Calibrating MEPDG Inputs Prediction Models for Asphalt Mixes Containing Reclaimed Asphalt Pavement

By

Saman Esfandiarpour

A thesis submitted to the Faculty of Graduate Studies of

The University of Manitoba

in partial fulfilment of the requirements of the degree of

Doctor of Philosophy

Department of Civil Engineering

University of Manitoba

Winnipeg

Contents

LIST OF TABLES

LIST OF FIGURES

ABSTRACT

In this thesis, the pavement sustainability practices were implemented by using recycled asphalt shingles (RAS) and reclaimed asphalt pavement (RAP) in asphalt pavements. Laboratory performance of mixes containing RAS and RAP were evaluated and characterized for a cold climate such as Manitoba, Canada. In addition, pavement sustainability practices were implemented by generating a database of measured values from laboratory test results to develop and perform local calibration alternatives on dynamic modulus and creep compliance predictive models used in Pavement ME Design software, and to assess the impact of locally calibrated MEPDG models on long-term performance of mixes. Laboratory results showed that 15% RAP can be used in an asphalt mix without changing the virgin asphalt binder grade when the design binder is PG 58-28. It was found that the globally calibrated MEPDG creep compliance and dynamic modulus models are not able to accurately predict values, particularly for mixes used in cold climates, in part because these mixes constituted only a small fraction of the mixes used to develop these models. It was found that the nonlinear multiple regression is the preferred technique for local calibration of NCHRP 1-37A and NCHRP 1-40D E* models. It was noted that the

existence of high RAP mixes in calibration of the E* predictive model causes an adverse effect on the reliability of calibrated models. In addition, it was found that nonlinear regression and Artificial Neural Network (ANN) models can be used as two alternatives to reliably predict creep compliance values.

Results of the predicted distresses of mixes containing RAP using MEPDG software for Manitoba default Level 3, Manitoba calibrated Level 3, and Manitoba Level 1 demonstrated that the calibrated Level 3 Manitoba asphalt mix input data can be used for the design and analysis of the Manitoba mixes with comparable accuracy of the Manitoba Level 1 input data. As conducting laboratory tests for individual mixes is expensive and time consuming, utilizing locally calibrated reliable models to predict E* and creep compliance can tremendously reduce operating and testing expenses.

ACKNOWLEDGEMENTS

I would like to express my appreciation to my advisor, Dr. Ahmed Shalaby, for his continued support, encouragement, and technical guidance during this research. My sincere thanks to the members of my advisory committee: Dr. M. Alauddin Ahammed and Dr. Madjid Birouk for their technical advice and comments.

I would like also thank all the people who helped me to make this thesis complete. The supports from Manitoba Infrastructure, City of Winnipeg, and Green Manitoba is gratefully acknowledge. Special thanks to my colleagues in the Pavement Research Group, Civil Engineering Department, University of Manitoba.

I would like to dedicate this work to my parents for their love, unfailing encouragement and continued support.

CHAPTER 1-INTRODUCTION AND FRAMEWORK

1.1 Introduction and Background

Annually, more than 150 billion tons of raw materials are used into the construction and maintenance of roadways in the United States. The need to increase the pavement network will continue as the pavement ages and demand for the roads with higher capacity grows. This requires the increase in the use of raw materials and cost of construction by different Department of Transportations (DOT). This challenge can be met by implementing sustainability best practices (Santero 2009). A sustainable approach focuses on maintaining the pavement infrastructure without the excessive use of resources through three key factors in the process of decision making: environmental, social, and economic (FHWA 2015).

Many transportation agencies are integrating new practices to implement sustainable pavements. These sustainable practices tend to surpass the current standards and provide innovation towards meeting required regulations and standards (FHWA 2015). Sustainability best practices can be

considered in different pavement life cycle phases including material production, pavement design, construction and maintenance, use and end of life as shown in Figure 1.1 (Santero 2009, UCPRC 2010).

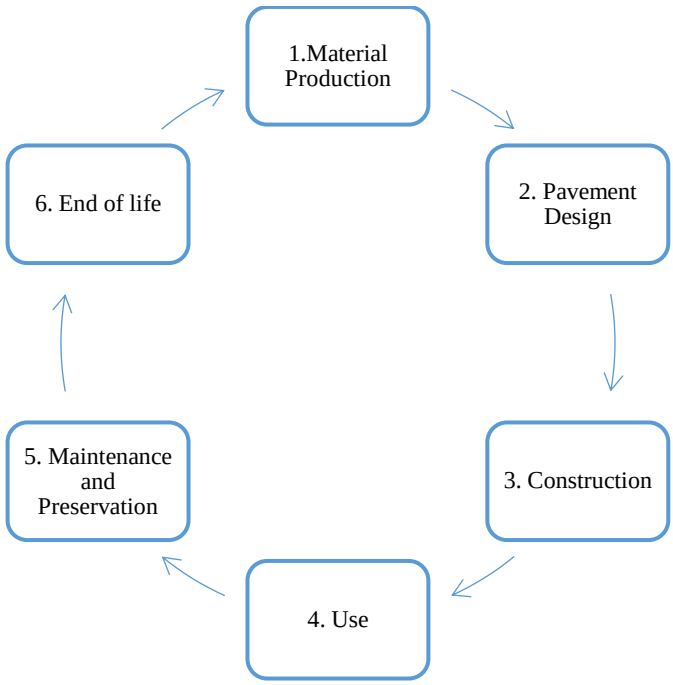

Figure 1.1: Pavement life cycle phases considered in sustainability best practices (Santero 2009)

This thesis considers only two phases; material and pavement design phases of sustainability best practices.

1.1.1 Sustainability in Material Production of the Asphalt Mix

The Federal Highway Administration (FHWA) has been encouraging the transportation agencies to use secondary materials in the construction and rehabilitation of highway infrastructure (NAPA 2016). Sustainability best practices for materials includes the reduction of the use of virgin materials by utilizing recycled and reclaimed materials.

Over the last two decades, the asphalt paving industry has been reusing materials in asphalt pavements and has promoted innovations to increase the maximum amount of recycling in asphalt pavements. Recycled materials have been used across North America in different parts of the road industry such as roadways, airports, parking lots, and many other locations (NAPA 2016).

Among the recycled materials, reclaimed asphalt pavement (RAP) and recycled asphalt shingles (RAS) have been implemented in asphalt pavements. In recent years, RAS and RAP have been used significantly to replace virgin asphalt binders and aggregates in the production of hot mix asphalt. The reduction in the use of virgin aggregates and virgin asphalt binders is paramount towards the successful implementation of sustainability best practices. (FHWA 2015). Utilizing RAS and RAP in new asphalt pavements provides many benefits (NAPA 2016) such as:

- Decrease in the production cost due to replacement of asphalt binder and aggregate,
- Decrease in the cost of transportation,
- Reduce the amount of waste disposal,
- Preserve aggregate, asphalt binder and energy,
- Reduce greenhouse gas emissions.

1.1.1.1 Reclaimed Asphalt Pavement (RAP)

Reclaimed asphalt pavement is an existing asphalt pavement, collected by milling or other operations, for use in a new HMA or base layer. RAP materials, typically consist of 95% aggregates and 5% asphalt binder. The use of RAP in asphalt mix provides many benefits such as the reduced demand for new materials, reduced transportation costs, and the preservation of natural sources. According to the National Asphalt Pavement Association (NAPA), it was estimated that

around 62.1 million tonnes of RAP were used in new asphalt pavement in the United States during 2010. This amount represents a saving of over 3 million tonnes of virgin asphalt binder. The use of RAP in asphalt mix increased to 67.8 million tonnes in United States in 2013 (Hansen and Copeland 2014).

The Federal Highway Administration suggests the use of RAP in pavement construction to be cost-effective and sustainable. It is reported that RAP is more economical when it is used in intermediate and surface layers of asphalt pavement. According to the FHWA, hot mix asphalt (HMA) with more than 25% RAP by weight of total mass is considered to be a high RAP content mix (Copeland 2011).

1.1.1.2 Recycled Asphalt Shingles

Asphalt roofing shingles are one of the most widely used roofing covers in Canada. Approximately 1.5 million tonnes of asphalt roofing shingles are discarded and replaced annually in Canada from residential and commercial facilities. The discarded roofing shingles represent approximately 10% of all residential and commercial waste reaching landfills (Ddamba 2012). Two types of base materials are used to produce asphalt shingles; organic and fibreglass. Both types of base material are made in a similar manner with asphalt, or modified asphalt, covered with granules. Organic shingles are made with a base mat of organic material such as paper, wood or other materials saturated with asphalt to make a waterproof top coating of adhesive asphalt and granules. Fibreglass shingles have a base layer of glass fiber-reinforced mat coated with asphalt and mineral fillers. Rand (2013) reported that asphalt shingles typically contain 30% aged asphalt binder by total weight, with organic asphalt shingles having approximately 1.6 times more binder content than fibreglass shingles. There are two types of recycled shingle scraps; Tear-off Scrap Shingle

(TOSS) which are removed from roofs, and Manufacture Waste Scrap Shingles (MWSS) which are discarded during the manufacturing process. Tear-off asphalt shingles are typically richer in asphalt and more readily available to be recycled compared to manufacture waste shingles. However, the asphalt binder obtained from TOSS is more oxidized (aged) than that of the MWSS due to the extended exposure to environmental conditions (Johnson et al. 2010).

In North America, the use of RAS in HMA has gained popularity because of its economic and environmental benefits. Approximately 1.9 million tons of RAS was used in asphalt pavements in 2012 (NCHRP SYNTHESIS-495 2016). RAS in HMA mixes reduces the amount of virgin asphalt binder required in HMA, and saves in production costs. While the use of RAS has economic and environmental benefits, the percentage of aged asphalt binder obtained from RAS must be properly designed for HMA mixes in order to ensure acceptable pavement performance.

1.1.2 Sustainability in Pavement Design Process

The other phase of a sustainable pavement is in the pavement design process. Design improvements can be derived from the use of new tools to obtain a better understanding of design parameters and performance. For many years, AASHTO 1993 (AASHTO Guide for Design of Pavement Structures) was the common approach for pavement structural design. The AASHTO 1993 design is based on empirical models which were developed based on limited field data and pavement structures.

The Mechanistic-Empirical Pavement Design Guide (MEPDG) was introduced in 2007 by the National Cooperative Highway Research Program (NCHRP 2004) as an improved methodology of pavement design and analysis. The new guide incorporates climate data, traffic loads and

material characteristics that can have an effect on pavement performance.

1.1.2.1 Pavement ME Design Software

The AASHTOWare Pavement ME Design program uses the MEPDG to design and analyze flexible and rigid pavement structures. This software uses the material properties to mechanistically compute the pavement responses such as strains, stresses, and deformations under specific design traffic loadings and climate data, and empirically relates damage to the pavement performance over time (AASHTO 2015). Flintsch and McGhee (2009) stated that "mechanistic–empirical (M-E) procedures use pavement models based on the mechanics of materials to predict pavement responses (deflections, strains, and stresses) and empirically based on transfer functions to estimate distress initiation and development based on these responses" (Flintsch and McGhee 2009). The transfer functions correlate pavement responses to pavement distresses. The flexible pavement distresses included in this software are surface roughness, total permanent deformation (rutting), asphalt layer permanent deformation, asphalt bottom-up fatigue cracking, asphalt top-down fatigue cracking, and asphalt thermal cracking. The distress prediction models require inputs to be defined by the user. The user defined inputs include asphalt, base, subbase and subgrade materials characteristics, traffic loading (include truck volume, truck traffic growth rate, axle load spectra, and truck class distribution, etc.), and climate data for a proposed/trial pavement structure.

Based upon the quality and quantity of available data for each material property, there are three levels of input options in MEPDG (NCHRP 2004). Level 1 input option generally requires site specific material properties data which are obtained through laboratory or field testing. These data have the highest level of reliability and are expected to provide the most reliable design and analysis. The required main input parameters for asphalt layer, which are considered for modeling

with the MEPDG software using Level 1 input data, are shown in Table 1.1.

Table 1.1: Asphalt layer Level 1 input parameters in MEPDG software.

	Tests/Parameters	Description
Asphalt Mix	Mix Design	VMA %, Va %, and asphalt content percentages
	Aggregate Gradation	-
	Dynamic modulus	4 different temperatures (-10°C, 5°C, 25°C, 40°C) and 6 frequencies (0.1 Hz., 0.5 Hz., 1 Hz., 5 Hz., 10 Hz., 25 Hz.)
	Creep Compliance	3 temperatures (-20°C,-10°C, and 0°C)
	Indirect Tensile Strength	at (-10°C)
Asphalt Binder	Performance Grade	Low and high temperature performance of virgin and recovered binder
	Complex Shear Modulus (G*)	
	Phase angle (δ)	

Level 2 inputs have an intermediate level of reliability. The input data are generally obtained through limited laboratory or field testing or estimated from correlations with other measured properties. Level 3 inputs have the lowest level of reliability as typical agency data or software default inputs are used (AASHTO 2008).

Although Level 1 inputs for an asphalt mix provide more reliable results when compared to both Level 2 and Level 3 inputs, the comprehensive laboratory testing required to obtain Level 1 inputs is time consuming and expensive. When Level 1 inputs for an asphalt mix cannot be obtained, asphalt mix properties will be estimated using predictive models. For instance, the dynamic modulus and creep compliance of an asphalt concrete (AC) mix can be estimated from predictive models. The NCHRP 1-37A or NCHRP 1-40D models can be used to estimate the dynamic modulus (E*) and MEPDG creep compliance model is used to estimate creep compliance values. These predictive models were globally calibrated and were function of volumetric properties of asphalt mixes (AASHTO 2015). They do not necessarily represent the local conditions such as

various types of materials and specifications. Therefore, there is a need to locally calibrate these predictive models used in the MEPDG software to enhance the reliability of pavement distress predictions.

1.2 Statement of the Problem

The use of RAS and RAP in asphalt pavements is beneficial. However, a number of challenges have been reported by researchers. For instance, Copeland (2011) reported RAS and RAP asphalt binder could increase the potential of thermal cracking. The lack of uniformity in RAS and RAP, and the potential presence of asbestos in RAS are other concerns in the use of RAS and RAP (NAPA 2016). In addition to these concerns, the design and performance of RAS and/or RAP mixes in a cold region are required to be addressed.

Furthermore, the reliability of MEPDG inputs predictive models should be evaluated. Both NCHRP 1-37A and NCHRP 1-40D models have been incorporated into the MEPDG program to estimate the dynamic modulus, whereas MEPDG creep compliance prediction model is used to predict the creep compliance values when Level 2 and Level 3 inputs for asphalt mix and asphalt binder are used. These predictive models are not necessarily accurate or consistent for different mixes in all regions since they were globally calibrated. Therefore, it is essential to develop a database for local mixes and materials and perform a local calibration on the predictive models used in MEPDG software (Pavement ME Design).

In this thesis, the sustainability practices are examined by using RAS and RAP in asphalt pavements along with optimizing the performance of recycled mixes. Laboratory low and high temperature performance of RAS and/or RAP mixes are evaluated for a cold climate such as

Manitoba, Canada. In addition, pavement sustainability practices are implemented by developing a database of measured values from laboratory tests to perform local calibration on MEPDG inputs prediction models for AC mixes. The reliability of globally calibrated predictive models used in MEPDG software for local mixes are evaluated, and the potential calibration tools for mixes containing RAP are investigated.

1.3 Goals and Objectives

The goals and objectives of this thesis are:

1. **Laboratory Characterization and Evaluation of Asphalt Mixes Containing RAS and RAP.** This research investigates the mechanical performance of RAS and RAP mixes. The potential rut resistance and thermal resistance of asphalt mixes are evaluated. The following objectives are included to address this goal:
    - Determine and evaluate the dynamic modulus of HMA mixes containing different amounts of RAS and RAP.
    - Evaluate the impact of RAS and/or RAP mixes on the dynamic modulus.
    - Determine and evaluate creep compliance and indirect tensile (IDT) strength tests results of HMA mixes containing RAS and RAP.
    - Examine the impact of RAS and/or RAP on creep compliance and IDT strength.
2. **Develop Local Calibration of MEPDG Inputs Predictive Models.** The MEPDG program uses predictive models to estimate some properties of asphalt mixes for the purpose of analysis and design. The reliability of these models should be evaluated and calibrated accordingly based

on local materials and mixes. The following objectives are included to meet the goal of performing local calibration alternatives on the MEPDG inputs predictive models:

- Evaluate the reliability of NCHRP 1-37A and NCHRP 1-40D dynamic modulus predictive models used in MEPDG software for AC mixes containing RAP.
- Develop two regression models; exponential fit of model outputs and nonlinear multiple regression to predict E* values.
- Evaluate the reliability of MEPDG creep compliance predictive model for AC mixes containing different amounts of RAP.
- Develop two alternatives, including a nonlinear multiple regression and an artificial neural network, to locally calibrate the MEPDG creep compliance model.

3. **Assess the Impact of Locally Calibrated MEPDG Models.** It is critical to determine if the use of values obtained from calibrated E* and creep compliance models in place of default values from globally calibrated will result in any difference in performance of the mixes containing RAP. The following steps are included to address this goal:
    - Evaluate the long-term performance of mixes containing RAP for Level 1 asphalt input data using MEPDG software.
    - Evaluate the performance of mixes containing RAP for default and calibrated Level 3 asphalt input data using MEPDG software.
    - Compare the predicted distresses of mixes for different Levels.

Comparing and combining the laboratory performance and MEPDG predicted performances of mixes will bring more reliable conclusions in the evaluation of mixes containing RAP. This approach will assist in the use of RAS and RAP in HMA and enhance the asphalt pavement

sustainability.

1.4 Significance of the Study

This thesis provides laboratory values of mechanistic properties of RAS and RAP mixes in Manitoba, Canada. The laboratory values are used in the analysis and design of RAS and RAP mixes. Laboratory test results can be used to develop a comprehensive laboratory database and to calibrate the prediction models used by MEPDG software. The locally calibrated asphalt mix inputs predictive models can provide more reliable analysis and design of asphalt pavement containing RAP. Improving reliability of AC prediction models will enhance the sustainability practices by reducing the risk and uncertainty regarding the adverse impacts of RAP mixes.

The mechanical characteristics of the RAS and/or RAP mixes will assist the City of Winnipeg (COW) and Manitoba Infrastructure (MI) to establish the allowable amount of RAS and RAP in asphalt mix without sacrificing the HMA performance.

The calibrated models can assist to achieve a reliable analysis and design of asphalt pavements while saving money. As conducting laboratory tests for individual mixes is expensive and time consuming, utilizing locally calibrated reliable models to predict E* and creep compliance can tremendously reduce operating and testing expenses.

1.5 Research Approach

The research program of this thesis consists of the laboratory testing, developing a database of laboratory-measured values, and conducting local calibration on MEPDG inputs models based on laboratory-measured data. In the first phase, eleven types of mixes with different amounts of RAS

and/or RAP from two material sources were prepared and laboratory tests were conducted. Two types of specimens were prepared; specimens from bulk field mix, and the University of Manitoba laboratory mix design specimens. Bulk field mixes were prepared and compacted in the laboratory from loose asphalt mixes, collected during the paving process. The University of Manitoba mixes were designed, prepared, and compacted in the laboratory. Creep compliance and dynamic modulus tests were conducted on specimens to determine mechanical characteristics of the mixes.

During the second phase, laboratory results were used to assess the MEPDG inputs prediction models. Additional mixes were tested to develop a database for creep compliance and dynamic modulus results. The MEPDG predictive models were used to estimate the dynamic modulus and creep compliance values. The laboratory test results were compared to predicted dynamic modulus and creep compliance values. Matlab software was used for conducting calibration techniques and statistical analysis. Local calibration alternatives were performed with the intent of improving the accuracy of the predictions. Finally, the effect of locally and globally calibrated models on long-term performance of AC mixes were evaluated.

1.6 Thesis Organization

This thesis is organized as follows:

Chapter 1 presents the statement of problem, the objectives, significance of the research, and research approach.

Chapter 2 presents an overview of laboratory and field performance of RAS and RAP mixes as well as a summary of allowable amounts of RAS and RAP in HMA by some transportation

agencies. This chapter also presents the globally calibrated dynamic modulus and creep compliance predictive models used in MEPDG software and describes relevant studies on the respective models.

Chapter 3 presents the research methodology, various properties of the investigated materials, and outline of experimental programs.

Chapter 4 describes the high and low temperature performance of the investigated mixes through laboratory-measured test results. This chapter presents the potential rutting resistance and low temperature performance of the mixes based on pavement stiffness.

Chapter 5 presents the alternative methods for calibration of dynamic modulus predictive models. This chapter also discusses how to increase the reliability of predicted dynamic modulus values.

Chapter 6 describes the options to improve the reliability of the MEPDG creep compliance prediction models.

Chapter 7 details the impact of globally and locally calibrated models on the analysis and performance of a built section in Manitoba using MEPDG software.

Chapter 8 presents a summary and the conclusions of this research along with recommendations for the future work.

Appendix A presents the field performance results of two mixes containing RAS and RAP from the City of Winnipeg projects.

CHAPTER 2 - LITERATURE REVIEW AND RESEARCH NEEDS

Transportation agencies, companies, and institutes have been seeking ways to utilize sustainable approaches to maximize benefits as part of daily operations. According to Federal Highway Administration, sustainable pavement is not entirely achieved yet (FHWA 2015). Implementing sustainability best practices can improve the existing practices. The sustainability best practices introduce some innovative approaches to enhance the current common practices while they meet the standards. Santero (2009) divided pavement life cycle into six phases to be considered in sustainability best practices. These phases are material production, pavement design, construction, use, maintenance and preservation, and end of life.

This thesis considers only two phases; material and pavement design phases of sustainability best practices. More details of these phases can be found in a reference document published by FHWA "Towards sustainable pavement systems "(FHWA 2015). The first part of this literature review considered the pavement materials in sustainability best practices using RAS and RAP in HMA. The second part focused on the pavement design phase of sustainability best practices that mainly

provided an overview of Pavement ME Design program and previous research of using MEPDG software models, analysis and design.

2.1 Asphalt Mix Materials

A typical asphalt concrete pavement roughly consists of 95% aggregate particles of different sizes and 5% asphalt binder (Copeland 2011). One phase of sustainability best practices is the use of pavement materials. Reduction in the use of virgin aggregate and asphalt binder by using RAS and RAP can be part of pavement materials phase (FHWA 2015).

The following sections summarize the previous work using RAS and RAP in asphalt mixes. In addition, these sections describe the use of RAS and RAP through several material specifications and selection, processing and laboratory performance evaluation.

2.1.1 Methods of Incorporating RAS and RAP in HMA

Processing of roofing shingles is the primary step to produce mixes containing RAS. Manufacturing Waste Shingles (MWS) generally are more desirable to be recycled since they contain less contaminant and fewer deleterious materials such as metal, wood, and plastic. However, the availability of MWS is limited compared to Tear Off Shingles (TOS). There are much more TOS available from roofing replacement. TOS usually are more aged (oxidized) and require more inspection, separation of unwanted materials and tests for potential asbestos content (Zhou et al. 2012).

There are two methods for incorporating shingles in an asphalt mix; wet and dry. In the dry method, RAS and/or RAP materials are heated and then mixed with heated virgin aggregates and heated

binder.

Based on past experiences, some states may have different approaches for incorporation of RAS and/or RAP in HMA. For example, the Texas Transportation Institute suggested two steps for RAS incorporation in HMA using dry method. In the first step, RAS is heated at 60°C for 12 to 15 hours (overnight) and in the second step RAS is heated at mixing temperature for two hours before mixed with virgin binder and aggregate (Zhou et. al 2011).

In the wet method, RAS should be ground to ultra-fine particles. The fine RAS particle is blended with asphalt binder using mechanical shear mixer at high temperature (180°C) at a speed rate of 1500 rpm for minimum of 30 minutes (Salari 2012).

There are two main scenarios of RAP contribution in asphalt mixes. The first scenario is "black rock" which has no contribution of RAP binder in asphalt mix. In fact the RAP particles act as aggregate in the mix. The second scenario is mingling the RAP binder with virgin binder. To find out the best possible scenario, many binder tests were carried out under NCHRP Project 9-12, "Incorporation of Reclaimed Asphalt Pavement in the Superpave System". Binder test results indicated that the second scenario which was blending the RAP binder and aggregate occurs mostly in the mix. It is necessary to characterize the RAP binder since it can have direct effect on HMA properties.

RAP is added to asphalt mix through dry method. In order to effectively release the RAP binder, RAP particles are usually preheated for specific time and temperature before mix with virgin aggregate and asphalt binder. There are two well-known RAP mixing procedures; National Cooperative Highway Research Program (NCHRP) method and Field Simulation method (FS). In

NCHRP method, the RAP is preheated at the range of 110°C to 150°C for two hours before being blended with virgin aggregate and binder at mixing temperature (McDaniel 2000). In FS method, RAP is mixed with very high heated virgin aggregate (usually 215°C) for 1 to 8 minutes before being mixed with virgin binder at mixing temperature (Nguyen 2009).

2.1.2 Laboratory Evaluation of RAS and RAP Mixes

2.1.2.1 Laboratory Evaluation of RAS Mixes

Sengoz and Topal (2004) indicated that up to 5% shingle waste by weight of total asphalt mix was used in HMA. Results showed that the use of RAS in hot regions improves the rutting resistance of pavements due to an increase in the stiffness of the mix.

Watson et al. (2010) evaluated the effect of RAS gradation on HMA. The authors found that the gradation of RAS can have significant impact on the performance of HMA. The finer the RAS, the more RAS binder incorporate into the HMA mix. However, authors did not consider preheating RAS before being mixed with virgin aggregate for RAS to release the binder.

Maupin (2010) examined the field and laboratory performance of asphalt mixes containing shingles in Virginia HMA samples. Maupin's results showed that 4% to 5 % shingles can be effectively used in HMA based on various tests such as indirect tension, rut and fatigue resistance using the asphalt pavement analyzer (APA).

Abbas et al. (2013) conducted different tests to examine the impact of RAS on physical and chemical properties of virgin binder. The results showed that RAS binder can improve the permanent deformation, however, the susceptibility to low temperature cracking increases. Abbas

et al. also found that the addition of RAS dramatically increases the level of aging (based on pressure aging vessel conditioning). This indicates that RAS binder will mostly affect the long-term cracking performance of the asphalt mix.

Ddamba (2011) analyzed the performance of mix including RAS in Ontario. Ddamba found that 6% RAS has the best rutting and cracking performance. Moreover, it was found that using RAS alone performed better than combined use of RAS and RAP in HMA mixes. However, this research did not consider long-term field performance.

2.1.2.2 Laboratory Evaluation of RAP Mixes

According to National Cooperative Highway Research Program (NCHRP) 452, when the RAP content is low (usually 10-20 percent RAP), it is not necessary to conduct the binder test due to low RAP binder contribution in the mix. However, higher percentage of RAP could have an influence on asphalt binder of the asphalt mix. Therefore, softer binder must be used. Table 2.1 shows the recommended binder selection according to RAP contents by NCHRP 452.

Table 2.1: Binder selection guideline for RAP mixes (NCHRP-452 2001)

Recommended Virgin Asphalt Binder Grade	RAP Percentage		
	Recovered RAP Binder Grade		
	PG xx-22	PG xx-16	PG xx-10 or higher
No change in binder selection	<20%	<15%	<10%
Select virgin binder one grade softer than normal (e.g., select a PG 58-28 if a PG 64-22 would normally be used)	20–30%	15–25%	10–15%
Follow recommendations from blending charts	>30%	>25%	>15%

The virgin binder selection, based on blending charts, is a function of blended final binder and

RAP binder properties obtained from dynamic shear rhometer (DSR) test, and bending beam rhometer (BBR) test. The performance grade of RAS or RAP asphalt binder can vary from one location to another due to different age and mix design. Therefore, it is critical to determine the performance grade of RAS and/or RAP binder prior use in the mix.

Most highway agencies require the contractor to change the virgin binder grade when the RAP content exceeds 15-20% (McDaniel et al. 2012). Many studies established the effect of high RAP (more than 20%) on virgin binder and asphalt mix. Some of those studies are discussed below.

One of the objectives of NCHRP Project 9-12 (2000) was to evaluate the influence of RAP on physical properties of asphalt mix. In this study, two types of virgin binder and three RAP sources were used. Asphalt mixes contained 0, 10, 20 and 40 percent RAP. Frequency sweep, indirect tensile creep, and beam fatigue test were carried on the RAP samples. Results showed that stiffness of the mixes increases and fatigue life decreases by increasing the RAP percent. In this study, the use of soft binder was recommended when 40% RAP was used (McDaniel 2000).

In 2005, Daniel and Lachance applied 0, 15, 25, and 40 percent RAP in HMA. PG 58-28 was selected as virgin binder and the gradation of all mixes was kept almost the same. The voids in mineral aggregate (VMA) and voids filled with asphalt (VFA) increased as RAP content increased. The dynamic modulus was increased when higher amounts of RAP were used. However, no trend was obtained for creep compliance result due to inconsistency in RAP gradation, since unfractionated RAP was used in HMA. The inconsistency of results can be attributed to different heating time, which resulted in releasing different amounts of RAP binder in the HMA.

Shu et al. (2008) assessed the effect of 0, 10, 20, and 30 percent RAP on asphalt mix with five

percent optimum asphalt binder. The virgin binder had a performance grade of PG 64-22. The RAP particles were screened through the No.4 (4.75 mm) sieve. The RAP asphalt binder content was found to be 5.5%. Results showed that the IDT strength at (25°C) increases as RAP content increases. This indicates that RAP makes the mix brittle. In addition, the resilient modulus and fatigue resistance of the mix increase as RAP increases.

Mogawer et al. (2012) assessed the performance of plant produced HMA containing RAP (0, 20, 30, and 40%). In order to evaluate the influence of softer binder on RAP mixes, four PG binder grades PG52-34, PG58-28, PG64-22 and PG64-28 were used. Results indicated that the stiffness of mix increases by increasing the RAP content, however, the mix stiffness decreases when softer binder is used. The recovered binder test results showed that RAP increases the stiffness at the high temperature than that of the low temperature and when the softer binder is used the low temperature properties is improved. Workability result showed that increasing the RAP content can adversely impact the workability while the use of soft binder improves the workability.

Islam et al. (2014) examined the effect of up to 35% RAP on asphalt binder and asphalt mix performance in the laboratory. The results showed that RAP improves the dynamic modulus and it has no significant effect on moisture susceptibility. Furthermore, 35% RAP mix created less permanent strain indicating higher rut resistance (Islam 2014).

In a study in Virginia, performance of RAP on mix containing high (up to 45%) RAP in asphalt mix was evaluated, whereas, according to the Virginia DOT specification 30% RAP is allowed to be used in the surface layer of asphalt mix. Loose mixes were collected from field and prepared in the laboratory to examine the high RAP mixes properties. Results showed that 45% RAP mix can be successfully designed and used in HMA. According to flow number (permanent deformation)

and dynamic modulus test results, the 40% and 45% mixes should perform comparable to the 20% and 30% RAP mixes. Authors recommended that the field performance should be investigated in future to validate the long-term performance of high RAP mix (Diefenderfer and Nair 2014).

McDaniel et al. (2012) evaluated the characteristics of plant produced HMA containing RAP. It was found that the stiffness of the mix increases by increasing the RAP content especially at intermediate and high temperature. A softer binder showed reduction in stiffness at low and high temperature as expected. In a study in University of Iowa, Fractionated RAP with 30%, 40% and 50% virgin binder replacement was used in asphalt mix. It was found that FRAP decreases the amount of fine aggregate and improves the volumetric mix design criteria (Shannon 2012).

Hajj et al. (2011) evaluated the moisture damage and thermal cracking resistance of HMA with 0, 15 and 50% RAP in Manitoba. The PG 58-28 virgin binder was used for different percentage of RAP. In order to determine the difference between the plant mixes and laboratory compacted samples, the raw materials were also collected. The PG grade of extracted binder showed that mix containing 15 % RAP has the same performance grade (PG 52-28) as the virgin binder. When 50 % RAP was used, the performance grade of binder changed from PG 58-28 and PG 58-34 to PG 64-16 and PG 64-22, respectively. Samples were conditioned in 0 to 3 freeze and thaw cycles before conducting tensile strength ratio (TSR) and dynamic modulus test. The results showed that the moisture damage trends were almost similar for all RAP mixes. The plant produced HMA samples were determined to be stiffer when it was compared to laboratory compacted samples. Dynamic modulus decreased by increasing the number of freeze and thaw cycles. Thermal Stress Restrained Specimen Test (TSRST) results showed mixes containing 0% RAP and 15% RAP have similar low critical temperature. The 50 % RAP mix had few degrees warmer low critical

temperature (lower thermal cracking resistance) when it was compared to the virgin binder. Softer binder improved the TSRST fracture temperature and therefore thermal cracking resistance.

2.1.2.3 Incorporation of RAS and RAP in HMA

In recent years, many departments of transportation conducted research to determine the impact of RAS and RAP in asphalt pavement. The following summarizes some of previous experiences of RAS and RAP in HMA.

An extensive study in Minnesota investigated the influence of RAS and RAP in HMA, the effect of soft binder, and the difference in performance between MWSS and TOSS in HMA (Johnson et al. 2010). Seventeen mixes containing variable amounts of RAS and RAP were evaluated. The virgin binder was selected as PG58-28 for all mixes except when 25% RAP and 5% RAS (for both TOSS and MWSS) were used. For these mixes, a softer binder (PG 52-34) was used. Two sources of RAP were used in this study. The RAP-1 and RAP-2 contained 5.6% and 4% asphalt cement, respectively. Table 2.2 shows the detail of RAS and RAP contents in HMA and PG grade of binder for each mix. The results showed that RAP and/or RAS increases the PG grade of mix particularly the high temperature grade. Use of softer binder showed improvement in high and low temperature performance grades. As expected, increase in RAP and/or RAS showed an increase in stiffness of the asphalt mix. According to the dynamic modulus tests results, a softer binder decreased the stiffness of the mix. The TOSS mix showed better rutting resistance compared to the MWSS mixes.

Table 2.2: Different amounts of RAS and RAP in HMA (Johnson et al. 2010)

Mix No.	Mix ID	RAP (%)	RAS – TOSS (%)	RAS – MWSS (%)	PG Grade
1	PG 58-28	0	0	0	58-28
2	15% RAP-1	0	0	0	70-16
3	25% RAP-1	0	0	0	76-16
4	30% RAP-1	0	0	0	70-22
5	15% RAP-1 5% MWSS	15	0	5	76-16
6	15% RAP-1 5% TOSS	25	5	0	76-16
7	25% RAP-1 5% TOSS	25	5	0	82-10
8	25% RAP-1 5% MWSS	25	0	5	76-16
9	25% RAP-1 5% TOSS 51-34	25	5	0	70-16
10	25% RAP-1 5% MWSS 51-34	25	0	5	70-22
11	25% RAP-1 3% TOSS	25	3	0	76-16
12	25% RAP-1 3% MWSS	25	0	3	76-16
13	15% RAP-1 3% TOSS	15	3	0	76-16
14	15% RAP-1 3% MWSS	15	0	3	76-16
15	10% RAP-1 5% TOSS	10	5	0	76-16
16	15% RAP-2 5% TOSS	15	5	0	76-16
17	5% TOSS	0	5	0	70-22

Results showed that use of recycled materials generally improve the rut resistance due to increase in stiffness in the mix. TOSS mix showed more sensitive to moisture damage as compared to MWSS mix. In addition, it was found that when the binder replacement limited by 30% of virgin binder, the mixes showed better performance (Johnson et al. 2010).

Wu et al. (2014) investigated the use of 3% RAS and 15% RAP into HMA overlay in Washington. The tear-off recycled shingles with asphalt content in the range of 16% to 23% were used in this study. The percent of RAS and RAP were selected based on less than 30% binder replacement in the mix. The virgin binder was PG 64-22 and the design asphalt content was 5.5%. Results showed that the rutting resistance of the binder is improved by the addition of RAS and RAP. The fatigue and thermal cracking resistance did not show significant change by the addition of RAS and RAP

(Wu et al. 2014).

Ozer et al. (2013) investigated the impact of high percentages of recycled asphalt binder replacement (43% to 64% by weight of virgin binder) on HMA. Ozer et al. found that the complex shear modulus (stiffness) increased at high temperature with increasing amounts of RAS and RAP binder in the mixes, and that when the amounts of RAS and RAP increased in the HMA, rutting resistance improved while fatigue life decreased.

In a study in British Columbia, effect of RAS and RAP on asphalt mix was evaluated. Sample mixes consisted of 15% RAP and 3% to 5% RAS. Results from the dynamic modulus, resilient modulus, and rutting resistance testing in the Asphalt Pavement Analyzer (APA) showed RAS mixes perform comparably to control mix (Uzarowski et al. 2010).

Watson et al. (2011) assessed the effect of combination of RAS and RAP in HMA. Two field projects were considered to be assessed in this research. The asphalt mixes consisted of 15% RAP and 5% RAS (TOSS and MWSS). Survey results after three years of service showed that the section containing 15% RAP and 5% TOSS RAS showed the best performance. Authors concluded that the RAS and RAP did not show to be a dominant parameter in the asphalt mix performance.

Lippert and Brownlee (2012) and Williams et al. (2011) conducted various studies on RAS mixes for Illinois Department of Transportation, The field and laboratory results showed that 5% RAS decreased the permanent deformation (rutting), however low temperature cracking increased as the amounts of RAS increased. Authors also reported that use of RAS in HMA in Illinois increased around 250% in 2012 compared to 2011.

2.1.3 Allowable RAS and RAP in AC Mix by Different Transportation Agencies

The allowable amount of recycled and reclaimed binder which can be used in HMA is an important issue in the use of RAS and RAP. Since recycled and reclaimed binders are usually too stiff compared to virgin asphalt, the binder replacement percentage can significantly impact the properties of asphalt mix. For instance, high percentage of binder replacement (percentage of recycled and reclaimed binder derived from RAS and RAP) in HMA can increase the potential of thermal cracking. At the lower layer, higher amount of binder replacement is usually allowed since it is not subject to the same tire stress and extreme low temperature. Therefore, it is essential to determine the maximum allowable amounts of RAS and RAP in asphalt mix layers.

The allowable RAS and/or RAP is limited by highway agencies to avoid sacrificing the asphalt mix short term and long-term performance. Department of transportation in many states either established specifications related to RAS and/or RAP allowable usage or have research or pilot projects going on to provide acceptable amounts of RAP and/or RAS in HMA. A summary of maximum allowable amounts of RAS and/or RAP in some states are presented below (Bonaquist 2011).

Indiana DOT allows a maximum of 3% manufacturing waste RAS on surface layer and 5% in other layers. Indiana DOT established an equivalent for substitution of RAS and RAP; 1% RAS is equivalent to 5% RAP. Maryland DOT also permits up to 5% manufacturing waste RAS in asphalt mix except in gap-graded mixes and mixes with polymer binders (Hansen 2014).

In 2010, WisDOT established the maximum percent binder replacement which can be used in different asphalt layers. Table 2.3 shows the maximum allowable percent binder replacement for

RAP, RAS, fractionated reclaimed asphalt pavement (FRAP), and their combination.

Table 2.3 WisDOT 2010 maximum allowable percent binder replacement

Recycled and Reclaimed Materials	RAS	RAP	FRAP	RAS and RAP	RAS and FRAP	RAS, RAP, and FRAP
Lower Layers	20	35	35	30	30	30
Upper Layers	15	20	25	20	25	25

RAS: Recycled asphalt shingles
RAP: Reclaimed asphalt pavement
FRAP: Fractionated recycled asphalt pavement

Minnesota Department of Transportation established the amounts of RAS and RAP content in asphalt mix based on asphalt binder replacement (ABR). Table 2.4 shows the allowable RAS and RAP percent in Minnesota.

Table 2.4 Allowable RAS and RAP contents in Minnesota.

Specified Asphalt Binder Grade	**Lift**	**Minimum Ratio of Virgin Asphalt Binder to Total Asphalt Binder**		
		RAP only	**RAS only**	**RAS and RAP**
PG XX-28 PG 52-34 PG 49-34 PG 64-22	Wear	70	70	70
	Non-Wear	70	70	65
PG 58-34 PG 64-34 PG 70-34	Wear	80	80	80
	Non-Wear	80	80	80

Source: MnDOT (2013; Table 2360-8).

In 2010, the Ontario Ministry of Transportation limited the use of RAP (under highway specification OPSS 1150) in the surface layer and binder (intermediate layer) up to 15% and 30%, respectively. Based on this specification, use of more than 50% RAP is not permitted in any mixes

(Ontario Provincial Standard Specification 2010).

Missouri permits the use of RAS up to 3% in asphalt mix without changing the PG binder if the binder replacement is less than 30%. If the ratio of virgin binder to total binder is between 60 to 70 percent, a softer virgin binder PG 52-28 or PG 58-28 shall be used instead of PG 64-22. RAP is allowed to be used in mix up to 20% without any change in PG binder (MO DOT Engineering Policy Guide RSS 2011). The Massachusetts DOT allows up to 5% manufacturing waste RAS in asphalt mix except in surface mix layer (Mass Dot 2010).

Virginia Department of Transportation specified the allowable amount of RAP, RAS, and combined RAS and RAP in surface, intermediate, and base layer of asphalt mix. The maximum asphalt binder replacement was addressed for different layers as well (VDOT 2016). Table 2.5 shows the Virginia specification.

Table 2.5 Allowable RAS and RAP contents in Virginia

Mix	**Maximum Allowable Binder Replacement, %**		**Maximum Allowable Binder Replacement for Mix with Both RAS and RAP, %**
	RAP	**RAS**	**RAS and RAP**
Surface	< 25 %	5	30
Intermediate	25% - 30%	5	30
Base	25% to 35%	5	30

Note: [1]RAP= Recycled asphalt pavement
[2]RAS= Reclaimed asphalt shingles

Texas Department of Transportation established the combined amounts of RAS and RAP asphalt binder in asphalt mix. Table 2.6 summarized the allowable RAS and RAP percent and binder replacement in Texas (NCHRP SYNTHESIS 2016).

Table 2.6 Allowable RAS and RAP contents in Texas

Originally Specified PG Binder	Allowable Substitute PG Binder	Maximum Asphalt Binder Replacement [1] for Asphalt Mixes, %		
		Surface	Intermediate	Base
76-22[2]	70-22 or 64-22	20	20	20
	70-28 or 64-28	30	35	40
70-22[2]	64-22	20	20	20
	64-28 or 58-28	30	35	40
64-22[2]	58-28	30	35	40
76-28[2]	70-28 or 64-28	20	20	20
	64-34	30	35	40
70-28[2]	64-28 or 64-28	20	20	20
	64-34 or 58-34	30	35	40
64-28[2]	58-28	20	20	20
	58-34	30	35	40

Note: [1] Combined recycled binder from RAS and RAP

[2] nNo more than 20.0% recycled binder when using this originally specified PG binder.

Nebraska DOT certified the use of RAP based on the Equivalent Single Axle Load (ESAL) level. If the maximum allowable amount of RAP is exceeded for a given mix, the PG grade must be lowered one grade (Shannon 2012). Table 2.7 summarized the Nebraska RAP specification.

Table 2.7 Allowable RAP contents in Nebraska

Traffic Level, (MESAL)	Maximum Allowable RAP Content, % of Mix
<3	35
3 to <10	25
10 to <30	15

MESAL=million equivalent single axle load

2.2 Mechanistic-Empirical Pavement Design Guide (MEPDG)

Federal Highway Administration stated that the use of tools to improve the design of pavements, and better understanding of design parameters and pavement performance are keys to the sustainability best practices in pavement design (FHWA 2015). Pavement ME Design program is a tool that uses the mechanistic-empirical pavement design procedures in the analysis and design of pavements.

Many agencies in North America are in the process of adopting this new design method. Some agencies have shown a significant advancement to implement the MEPDG and to develop an appropriate database for calibrating the MEPDG distress prediction models.

Iowa Department of Transportation reported that change in asphalt layer thickness does not show significant influence on alligator cracking, transverse cracking and IRI. Also, the MEPDG predicted results showed that alligator cracking, longitudinal cracking, and rutting are highly sensitive to truck volume (Ceylan 2009).

Galal and Chehab (2005) reported that the different dynamic modulus values in Level 1 and Level 3 can impact the predicted rutting and longitudinal fatigue cracking. Level 1 dynamic modulus values provided closer prediction to field distresses when it compared to Level 3.

The reliability of pavement distresses can be improved if the predictive models in MEPDG software are calibrated based on local conditions. AASHTO recommends performing local calibration to reduce the possible bias and error in prediction of the pavement distresses (AASHTO 2015).

2.2.1 Predictive Models Used in MEPDG Software

The transfer functions which predict the performance of the pavements in Pavement ME Design program were mainly developed nationally based on data from different sites in North America (AASHTO 2010). The transfer functions require the use of material properties of the pavement as inputs. The material properties are generally tested and measured in the laboratory. When the laboratory-measured properties (Level 1 input data) are not available, the predictive models are used to estimate these properties. For instance, MEPDG software uses the NCHRP 1-37A or NCHRP 1-40D model for estimating dynamic modulus and utilizes MEPDG creep compliance predictive model to estimate creep compliance values, when Level 3 asphalt mix and binder inputs are used for design and analysis of the asphalt pavement.

Although these models were globally calibrated and validated mostly based on long-term pavement performance program database, they do not necessarily represent the local conditions such as various types of materials and specifications. Therefore, there is a need to locally calibrate these predictive models used in MEPDG software to enhance the reliability of pavement distress predictions. Mechanistic-empirical pavement design guide recommends to calibrate the models based on local materials and mixes before design and analysis of the pavements (AASHTO 2010). The following sections discuss the uncalibrated (globally calibrated) and calibrated (locally) dynamic modulus and creep compliance predictive models used in MEPDG software.

2.2.2 Dynamic Modulus Prediction Models of Asphalt Pavement

In the MEPDG and its software Pavement ME Design, the dynamic modulus of an AC mix is a required input for design and performance prediction. For Level 1 inputs, the dynamic modulus is

measured in the laboratory in accordance with the AASHTO T342 test method (AASHTO 2011). When Level 1 inputs for the AC mix cannot be obtained, the dynamic modulus can be estimated from correlations with other properties of the AC mix (NCHRP 2004). The NCHRP 1-37A and NCHRP 1-40D models have been incorporated into the MEPDG program to estimate E* when Level 2 and Level 3 inputs for asphalt mix and asphalt binder are used in the design and analysis of pavement structures.

2.2.2.1 NCHRP 1-37A Model

This model estimates E* in Level 2 and Level 3. A total of 2750 data points from asphalt mixes containing unmodified and modified asphalt binders were used in developing the coefficients of the NCHRP 1-37A model. This model assumes a sigmoid function of inputs for the AC mix. It is constructed based upon asphalt binder viscosity and asphalt mix volumetric properties (NCHRP, 2004). Equation 2.1 shows the NCHRP 1-37A model.

$$\text{Log}_{10}\, E^* = -1.249937 + 0.02923\rho_{200} - 0.001767(\rho_{200})^2 - 0.002841\,\rho_4 - 0.058097 V_a - 0.802208\frac{V_{beff}}{V_{beff}+V_a} + \frac{3.871977 - 0.0021\rho_4 + 0.003958\,\rho_{38} - 0.000017(\rho_{38})^2 + 0.00547\rho_{34}}{1+e^{(-0.603313 - 0.313351(logf) - 0.393532(log\eta))}} \quad (2.1)$$

Where, E* = dynamic modulus of the mix, 10^5 psi, η = bitumen (asphalt binder) viscosity, 10^6 Poise; f = loading frequency, Hz.; V_a = air voids content, %; V_{beff} = effective bitumen content, % by volume; ρ_{34} = cumulative % retained on the 3/4 in. (19 mm) sieve; ρ_{38} = cumulative % retained on the 3/8 in. (9.5 mm) sieve; ρ_4 = cumulative % retained on the #4 sieve; ρ_{200} = % passing the #200 sieve.

2.2.2.2 NCHRP 1-40D Model

A new model was developed based on 7400 data points from 346 mixes to predict the E* of asphalt mixes. This model is a sigmoid function of volumetric properties, aggregate gradation similar to NCHRP 1-37A model, however, complex shear modulus (G*) and phase angle (δ) of asphalt binder were used to characterize the asphalt binder instead of asphalt binder viscosity (Bari and Witczak 2006, Witczak et. al 2006). In 2006, this model was revised under NCHRP 1-40D project to be implemented in MEPDG program. This model is shown in Equation 2.2.

$$\begin{aligned}\text{Log}_{10}\,E^* = {} & -0.349+0.754(|G_b^*|^{-0.0052})^*(6.65-0.032\,\rho_{200}+0.0027(\rho_{200})^2+0.011\,\rho_4 \\ & -0.0001(\rho_4)^2+0.006\,\rho_{38}-0.00014(\rho_{38})^2-0.08V_a-1.06\left(\frac{V_{beff}}{V_{beff}+V_a}\right)) \\ & +\frac{2.558+0.032Va+0.713\left(\frac{V_{beff}}{V_{beff}+V_a}\right)+0.0124\,\rho_{38}-0.0001(\rho_{38})^2-0.0098\rho_{34}}{1+e^{(-0.7814-0.5785\left(\log\left|G_b^*\right|\right)+0.8834log(\delta_b))}}\end{aligned} \quad (2.2)$$

El-Badawy et al. (2012) reported that NCHRP 1-40D model was revised in 2007, shortly after it was first released. The revised model, Equation 2.3, is the one being implemented in MEPDG software since Version 0.9 to date.

$$\begin{aligned}\text{Log}_{10}\,E^* = {} & -0.02+0.758(|G_b^*|^{-0.0009})^*(6.8232-0.03274\,\rho_{200}+0.00431(\rho_{200})^2+0.0104\,\rho_4 \\ & -0.00012(\rho_4)^2+0.00678\,\rho_{38}-0.00016(\rho_{38})^2-0.0796V_a-1.1689\left(\frac{V_{beff}}{V_{beff}+V_a}\right))+ \\ & \frac{1.437+0.03313Va+0.6926\left(\frac{V_{beff}}{V_{beff}+V_a}\right)+0.00891\,\rho_{38}-0.00007(\rho_{38})^2-0.0081\rho_{34}}{1+e^{(-4.5868-0.8176\left(\log\left|G_b^*\right|\right)+3.2738\,log(\delta_b))}}\end{aligned} \quad (2.3)$$

Where, E* = dynamic modulus of the mix, psi, $|G_b^*|$= dynamic shear modulus of binder, Pa; δ_b = phase angle, degree; V_a = air voids content, %; V_{beff} = effective bitumen content, % by volume; ρ_{34} = cumulative % retained on the 3/4 in. (19 mm) sieve; ρ_{38} = cumulative % retained on the 3/8 in. (9.5 mm) sieve; ρ_4 = cumulative % retained on the #4 sieve; ρ_{200} = % passing the #200 sieve.

Both NCHRP 1-37A and NCHRP 1-40D require asphalt binder properties such as viscosity, complex shear modulus and phase angle to predict the dynamic modulus at different temperatures.

2.2.2.3 NCHRP1-37A Asphalt Binder Characterization

For the Level 1 inputs, the complex shear modulus (G*) and phase angle (δ) of the asphalt binder at different temperatures (at least 3 temperatures) are required. Equation 2.4 is used to compute the viscosity of asphalt binder at different temperatures based on G* and δ.

$$\eta = \frac{G^*}{10}\left(\frac{1}{Sin\ \delta}\right)^{4.8628} \tag{2.4}$$

Where, G* = complex shear modulus, Pa; δ = phase angle, degrees; η = binder viscosity, cP.

Once asphalt binder viscosity is determined, the viscosity-temperature relationship recommended by ASTM is used to determine the viscosity at any desired temperature (ASTM 2009). The linear regression is performed to obtain the regression parameters in Equation 2.5.

$$\log\log\eta = A + VTS\log TR \tag{2.5}$$

Where, η = binder viscosity, cP; T_R = temperature, Rankine; A = regression intercept; VTS = regression slope of viscosity temperature susceptibility. In Level 3 inputs, the default values of VTS and A parameters are used for the selected asphalt binder. Then, Equation 2.5 is used to compute the viscosity of the asphalt binder at desired temperature.

2.2.2.4 NCHRP 1-40D Asphalt Binder Characterization

For the Level 1 and Level 2 inputs, the binder viscosity is determined by using the complex shear modulus and phase angle of the asphalt binder, through Equations 2.4 and 2.5. The binder complex shear modulus and phase angle at desired temperatures and frequencies are determined using Equations 2.6-2.11. The calculated asphalt binder G* and δ are used in NCHRP 1-40D to predict E* (Witczak et al. 2006).

$$\log\log \eta_{fs,T} = A' + VTS' \log T_R \quad (2.6)$$

$$A' = 0.9699\, f_s^{-0.0527}\, A \quad (2.7)$$

$$VTS' = 0.9668\, f_s^{-0.0575}\, VTS \quad (2.8)$$

$$f_s = f_c / 2\pi \quad (2.9)$$

$$\delta = 90 - (-7.3146 - 2.6162\, VTS') \log(f_s \eta_{fs,T}) + (0.1124 + 0.2029 * VTS') * \log(f_s \eta_{fs,T})^2 \quad (2.10)$$

$$|G_b^*| = 0.0051\, f_s\, \eta_{fs,T} (Sin\, \delta_b)^{7.1542 - 0.4929\, fs + 0.0211\, fs^2} \quad (2.11)$$

Where, A′= adjusted A; VTS′ = adjusted VTS; fs = loading frequency in dynamic shear loading mode as used in the dynamic shear rheometer (DSR) test to measure |Gb*| and δb, Hz; fc = loading

frequency in dynamic compression loading as used in the E* test of HMA mixes, Hz; η_(fs,T) = viscosity of asphalt binder as a function of both loading frequency (f) and temperature (T), cP; |Gb*| = dynamic shear modulus of binder, Pa; δ_b= phase angle, degree.

Equations 2.6 to 2.11 were developed based on nonlinear regression technique to eliminate the direct use of viscosity and replace it with G* and δ (Witczak et al. 2006). For Level 3 inputs, similar to NCHRP 1-37A the default values of VTS and A parameters are firstly used to calculate the viscosity of the selected asphalt binder and then Equations 2.6 to 2.11 are used to estimate the asphalt binder G* and δ. Once required asphalt properties are determined from abovementioned methods, the prediction models are used to estimate the E* values.

2.2.2.5 Past Experience of E* Predictive Models and Local Calibrations

The reliability of the estimated E* from NCHRP models was evaluated by several researchers. Table 2.8 summarizes several studies that conducted the NCHRP E* predictive models calibration. According to a multitude of research studies, there were noticeable inconsistencies in predicting of E* values when globally calibrated NCHRP models were used. For instance, Clyne et al. (2009) reported that NCHRP 1-37A model underestimates the E* values at high temperature. Kim et al. (2005) also found that the estimated E* values from NCHRP 1-37A model show a better fit with the measured values at the low temperature than at the high temperature. Jeong (2010), Abu Abdo et al. (2009), Yousefdoost et al. (2013) reported that NCHRP 1-37A model underestimates E* in all range temperatures. However, other researchers claimed that the NCHRP 1-37A model tends to overestimate E* over the entire range of temperatures (Singh et al. 2011a, Martinez et al. 2009, Far et al. 2009, Esfandiarpour et al. 2015, Obulareddy et al. 2006, Singh et al. 2011b).

Table 2.8: Calibration of NCHRP dynamic modulus predictive models

Source	Number of Mixes	Number of date points	Calibration Type	Calibrated model
El-Badawy et. al (2012)	27	1128	Local mixes, Idaho, USA	NCHRP 1-37A
You et. al (2012)	14	1341	Local mixes, Michigan, USA	NCHRP 1-40D
Georgouli et. al (2016)	15	1350	Local mixes, Athens, Greece	NCHRP 1-40D
Biligiri and Way (2014)	N.A.	2834	Local mixes, Arizona, USA	NCHRP 1-37A, NCHRP 1-40D
Ceylan et. al (2009)	346	7400	National mixes, USA	NCHRP 1-37A, NCHRP 1-40D

When it comes to comparison of NCHRP 1-37A and NCHRP 1-40D models, Witczak et al. (2006) and Birgisson et al. (2005) reported that NCHRP 1-40D model is reasonably accurate and is able to predict better E* predictions compared to NCHRP 1-37A model. Others, however, claimed that NCHRP 1-37A model is fairly accurate in estimating the E* compared to NCHRP 1-40D (Martinez et al. 2009, Awed et al. 2009, Robbins et al. 2011, Khattab et al. 2014).

The accuracy of the estimated E* varies with type of mix, temperature, air voids and other volumetric properties [Bari and Witczak 2006, Singh et al. 2011a, Harran and Shalaby 2009]. The models are based on the analysis of a broad dataset of mixes, however it is recommended to calibrate the models to local mix properties and binder types. Inconsistency in prediction of E*, as mentioned earlier, leads researchers to evaluate the NCHRP predictive models for local mixes and to utilize calibration methods on NCHRP models.

AASHTO (2010) recommended the local calibration of MEPDG models, however some users are still using globally calibrated MEPDG models due to lack of an adequate local calibration

database. In recent years, the use of RAP in HMA has increased due to economic and sustainability benefits. It is necessary to investigate potential local calibration tools for mixes containing RAP, and to evaluate the accuracy of uncalibrated E* models, and calibrated E* models for mixes containing RAP.

2.2.3 Creep Compliance Prediction Models of Asphalt Pavement

Thermal cracking is one of the principal asphalt pavement distresses that typically appear early in the service life. There are two types of thermal cracking; 1) low temperature cracking which occurs due to cold temperature and is more common in cold regions, 2) Thermal fatigue cracking which is function of thermal cycling (Shalaby et al. 1996).

In the Mechanistic-Empirical Pavement Design software, the thermal cracking model is used to predict the low temperature performance (NCHRP 2004). The thermal cracking model requires creep compliance values of the mix as an essential input. Creep compliance values can be measured in laboratory and used as inputs in thermal cracking model.

Based upon the quality and quantity of the available material properties data, there are three levels of input options in the MEPDG program (NCHRP 2004). When Level 1 inputs cannot be obtained, creep compliance values can be estimated from correlations with other properties of the AC mixes (NCHRP 2004).

In Level 1 input data, laboratory-measured creep compliance values at three temperatures (-20, -10, and 0°C) are required. Level 2 input data requires measured creep compliance values at only -10 °C, and for Level 3 input data no measured values are required. The creep compliance values are predicted at three temperatures (-20, -10, and 0°C) in Level 3 and two temperatures (-20 and

0°C) in Level 2. The measured and/or predicted creep compliance values are then used to predict thermal cracking. Hence, bias in prediction of creep compliance values in Level 2 and particularly in Level 3 would impact the thermal cracking prediction.

2.2.3.1 Creep Compliance Model

The MEPDG software implements a regression model to estimate creep compliance when measured values are not available. The MEPDG creep compliance prediction model is based on asphalt binder and volumetric properties of asphalt mix. The creep compliance model was developed based on 714 data points from 32 mixes (NCHRP 2006). The creep compliance predictive model is shown in Equation 2.12 (AASHTO 2015).

$$D(t) = D_1 t^m \quad (2.12)$$

Where, D_1 and m are regression coefficients and t is loading time in seconds. D_1 and m are obtained based on volumetric properties of the mix as follows (AASHTO 2015):

$$\log(D1) = -8.5241 + 0.01306T + 0.7957 \log(Va) + 2.0103 \log(VFA) - 1.923 \log(A) \quad (2.13)$$

$$m = 1.1628 - 0.00185\,T - 0.04596\,Va - 0.01126\,VFA + 0.00247\,Pen77 + 0.001683\,(Pen77)^{0.4605T} \quad (2.14)$$

Where, T = test temperature 0, -10, and -20, (°C), Va = air voids, (%), VFA = void filled with asphalt, (%), A = intercept of asphalt binder viscosity-temperature relationship, Pen77 = penetration at 77 °F.

2.2.3.2 Characterizing Asphalt Binder

When Level 3 input data are used, MEPDG requires a classification of the asphalt binder by either its penetration grade, viscosity grade, or its performance grade. As mentioned before, penetration

grade is an essential input for predicting creep compliance. If the binder is classified using its performance grade, the penetration grade can be estimated by using default values of viscosity-temperature regression parameters. The viscosity-temperature relationship was shown in Equation 2.5 (ASTM D2493M 2009). Based on A and VTS values, the penetration grade of asphalt binder can be estimated (NCHRP 2004). In Level 3 inputs, the default values of A and VTS parameters are used for the selected asphalt binder. Equation 2.15 shows the relationship between the penetration and viscosity.

$$\text{Pen}_{77} = 10^{\,290.5013 - \sqrt{81177.288 + 257.0694 * 10^{\,(A + 2.72973 * VTS)}}} \tag{2.15}$$

The slope of creep compliance master curve known as "m" parameter is used to compute the crack propagation (Equation 2.12). Zborowski and Kaloush (2011) recommended that the other creep compliance parameter "D_1" be included in the thermal cracking model.

Yin et al. (2009) reported that Level 3 creep compliance model tends to overpredict creep compliance values. As a result, the predicted thermal crack length from Level 3 creep compliance input data was noticeably underestimated compared to those of Level 1. Bias in estimation of thermal cracking can lead to less reliable predictions of the international roughness index (IRI), and subsequently the predicted service life, and life cycle cost estimates.

Local calibration is a process of minimizing the difference between predicted values and measured values by applying calibration factors to inputs or outputs, or by utilizing a different model form. The need for calibration is more critical when there are insufficient laboratory data to support the mechanistic-empirical models. There are various techniques for calibration of predictive models. Linear and nonlinear regression are very common calibration techniques among other calibration

methods. The regression models minimize the least squared residuals between predicted and measured values. Regression-based calibration is expected to improve the accuracy of predictions (Esfandiarpour and Shalaby 2016, Georgouli et al. 2015, You et al., 2012, Khattab et al., 2014). An alternative method is artificial neural network (ANN). The MEPDG software already implements ANN as a powerful soft computing technique (NCHRP 2004).

ANNs have been extensively used to predict the dynamic modulus and fatigue life of asphalt pavements (Ceylan et al. 2009, Singh et al. 2012). Zeghal (2008) reported that ANN method is a valuable and accurate alternative to predict creep compliance values. Jamrah and Kutay (2015) recently used an ANN model to calibrate creep compliance values based on nine mix parameters from job mix formula properties, and found the model to be a reliable method to predict creep compliance more accurately.

Therefore, there is a need to compare the reliability of predicted creep compliance values from globally calibrated MEPDG model with locally calibrated models.

2.3 Literature Summary and Research Need

As presented and discussed, previous studies considered the effect of different amounts of RAS and RAP in HMA based on the available sources to find a mix design that meets the local specifications and standards. Therefore, it is essential to conduct a research to evaluate the performance of RAS and RAP in HMA at high temperatures particularly in a cold region. In addition, previous studies reported inconsistency in some of asphalt mixes behaviours that contain RAS and/or RAP. Therefore, there is a need to perform laboratory tests to evaluate the impact of RAS and RAP in HMA for local materials and mixes.

When it comes to the use of MEPDG software, globally calibrated predictive models used in Pavement ME Design program were shown to have poor and inconsistent predictions. The calibration of these models based on local materials and mixes is critical. A considerable amount of research has been focused on using the MEPDG software to either implement or predict the typical asphalt mix performance, however, few studies has been conducted to calibrate the MEPDG inputs prediction models particularly for the local mixes containing reclaimed and/or recycled materials.

Based on the established issues, the investigation to evaluate the use of RAS and RAP in HMA and also to develop a database (from laboratory values) to calibrate the MEPDG inputs predictive models based on local materials and local mixes are relevant for this thesis.

CHAPTER 3 - MATERIALS AND EXPERIMENTAL PROGRAMS

3.1 Introduction

The research in this thesis required the determination of asphalt mix and asphalt binder properties of Manitoba RAS and/or RAP mixes. The low and high temperatures performances of HMA containing RAS and/or RAP were assessed based on laboratory tests. The MEPDG software (Pavement ME Design) was used to evaluate the long-term performance of mixes. Table 3.1 summarizes the RAS and/or RAP mix performance evaluation approaches.

Laboratory evaluation consisted of asphalt binder and asphalt mix tests. Different RAS and RAP mixes were prepared and tested to determine the low and high temperatures performances of the mixes. The required input data for MEPDG software was measured in the laboratory and introduced to Pavement ME Design program to estimate the long-term performance based on mechanistic-empirical models.

Table 3.1: Performance assessment of HMA containing RAS and/or RAP

Types of Evaluation	Measured Properties	Assessment
Laboratory test evaluation	• Creep compliance value • IDT strength • Dynamic modulus	➢ Low temperature performance ➢ High temperature performance
MEPDG software (Pavement ME Design Software)	• Rutting • AC top down cracking (Longitudinal cracking) • Thermal cracking • AC bottom up cracking (Alligator cracking)	➢ Long-term performance

3.2 Investigated Laboratory AC Mixes

3.2.1 Properties of RAS and RAP

The local aggregates, asphalt binder and local RAS and RAP in Manitoba were used to prepare the mixes. Asphalt mix design and asphalt binder properties of RAS and/or RAP mixes used in this thesis were assessed as well.

3.2.1.1 Asphalt Roofing Shingle Processing in Manitoba

Shingle recyclers in the City of Winnipeg are fairly new with only six years of operation. Shingle recyclers in the City of Winnipeg collect, shred, and process discarded asphalt roofing shingles for use in asphalt paving. Recyclers collect roofing shingles from various parts of the City and transfer them to a central recycling depot. The process of RAS includes removing non-debris materials such as nail, plastic and wood, then shredding, grinding and screening the processed shingles to

specified gradations suitable for HMA production.

For laboratory testing in this study, samples of processed asphalt roofing shingles were referred to be examined for asbestos content according to ASTM E2356 (EPA method 600/R). As described in ASTM E2356, the asbestos content of the asphalt shingle must be less than 1 percent. Table 3.2 shows the laboratory analysis report of the asphalt roofing shingles samples. The laboratory results showed the roofing shingles had 8-15% cellulous fibre and 85-92% non-fibrous material. Asbestos was not detected in the asphalt shingles samples.

RAS binder was extracted through asphalt binder tests. The RAS used in this study consisted of approximately 31.5% asphalt binder. The extracted RAS binder performance grade was PG 70-10.

Table 3.2: Laboratory analysis report of asphalt roofing shingles samples

LABORATORY ANALYSIS REPORT

Asbestos Identification by EPA Method[1] 600/R-93/116, EPA 600/M4-82-020

ACCOUNT #: 4201-13-275
CLIENT: Winnipeg Air Testing
ADDRESS: 121 Keedian Drive
East St. Paul, MB R2E 0K3
PROJECT NAME: Vq Manitoba
JOB LOCATION:
PROJECT NO.:
PO NO.:

DATE COLLECTED: 3/3/2013
DATE RECEIVED: 4/4/2013
DATE ANALYZED: 4/11/2013
DATE REPORTED: 4/11/2013

SampleType: BULK

Client Sample No.	SLI Sample/ Layer ID	Sample Identification/ Layer Name	PLM Analysis Results: Asbestos Fibers	PLM Analysis Results: Other Materials
A	31839185	Shingle Asphalt		
Layer 1:		Asphalt Shingle Black, Bituminous/Fibrous	None Detected	8% CELLULOSE FIBER 92% NON FIBROUS MATERIAL
B	31839186	Shingle Asphalt		
Layer 1:		Asphalt Shingle Black/Red, Bituminous/Fibrous/Granular	None Detected	15% CELLULOSE FIBER 85% NON FIBROUS MATERIAL
C	31839187	Shingle Asphalt		
Layer 1:		Asphalt Shingle Black/Red, Bituminous/Fibrous/Granular	None Detected	15% CELLULOSE FIBER 85% NON FIBROUS MATERIAL

3.2.1.2 Reclaimed Asphalt Pavement

Reclaimed asphalt pavement is an existing asphalt pavement, collected by milling or other operations, for use in a new HMA or base layer. RAP has been using in asphalt pavement for about 20 years in Manitoba. Generally, RAP properties can be varied from one location to another. Asphalt mixes in Manitoba typically consisted of 5% asphalt binder. The RAP used in this thesis contained approximately 4.5% asphalt binder. The extracted RAP asphalt binder performance grade was PG 64-28.

3.2.2 Mix Design and Volumetric Properties

In this thesis, eleven mixes (Mix 1 to Mix 11) containing various amounts of RAS and RAP as listed in Table 3.3, were considered for laboratory performance evaluation. More mixes (Mix12 to Mix 23) were prepared to be used in the evaluation of MEPDG predictive models (more detail of these mixes are presented in Chapter 5 and Chapter 6). Each mix ID consists of an identification number followed by percent of RAS and RAP in the mix, respectively. Table 3.3 also shows the amounts of RAS and RAP in each mix along with the type of mixes. Field mixes are referred to the mixes which were collected from field during paving process and then compacted in the laboratory. Figure 3.1 shows the field mix sampling. The University of Manitoba (U of M) laboratory trial mixes were designed, prepared, and compacted in the laboratory using the Superpave gyratory compactor.

Table 3.3: Amounts of RAS and RAP in investigated mixes

	Mix No.	Mix ID	RAS %	RAP %	Description	Type of Mix
Used for the laboratory evaluation (Chapter 4)	Mix 1	Mix-0-0	0	0	0% RAS + 0% RAP	Field mix
	Mix 2	Mix-0-10	0	10	0% RAS + 10% RAP	Field mix
	Mix 3	Mix-0-15	0	15	0% RAS + 15% RAP	Field mix
	Mix 4	Mix-0-20	0	20	0% RAS + 20% RAP	Field mix
	Mix 5	Mix-0-40	0	40	0% RAS + 40% RAP	Field mix
	Mix 6	Mix-0-50	0	50	0% RAS + 50% RAP	Field mix
	Mix 7	Mix-0-50-S	0	50	0% RAS + 50% RAP	Field mix
	Mix 8	Mix-0-10_2	0	10	0% RAS + 10% RAP	Field mix
	Mix 9	Mix-3-10	3	10	3% RAS + 10% RAP	Field mix
	Mix 10	Mix-3-10_lab	3	10	3% RAS + 10% RAP	U of M Lab mix
	Mix 11	Mix-5-10_lab	5	10	5% RAS + 10% RAP	U of M Lab mix
Used for developing local calibration of predictive models (Chapters 5 and 6)	Mix 12	Mix-0-0_2	0	0	0% RAS + 0% RAP	Field mix
	Mix 13	Mix-0-0_3	0	0	0% RAS + 0% RAP	Field mix
	Mix 14	Mix-0-0_4	0	0	0% RAS + 0% RAP	Field mix
	Mix 15	Mix-0-0_5	0	0	0% RAS + 0% RAP	Field mix
	Mix 16	Mix-0-0_6	0	0	0% RAS + 0% RAP	Field mix
	Mix 17	Mix-0-0_7	0	0	0% RAS + 0% RAP	Field mix
	Mix 18	Mix-0-0_8	0	10	0% RAS + 0% RAP	Field mix
	Mix 19	Mix-0-10_3	0	10	0% RAS + 10% RAP	Field mix
	Mix 20	Mix-0-10_4	0	10	0% RAS +10% RAP	Field mix
	Mix 21	Mix-0-10_5	0	10	0% RAS +10% RAP	Field mix
	Mix 22	Mix-0-10_6	0	10	0% RAS +10% RAP	Field mix
	Mix 23	Mix-0-15_2	0	15	0% RAS + 15% RAP	Field mix
	Mix 24	Mix-0-15_3	0	15	0% RAS + 15% RAP	Field mix

Figure 3.1: Collecting bulk field mixes during paving

Table 3.4 shows the virgin asphalt binder PG used in each mix as well as the source of materials used for production of the mixes. Two sources were used in producing the HMA mixes. Source 1 is referred to the projects of the province of Manitoba. Source 2 is referred to the City of Winnipeg projects. Mix 1 to Mix7 were prepared using materials from Source 1 whereas Mix 8 to Mix 11 were prepared using materials from Source 2. The University of Manitoba (U of M) trial mixes were prepared using materials from Source 2. Mix 1 to Mix 9 were compacted in the laboratory from bulk field mixes. Mix 10 and Mix 11 were designed and prepared at the University of Manitoba laboratory.

Table 3.4: The virgin asphalt binder and sources of investigated mixes

Mix No.	Mix ID	RAS %	RAP %	Virgin Asphalt Binder PG	Jurisdiction /Sources
Mix 1	Mix-0-0	0	0	58-28	Source 1
Mix 2	Mix-0-10	0	10	58-28	Source 1
Mix 3	Mix-0-15	0	15	58-28	Source 1
Mix 4	Mix-0-20	0	20	58-28	Source 1
Mix 5	Mix-0-40	0	40	58-28	Source 1
Mix 6	Mix-0-50	0	50	58-28	Source 1
Mix 7	Mix-0-50-S	0	50	58-34	Source 1
Mix 8	Mix-0-10_2	0	10	58-28	Source 2
Mix 9	Mix-3-10	3	10	58-28	Source 2
Mix 10	Mix-3-10_lab	3	10	58-28	Source 2
Mix 11	Mix-5-10_lab	5	10	58-28	Source 2

An asphalt binder with performance grade of PG 58-28 (equivalent to a 150/200 penetration grade) was used as a virgin asphalt binder for all mixes except Mix 7. A softer asphalt binder with performance grade of PG 58-34 (200/300 penetration) was used as a virgin binder for Mix 7 to evaluate the effect of soft binder on the high RAP content mix. Mix 2 and Mix 8 contained 10% RAP with different aggregate gradations and different RAP sources.

The aggregate gradation of Source 1 and Source 2 mixes were different from each other. This difference may impact some mix performances. The aggregate gradations of the mixes are shown in Table 3.5 and Figure 3.2.

Table 3.5: Aggregate gradation of the mixes

Mix ID	Aggregate Gradation								
	19 mm	16 mm	12.5 mm	9.5 mm	4.75 mm	2.0 mm	425 µm	180 µm	75 µm
Mix-0-0	100.0	98.6	90.4	80.2	64.4	50.1	25.8	10.0	4.5
Mix-0-10	100.0	99.4	91.8	83.3	65.5	51.2	26.6	9.0	4.7
Mix-0-15	100.0	98.5	91.8	80.2	61.2	48.1	28.0	8.0	3.7
Mix-0-20	100.0	97.9	91.9	84.1	64.5	48.7	27.2	9.3	5.2
Mix-0-40	100.0	99.2	92.3	82.2	63.7	50.0	29.1	7.7	4.5
Mix-0-50	100.0	98.8	94.2	83.3	66.3	50.7	27.7	9.6	6.7
Mix-0-50-S	100.0	98.6	93.6	84.4	68.5	52.1	28.1	10.3	7.1
Mix-0-10_2	100.0	100	91.1	81.8	64.0	51.8	20.1	8.8	4.9
Mix-3-10	100.0	100	92.4	82.9	66.1	53.2	20.4	7.7	4.8
Mix-3-10_lab	100.0	100	91.4	81.1	62.4	51.2	19.7	7.5	4.8
Mix-5-10_lab	100.0	99.8	92.8	83.7	65.8	56.8	19.8	7.1	4.3

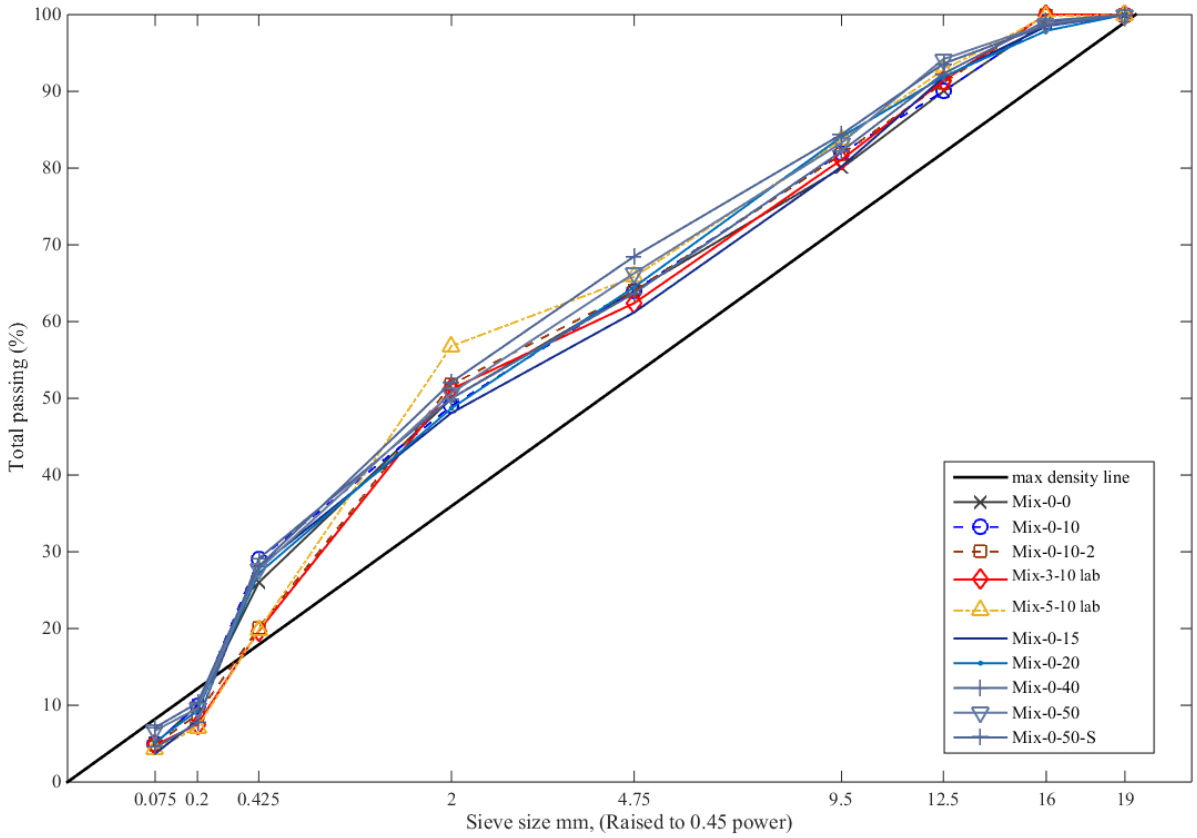

Figure 3.2: Aggregate gradation of mixes

The volumetric properties of mixes and extracted asphalt binder performance grades are presented in Table 3.6. The asphalt content of the mixes varies from 5.1% to 6% and the percent of air voids varied from 3.6 % to 4.3 %. The extracted asphalt binder grades of some of mixes were not available as indicated in Table 3.6. Manitoba Infrastructure (MI) provided the asphalt binder tests, including extraction and evaluating asphalt binder performance grade for the mixes.

Table 3.6: Volumetric properties of mixes and performance grade of extracted asphalt binder

Mix ID	Mix Properties					Extracted
	AC, %	VMA, %	Va, %	VFA, %	Gmm	Binder PG
Mix-0-0	6.0	15.2	4.2	72.7	2.445	58-28
Mix-0-10	5.9	14.7	3.7	75.0	2.436	58-28
Mix-0-15	5.9	13.7	3.8	72.3	2.437	58-28
Mix-0-20	5.3	13.5	3.9	71.3	2.499	N.A.
Mix-0-40	5.9	13.7	3.7	73.3	2.447	N.A.
Mix-0-50	5.2	12.2	3.6	70.6	2.516	64-16
Mix-0-50-S	5.1	12.0	3.6	69.8	2.526	64-22
Mix-0-10_2	5.2	14.2	4.3	70.2	2.496	58-28
Mix-3-10	5.3	14.5	4.1	70.9	2.498	64-28
Mix-3-10_lab	5.4	15.2	4.0	73.7	2.467	N.A.
Mix-5-10_lab	5.5	14.5	4.0	72.4	2.477	N.A.

AC=percent asphalt content; VMA= voids in mineral aggregates; V_a = percent air voids; VFA= voids filled with asphalt binder; G_{mm}= maximum theoretical spesific gravity;

All the specimens were compacted by mean of Superpave gyratory compactor. The number of gyrations was selected based on the traffic level and climate condition to simulate the actual field condition in accordance with AASHTO R 35-12. The number of design gyrations was selected to meet the required air voids (4%) in asphalt mix.

In order to prepare the laboratory specimens (Mix 10 and Mix 11), virgin aggregate was placed in the oven at 165°C overnight. RAS and RAP were heated at compaction temperature (135°C) for two hours before blending. The RAS and RAP were added to preheated virgin aggregate and then asphalt binder was introduced to the mix. The mix was blended at 150°C for 3 to 5 minutes until asphalt binder uniformly coated all aggregate particles. Then the loose mix was kept in the oven at compaction temperature for 4 hours for short term aging (AASHTO-R30 2015). Figure 3.3

shows the mixing temperature of samples for the dynamic modulus testing.

Figure 3.3: Mixing temperature of dynamic modulus samples

Finally, the loose mix was placed in the 150 mm (6 in.) mold for compaction using Superpave gyratory compactor. Then, all the specimens were sawed and/or cored to standard sizes. According to AASHTO T 322-07 and AASHTO T 342-11, at least 6 mm from both sides of each sample should be sawed to provide smooth and parallel surface and avoid the over compaction effect at each side. Figure 3.4 shows the gyratory compacted specimens.

a) Gyratory compacted creep samples

b) Sawed samples (creep compliance and IDT test)

c) Gyratory compacted dynamic samples

d) Cored and Sawed samples (dynamic modulus test)

Figure 3.4: Gyratory compacted specimens for laboratory tests

In order to prepare the bulk field mixes (Mix 1 to Mix 9) for laboratory compaction, the loose mix was re-heated at 60°C and then placed in an oven to reach the mixing temperature (150°C). The asphalt mixes were blended and then compacted using gyratory compactor. Next, all the samples were sawed and cored to conduct in asphalt mix tests.

3.3 Laboratory Test and Evaluation

Two main tests were conducted to evaluate the low and high temperatures performance of the mixes. Creep compliance test result was used to determine the potential of thermal cracking and dynamic modulus was measured to evaluate the rutting resistance of the mixes.

3.3.1 Creep Compliance Test

Creep compliance test is an essential test for Level 1 material properties input which is used for MEPDG thermal cracking prediction model. Creep compliance test is a non-destructive test which was applied on the asphalt mixes to evaluate their low temperature resistance. The creep compliance is time-dependent strain over applied stress under constant static load. The load must be applied to create horizontal deformation of 0.00125 mm to 0.0190 mm. Creep compliance tested used according to AASHTO T 322-07 (2011) "*Determining the Creep Compliance and Strength of Hot Mix Asphalt (HMA) Using the Indirect Tensile Test Device"*. The test temperature which is a function of the binder performance grade was selected as -20 °C, -10°C, and 0°C in accordance with AASHTO T 322-07 (2011). The average sample diameter is 150 mm (6 in.) and the average thickness is 40 to 60 mm.

3.3.2 Indirect Tensile (IDT) Strength Test

The indirect tensile strength test is an important indicator to characterize the HMA low temperature resistance. The test is destructive and operated at low temperature. The load with a specific rate was applied on the samples until failure. The IDT temperature is a function of binder performance grade. According to AASHTO 322-07 (2011) "*Determining the Creep Compliance and Strength*

of Hot Mix Asphalt (HMA) Using the Indirect Tensile Test Device", the IDT temperature for mix made using PG xx-28 binder is -10 °C which is the middle creep compliance test temperature.

3.3.3 Dynamic Modulus Test

The dynamic modulus defines the relationship between stress and strain under continuous sinusoidal loading. The dynamic modulus test output is stiffness of the mix which can be used to evaluate whether the mix is susceptible to performance issues including rutting and fatigue cracking. The dynamic modulus is a complex number. The absolute value of the complex modulus (|E*|) is defined as dynamic modulus. Phase angle is the angle (in degree) between stress peak and resulting strain peak under sinusoidal load. For a pure elastic material phase angle is zero ($\delta = 0$) and the complex modulus is equal to the absolute value (dynamic modulus) and for a pure viscous material phase angle is equal to 90 ($\delta = 90$). Figure 3.5 shows the typical sinusoidal stress and strain for an asphalt mix.

This test is usually applied at five temperatures and six different frequencies (start from lowest temperature and highest frequency) to consider all range of traffic speeds and temperatures which an asphalt pavement might experience. The dynamic modulus test was applied on the specimens (150 mm height and 100 mm diameter) at five temperatures (-10°C, 5°C, 25°C, 40°C, and 54°C) and six frequencies (25 Hz., 10 Hz., 5 Hz., 1 Hz., 0.5 Hz., and 0.1 Hz.) according to AASHTO T 342-11 "*Determining Dynamic Modulus of Hot Mix Asphalt (HMA)"*. Figure 3.6 shows the dynamic modulus sample testing.

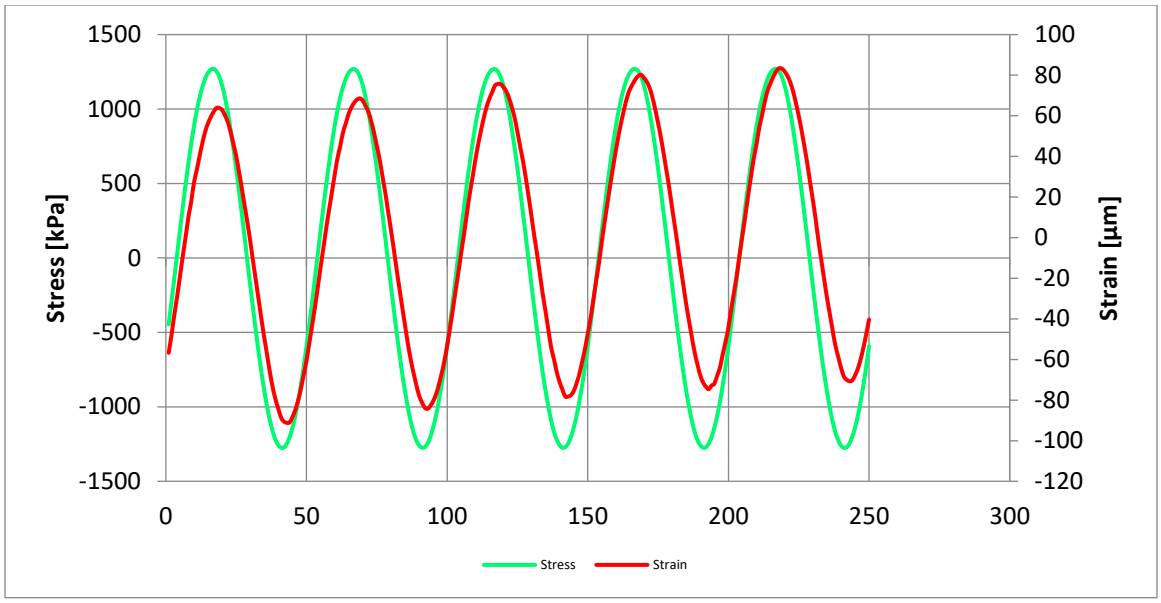

Figure 3.5: Stress and strain in dynamic modulus loading

Figure 3.6: Dynamic modulus sample testing

3.3.4 Asphalt Binder Tests

Asphalt cement is mostly obtained from crude petroleum through different refinery processes. Asphalt binder performance is basically a function of temperature and time of loading. By characterization of asphalt binder, the influence of temperature and stress on engineering properties of asphalt binder can be determined. The asphalt binder characterization assists to achieve better mix design and enhanced mix performance. Two binder tests, dynamic shear rhometer (DSR) and bending beam rhometer (BBR) are used to determine the performance grade (PG) of asphalt binder.

The DSR was conducted to obtain the complex shear modulus (G*) and phase angle (δ) of the asphalt binders. The complex shear modulus (G*) represents the resistance of asphalt binder to deformation under load. Phase angle (δ) is in radians and it is defined as the lag between sinusoidal stress and the resultant sinusoidal strain. DSR is used to determine the performance grade of the binders at medium and high temperatures. G* and δ are two main asphalt binder inputs in Pavement ME Design program. The binder tests were performed by MIT technician at University of Manitoba.

Usually, an aged binder obtained from RAS or RAP is more brittle at low temperature due to high level of oxidation and aging. The BBR test examines the low temperature creep stiffness and relaxation properties of an asphalt binder and provides the low critical temperature of the binder within which a binder can perform.

3.4 Long-Term Performance and Evaluation of the Mixes Using MEPDG Software

Pavement ME Design software is a tool to analyze and design the flexible and rigid pavements. This software is able to predict the long-term performance of the pavement based on different distress prediction models. The Pavement ME Design software can predict and compare the performance of the mixes for different Levels of inputs. This software can assist to determine the long-term performance of RAP mixes.

Different input data such as traffic and climate data are required to introduce to the software. The software is able to design and analyze the pavement structure based on targeted threshold. The design life of the asphalt pavement is usually selected to be 20 years. Winnipeg was selected as the climate condition for analyzing of asphalt pavement structures in this thesis. In the analysis for this thesis, the traffic loads, weather conditions, and structures were kept the same for all mixes. More details of input data will be presented in Chapter 7.

CHAPTER 4 - MECHANICAL TESTS FOR CHARACTERIZATION OF ASPHALT MIXES CONTAINING RAS AND RAP

4.1 Introduction

Laboratory tests were conducted on asphalt specimens to evaluate their low and high temperatures performances. Low temperature performance of the mixes were examined through creep compliance and IDT strength tests. As part of laboratory characterization, high temperature performance of mixes were evaluated by conducting the dynamic modulus test. The high temperature performance of the HMA is an impartial indicator for rutting resistance of the mixes. Rutting in HMA can have a major impact on road safety since ruts filled with water can cause hydroplaning of a vehicle. The following sections discuss the results of low and high temperatures performances of the AC mixes.

4.2 Evaluation of High Temperature Performance of AC Mixes Using Dynamics Modulus Test

The dynamic modulus (E*) test was carried out to simulate various traffic loads at different temperatures during the pavement life. A high dynamic modulus implies higher stiffness, or lower strains, under traffic loading.

An asphalt binder becomes soft at high temperature and stiff at low temperature. It should be noted that high stiffness is not always in favour of HMA performance. Although the high stiffness of AC is desirable at high temperature to avoid rutting, high stiffness adversely impacts the thermal resistance of HMA at low temperature. Therefore, it is critical to measure the dynamic modulus to determine the stiffness of the mixes at low and high temperatures.

In order to compare the dynamic modulus over a range of temperatures and loading frequencies, master curve was constructed for each mix. The dynamic modulus master curve provides the stiffness of the mix across a wide range of temperatures and loading frequencies. The reference temperature was selected as 25 °C according to AASHTO PP 62-10 "Developing dynamic modulus master curves for hot mix asphalt (HMA)" (AASHTO 2010). The form of dynamic modulus master curve usually is a sigmoid function. Equation 4.1 shows the general form of dynamic modulus master curve.

$$\log|E*| = \delta + \frac{(\alpha)}{1+ e^{\beta + \gamma \log fr}} \quad (4.1)$$

Where, $\delta, \alpha, \beta, \gamma$ are the fitting parameters and f_r is reduced frequency (Hz.).

Time-temperature shift factors are usually used to compute the reduced frequency. There are few Equations to calculate the shift factors. In this study the second-order polynomial or experimental approach was used to calculate the reduced frequency as it is recommended by AASHTO PP 62-10 (AASHTO 2010).

$$\log fr = \log f + a_1(T_R - T) + a_2(T_R - T)^2 \quad (4.2)$$

Where, fr= reduced frequency at the reference temperature; f= loading frequency at the test temperature; a_1 , a_2= fitting coefficients; T_R= reference temperature, °F; and T= the test temperature, °F.

The second-order polynomial is fitting function without assuming any shift function equation to relate the time and temperature (Pellinen et al. 2004). In this method, fitting parameters are calculated simultaneously by using non-linear least squares fitting.

The right side of a master curve presents the low temperature stiffness which impacts the thermal resistance of the mix. A low dynamic modulus at low temperature is desirable indicating that the AC mix is less brittle at low temperature.

Alternatively, the left side of the master curve corresponds to the low frequencies or high temperature stiffness. At high temperatures, AC mix is prone to rutting distress because an asphalt binder becomes soft at high temperature. High dynamic modulus at high temperature is desirable since it implies that the AC mix is stiff. It is expected that a mix with high dynamic modulus will have better rutting resistance at high temperatures. The intermediate temperature of the master curve reflects the fatigue resistance of the mix. Too stiff or too soft mix can result in lower fatigue

resistance of the mix (NCHRP-673 2011).

The dynamic modulus test was carried out on all specimens (bulk field mix and U of M laboratory mix design specimens). Raw data from the test was analyzed according to AASHTO T342-11 "Determining dynamic modulus of hot mix asphalt" (AASHTO-T342 20011). Table 4.1 shows the average values of dynamic modulus for investigated mixes at different temperatures and frequencies.

E* of different mixes were compared to E* of Mix-0-0 (virgin mix) with no RAS and RAP as the control mix in this chapter. E* values of Mix-0-0 at 40 °C were lower than other field mixes except Mix-0-10-2 with different source of materials. Comparing the E* of Mix-0-0 with Mix-0-10_2 from Table 4.1, revealed that the E* of the Mix-0-0 is higher than Mix-0-10_2 at 25 °C and 40 °C. Higher E* at 40 °C implies higher rutting resistance.

It is expected that as the RAP and/or RAS content increases in a mix the dynamic modulus of the mix increases too. However, it was noted that increase in RAP does not result in increase the dynamic modulus for all the mixes. The possible reasons of inconsistency in dynamic modulus values could be due to different aggregate gradations and asphalt content of asphalt mixes.

Table 4.1: Dynamic Modulus Value for Mixes at Different Temperatures and Frequencies.

	Mix	Dynamic Modulus (E*), MPa						
		Temp. (°C)	0.1 Hz	0.5 Hz	1 Hz	5 Hz	10 Hz	25 Hz
Bulk field mixes laboratory compacted	**Mix-0-0**	-10	19285	23299	24807	28174	29857	32265
		5	7609	10899	12424	16222	17990	20267
		25	1922	3149	3940	6232	7438	9457
		40	400	647	829	1550	1957	3016
	Mix-0-10	-10	19869	24431	26298	30547	32435	34146
		5	7307	10516	12026	15945	17577	19822
		25	2006	3364	4241	6841	8240	10294
		40	565	834	1017	1745	2221	3027
	Mix-0-15	-10	18565	22234	23707	26883	28287	29813
		5	7540	10553	12026	15547	17131	19314
		25	2530	4052	4944	7485	8937	10695
		40	638	981	1201	2028	2547	3479
	Mix-0-20	-10	21038	26095	28334	32537	34907	37792
		5	8297	12064	13739	18368	20673	23985
		25	2061	3587	4550	7586	9252	11298
		40	583	882	1096	1937	2457	3580
	Mix-0-40	-10	24154	28058	30251	32984	34520	35687
		5	10269	13876	15543	19462	21217	22947
		25	2403	3890	4789	7390	8804	10973
		40	633	967	1199	2095	2661	3606
	Mix-0-50	-10	29227	33806	35585	39420	41210	42866
		5	10170	13858	15395	19680	21283	23827
		25	2486	4026	4875	7688	9085	10954
		40	786	1223	1512	2599	3298	4308
	Mix-0-50-S	-10	28065	32922	34487	38374	39462	41097
		5	12519	16678	18506	22771	24830	26763
		25	2293	3735	4597	7292	8562	10805
		40	716	1076	1320	2228	2917	3847
	Mix-0-10_2	-10	21138	26062	28110	32752	34624	37015
		5	6948	10083	11690	15891	17860	20469
		25	1150	1978	2524	4290	5383	7259
		40	346	535	666	1182	1654	2320
	Mix-3-10	-10	19706	23697	25374	29149	30517	32191
		5	8446	11736	13306	17117	18966	21342
		25	1803	2933	3604	5538	6593	8128
		40	504	819	1051	1787	2399	3152
U of M lab mix design	**Mix-3-10_lab**	-10	16676	20177	21632	24976	26412	27492
		5	6221	8178	9347	12311	13742	15418
		25	1044	1714	2121	3442	4230	5291
		40	293	448	548	956	1320	1911
	Mix-5-10_lab	-10	16638	20401	22230	26054	26742	28032
		5	5524	7789	8913	11835	13323	15311
		25	1149	1824	2230	3509	4244	5101
		40	416	641	786	1315	1764	2333

The master curves of the field mixes are shown in Figure 4.1. In general, RAS and RAP increased the HMA stiffness particularly at medium and high temperatures. Mixes from Source 2 showed lower dynamic modulus values in comparison with Source 1 mixes.

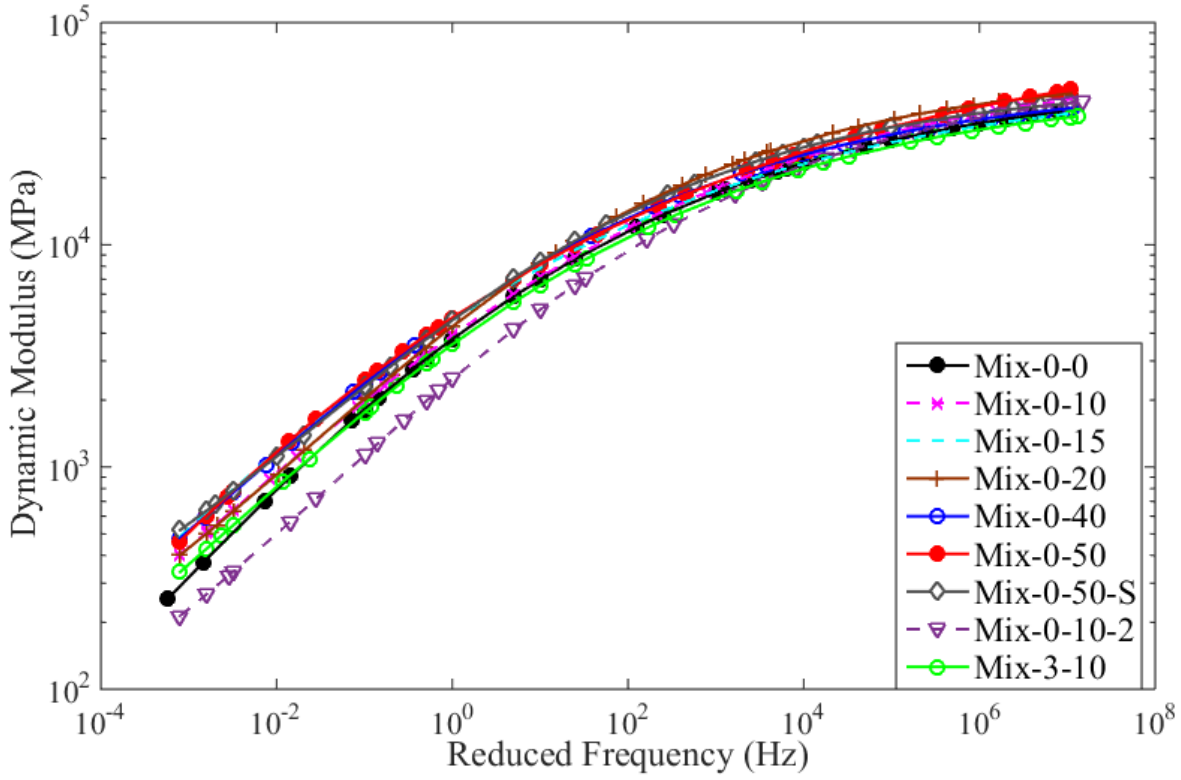

Figure 4.1: Dynamic modulus (E*) master curve of the field mixes

Source 1 mixes and Source 2 mixes were separated to have a detail assessment of the impact of recycled and/or reclaimed materials on mixes. Figure 4.2 shows the E* master curves for mixes from Source 1. The dynamic modulus of the mixes increased when the amounts of RAP increased in the mixes.

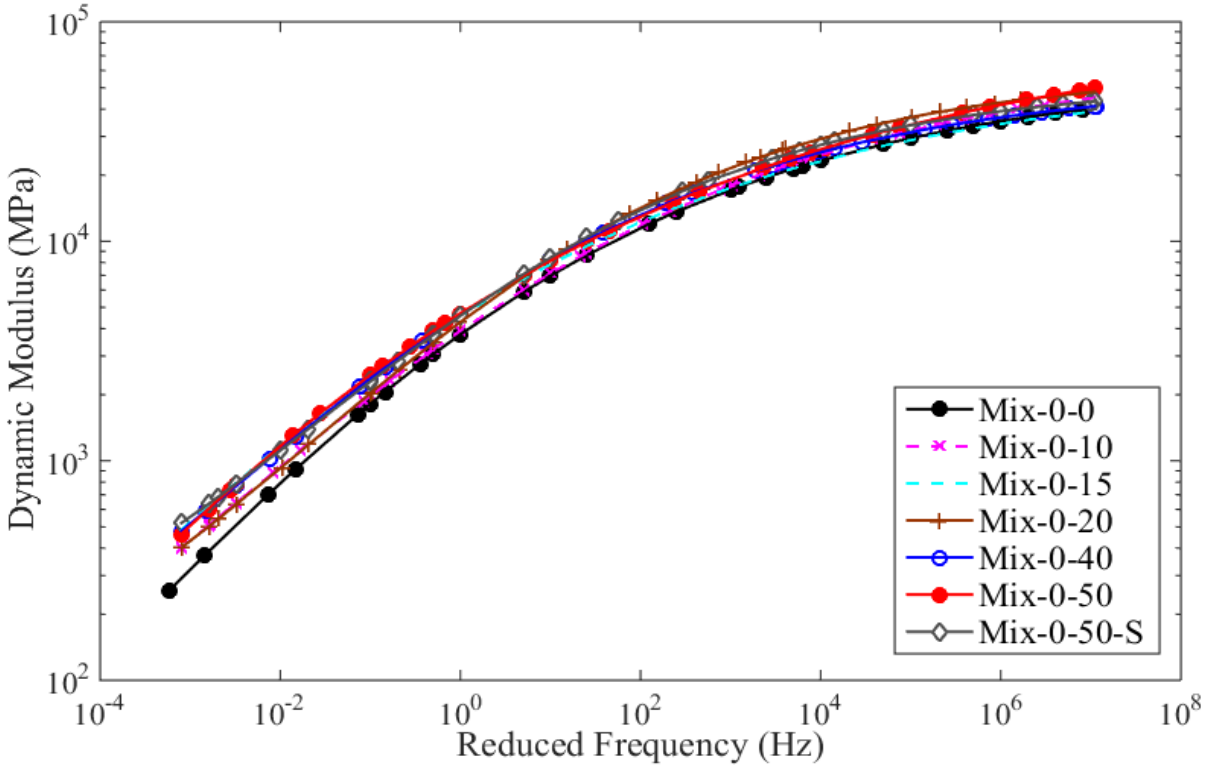

Figure 4.2: Dynamic modulus (E*) master curve of mixes from Source 1

Mix-0-10, Mix-0-15, and Mix-0-20 showed similar dynamic modulus at high temperature (left side of the master curves). However, Mix-0-20 showed higher values at intermediate and low temperatures. Mix-0-40, Mix-0-50, and Mix-0-50-S showed similar dynamic modulus master curve. The dynamic modulus of these mixes were higher than Mix-0-0 in all temperature ranges. It was noted that use of 15% RAP increases the rutting resistance of HMA without noticeable change in dynamic modulus at intermediate and low temperatures.

Figure 4.3 compares the dynamic modulus master curves of Mix-0-10_2 and Mix-3-10 from Source 2 and Mix-0-0 from Source 1. Mix-0-10_2 showed lower dynamic modulus values at high and intermediate temperatures when it was compared to master curve of virgin Mix-0-0. The

master curve of Mix-3-10 was comparable with Mix-0-0. It was noted that the use of 3% RAS resulted in an increase in dynamic modulus values when it was compared with Mix-0-10_2 with no RAS. Presence of aged RAS binder in a mix showed increase in stiffness of the asphalt mixes. The difference among dynamic modulus values of these mixes were more noticeable at high temperature than that of low temperature.

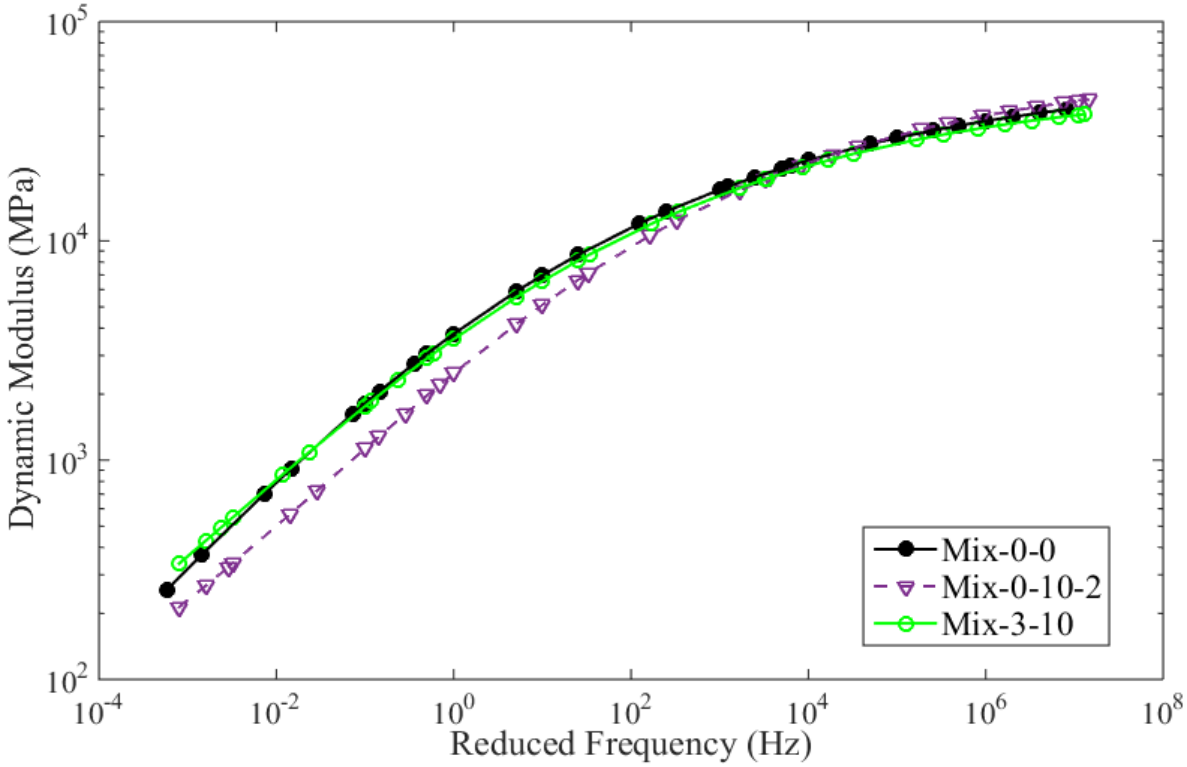

Figure 4.3: Dynamic modulus (E*) master curve of mixes from Source 2

Figure 4.4 compares the dynamic modulus master curve of U of M laboratory mixes (Mix-3-10-Lab and Mix-5-10-Lab) and Mix-0-0. It was found that the U of M laboratory design mixes have much lower dynamic modulus values when they were compared to Mix-0-0 (compacted bulk field mix laboratory). In addition, the dynamic modulus master curves of Mix-3-10-Lab and Mix-5-

10_lab were found to be very similar. This could occur due to inconsistency in RAS binder contribution to the AC mix.

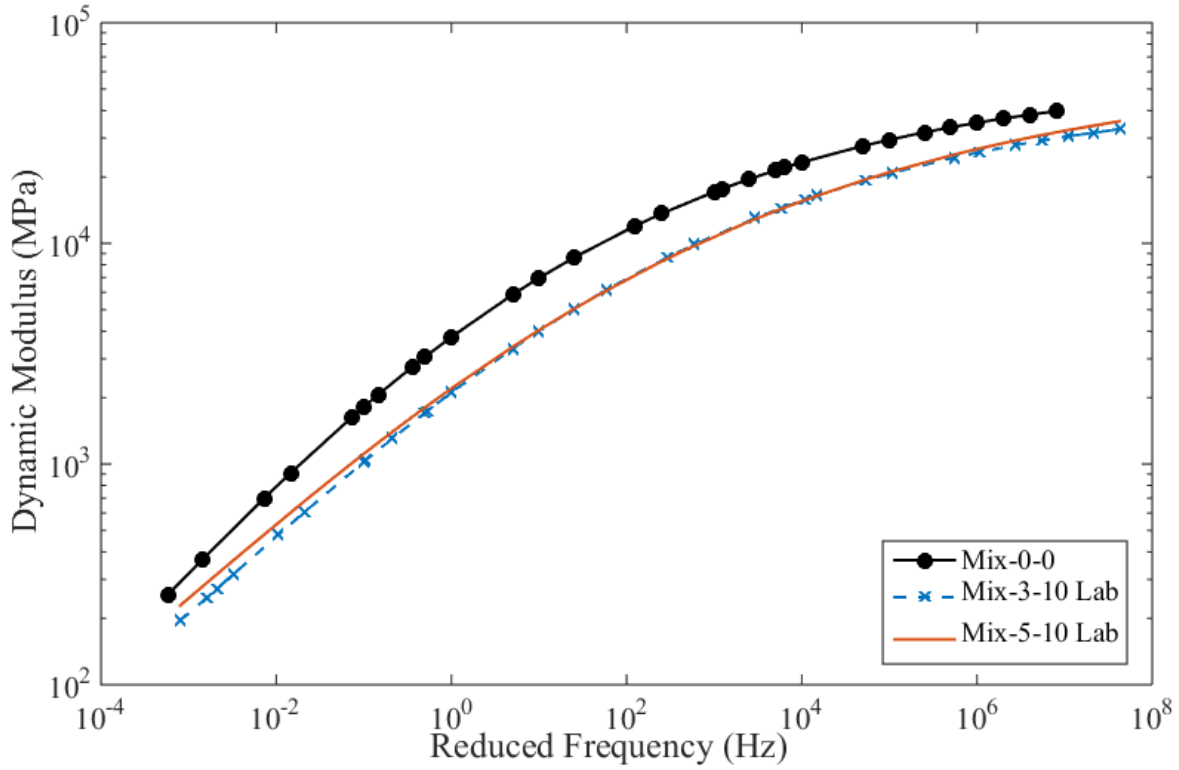

Figure 4.4: Dynamic modulus master curves of laboratory mix specimens and Mix-0-0

The difference in dynamic modulus master curves between the laboratory mix design specimens (Mix-3-10-Lab and Mix-5-10-Lab) and bulk field mix laboratory compacted specimens could be due to different level of age hardening of asphalt binder in the mixes, variation in asphalt binder content, type and equipment options (for preparing the mix), and moisture content (NCHRP SYNTHESIS-495 2016). In the field mixes, asphalt binder and aggregate particles are mixed in the drum and then stored in a silo prior to transport and placement which cause substantial amounts of age hardening in the field mix (NCHRP-673 2011). Therefore, it is expected that the field mix

specimens show higher stiffness compared to laboratory asphalt mix specimens.

4.2.1 Comparison of E* Master Curve of Laboratory Mix Specimens

In order to evaluate the performance of the laboratory mix specimens, the E* master curves of these two mixes were compared with two laboratory mixes from Ontario and Minnesota. These two mixes were chosen because of weather and climate similarity.

The Minnesota mix contained 5% RAS, and 5% asphalt content. An asphalt binder with PG 58-22 was used as a virgin binder for this mix. The Ontario mix contained 6% RAS, and 4.9% asphalt content. An asphalt binder with PG 52-34 was used as a virgin binder for this mix.

The comparison of dynamic modulus mater curves of the mixes are shown in Figure 4.5. The University of Manitoba laboratory mix showed lower stiffness at high temperature although the mix contained higher amounts of recycled materials (10% RAP and 5% RAS) compared to Minnesota mix (5% RAS) and Ontario mix (6% RAS). This implies that the University of Manitoba mix has lower rutting resistance compared to other mixes with similar RAS content. Possible reasons for this difference are differences in aggregate gradation, type or texture of aggregates used in these mixes, and asphalt binder content. Aggregate types, angularity and shape of aggregates significantly impact the dynamic modulus and rutting resistance of the mix. Increase in the angularity of the aggregate particles can be achieved by increasing the percentage of crushed aggregates used in the asphalt mix (Singh et al. 2013).

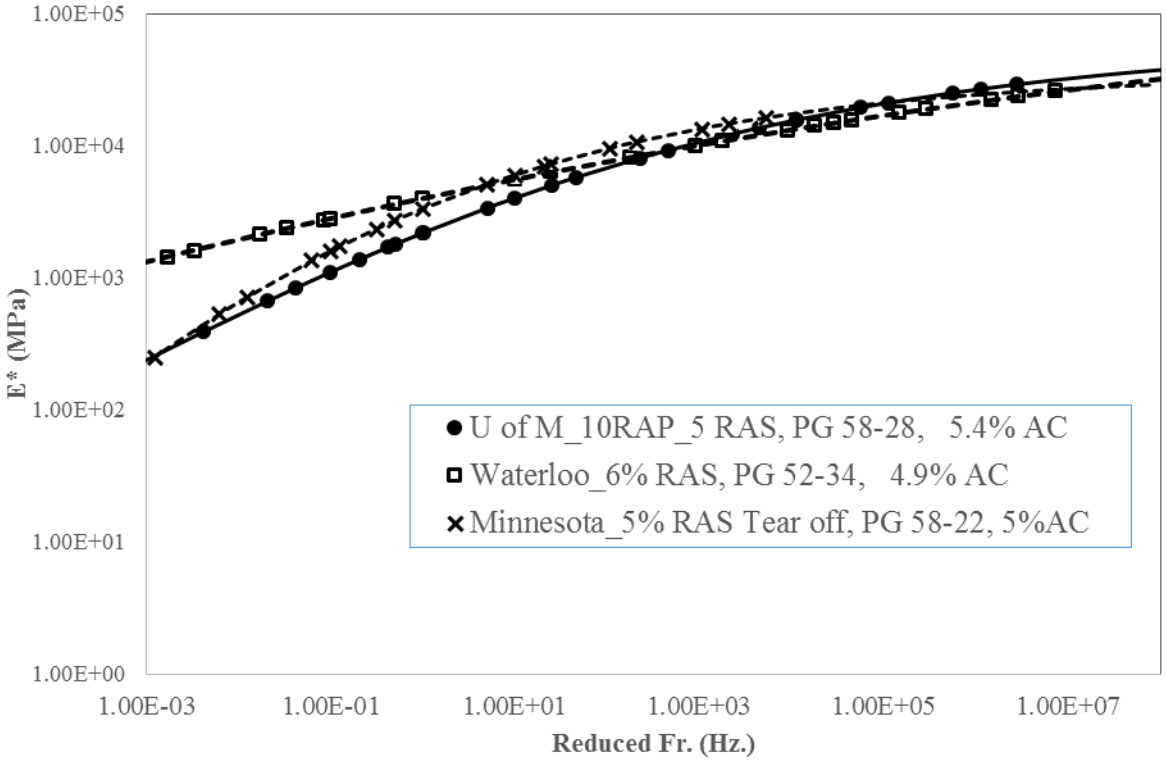

Figure 4.5: Comparison of Manitoba laboratory mix with Ontario and Minnesota laboratory mixes

4.3 Evaluation of Low Temperature Performance of AC Mixes Using Creep Compliance and IDT Strength Tests

Thermal cracking is one of the principal asphalt pavement distresses that typically appears early in the service life. Low temperature cracking occurs due to shrinkage of asphalt and is more common in cold regions.

The asphalt concrete is sensitive to temperature and time of loading. At low temperature, asphalt binder has the dominant impact on the AC performance (Goodrich 1991). Asphalt binder becomes hard and stiff at low temperature. A very stiff asphalt binder causes the mix brittle and vulnerable

to thermal cracking.

In Chapter 2, it was shown that aged RAS and RAP binder in a mix tends to increase the AC stiffness. Therefore, it is necessary to evaluate the stiffness of asphalt mixes at low temperature particularly for mixes containing RAS and RAP. To evaluate the low temperature performance of mixes two tests namely creep compliance and indirect tensile (IDT) strength tests were carried out. The creep compliance test data is a great indicator of low temperature performance. Moreover, the creep compliance is an essential input data in MEPDG software. The creep compliance values and IDT are used in thermal cracking model to predict the amount thermal cracking distresses in asphalt pavement. The tests were applied on the laboratory compacted specimens. Creep compliance was tested at three low temperatures; -20°C, -10°C, and 0°C whereas IDT strength was tested at -10°C. The results of creep compliance test for mixes are shown in Table 4.2.

In order to compare the overall creep compliance performance, the creep compliance master curve should be constructed. The creep compliance master curve is constructed at a reference temperature by shifting creep compliance values from different temperatures. This implies that the creep compliance at each temperature is shifted to align the master curve at reference temperature. The reduced temperature can be calculated by using time-temperature shift factor as follows:

$$T_r = \frac{T}{a\,(T)} \tag{4.3}$$

Where, $a(T)$ = shift factor and T_r = reduced temperature and T = the test temperature, (°C).

There are various shifting techniques. In this study, Williams, Landel and Ferry (WLF) method was used to construct the creep compliance master curve of the mixes (Pellinen *et*. al 2004).

Equation 4.4 shows the WLF shift factor equation. The middle temperature -10 °C is used as the reference temperature.

$$\log a(T) = \frac{-C_1(T-T_{ref})}{C_2+T-T_{ref}} \quad (4.4)$$

Where, $a(T)$ = shift factor, T_{ref} = reference temperature, (°C), T= test temperature, (°C), C_1, C_2 = constants parameters.

The general form of creep compliance master curve usually is an exponential sigmoid function, which was shown in Equation 2.12. A nonlinear regression was performed to fit the measured creep compliance data to general power law creep compliance master curve. Since there were three orders of magnitudes between creep compliance at 0°C and 20°C, the sum of squared error between log of measured creep compliance data and log of fitted data was minimized.

Table 4.2: Creep compliance test results of the mixes

Mix ID	Loading Time	Creep Compliance, 1/Gpa		
		Low Temp. (-20 °C)	Mid Temp. (-10 °C)	High Temp. (0 °C)
Mix-0-0	1	0.051	0.081	0.171
	2	0.054	0.085	0.190
	5	0.058	0.093	0.229
	10	0.063	0.102	0.272
	20	0.069	0.113	0.331
	50	0.081	0.135	0.453
	100	0.093	0.159	0.590
Mix-0-10	1	0.054	0.081	0.125
	2	0.056	0.086	0.136
	5	0.060	0.096	0.157
	10	0.065	0.106	0.181
	20	0.070	0.119	0.215
	50	0.079	0.143	0.284
	100	0.089	0.169	0.361
Mix-0-15	1	0.046	0.085	0.139
	2	0.048	0.090	0.152
	5	0.052	0.100	0.177
	10	0.055	0.110	0.205
	20	0.060	0.124	0.245
	50	0.069	0.150	0.323
	100	0.077	0.178	0.410
Mix-0-20	1	0.046	0.078	0.138
	2	0.048	0.084	0.154
	5	0.051	0.095	0.186
	10	0.054	0.107	0.224
	20	0.060	0.123	0.278
	50	0.068	0.157	0.392
	100	0.075	0.196	0.525
Mix-0-40	1	0.043	0.061	0.089
	2	0.046	0.064	0.097
	5	0.049	0.070	0.112
	10	0.051	0.075	0.130
	20	0.056	0.084	0.154
	50	0.063	0.099	0.203
	100	0.072	0.115	0.261
Mix-0-50	1	0.039	0.057	0.126
	2	0.040	0.060	0.145
	5	0.042	0.066	0.177
	10	0.044	0.074	0.224
	20	0.045	0.083	0.301
	50	0.049	0.106	0.450
	100	0.055	0.133	0.642
Mix-0-50_S	1	0.042	0.060	0.112
	2	0.043	0.063	0.128
	5	0.045	0.070	0.162
	10	0.048	0.078	0.200
	20	0.050	0.089	0.262
	50	0.054	0.109	0.387
	100	0.058	0.132	0.526

Mix-0-10_2	1	0.054	0.067	0.128
	2	0.056	0.072	0.139
	5	0.061	0.082	0.162
	10	0.066	0.094	0.188
	20	0.072	0.110	0.224
	50	0.084	0.148	0.298
	100	0.097	0.203	0.385
Mix-3-10	1	0.039	0.060	0.115
	2	0.040	0.063	0.125
	5	0.043	0.070	0.149
	10	0.046	0.078	0.174
	20	0.049	0.088	0.211
	50	0.057	0.110	0.284
	100	0.065	0.135	0.368
Mix-3-10_lab	1	0.041	0.063	0.120
	2	0.042	0.067	0.129
	5	0.045	0.073	0.152
	10	0.048	0.081	0.176
	20	0.052	0.092	0.212
	50	0.061	0.114	0.286
	100	0.069	0.140	0.373
Mix-5-10_lab	1	0.031	0.051	0.111
	2	0.033	0.055	0.121
	5	0.036	0.062	0.141
	10	0.039	0.071	0.164
	20	0.043	0.083	0.197
	50	0.051	0.109	0.266
	100	0.061	0.144	0.349

The regression coefficients (m and D_1) were determined and the creep compliance master curve was constructed at reference temperature of -10°C.

Figure 4.6 shows the creep compliance master curve of bulk field mixes (Mix 1 to Mix 9). A low creep compliance indicates a high stiffness. Therefore, it is desirable for an AC mix to have high creep compliance. The left side of the graph corresponds to low temperatures (-20°C and lower), while the right side of the graph corresponds to the high temperatures (0°C and higher).

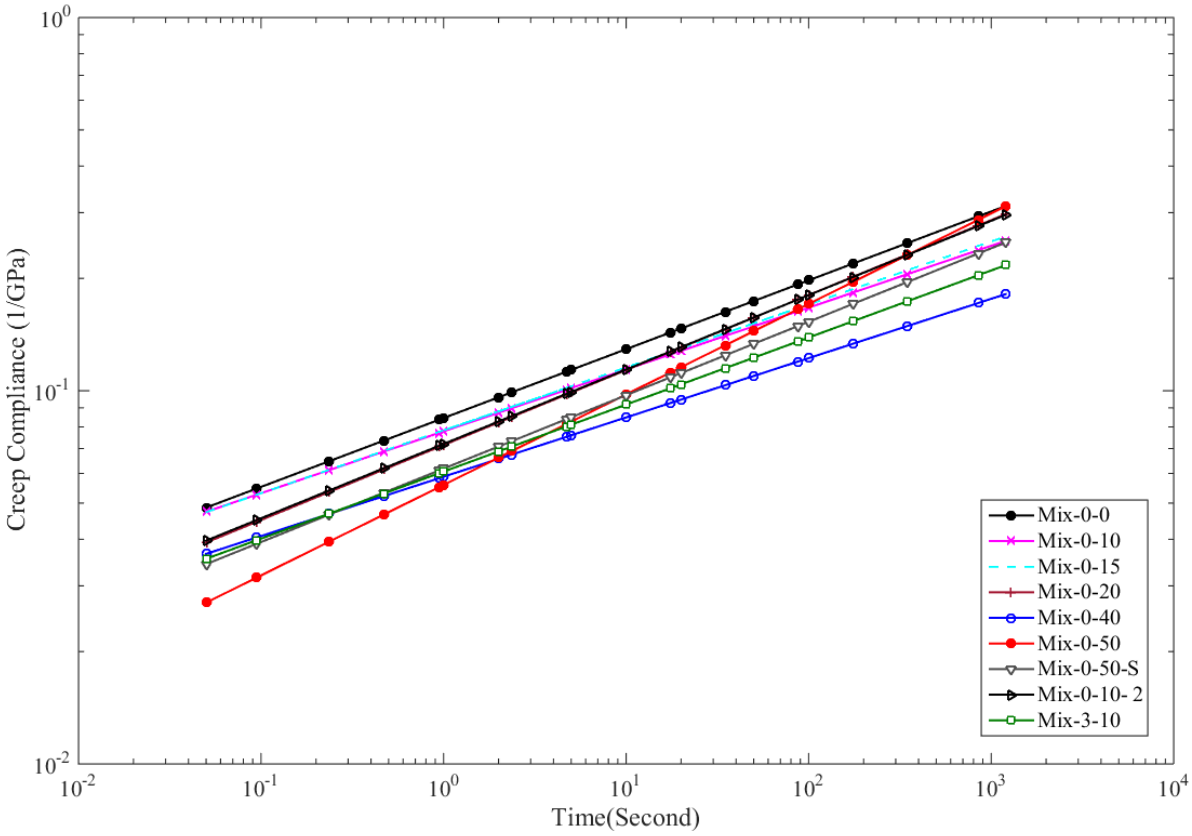

Figure 4.6: Creep compliance master curves for bulk field mixes (laboratory compacted)

Generally, as the amounts of RAS and RAP increased in the mixes the creep compliance values decreased. Master curve of Mix-0-10_2 from Source 2 was comparable with Mix-0-20 from Source 1. Master curve of Mix-3-10 was close to master curve of Mix-0-40 at very low temperature. It was noted that use of 3% RAS reduced the creep compliance values of Mix-3-10 when it was compared with Mix-0-10_2. The creep compliance values of Mix-3-10, Mix-0-40, and Mix-0-50-S were very similar at low temperature. However, these mixes showed different performance at high temperature. Mix-0-50 and Mix-5-10_lab showed substantially low creep compliance as compared to other mixes which indicates there are high chance of excessive thermal cracking.

Source 1 mixes and Source 2 mixes were separated to have a detailed evaluation of the effect of recycled and reclaimed materials on low temperature performance of mixes. Figure 4.7 shows the creep compliance results for mixes from Source 1. The creep compliance of the mixes decreased when the amounts of RAP increased in the mixes.

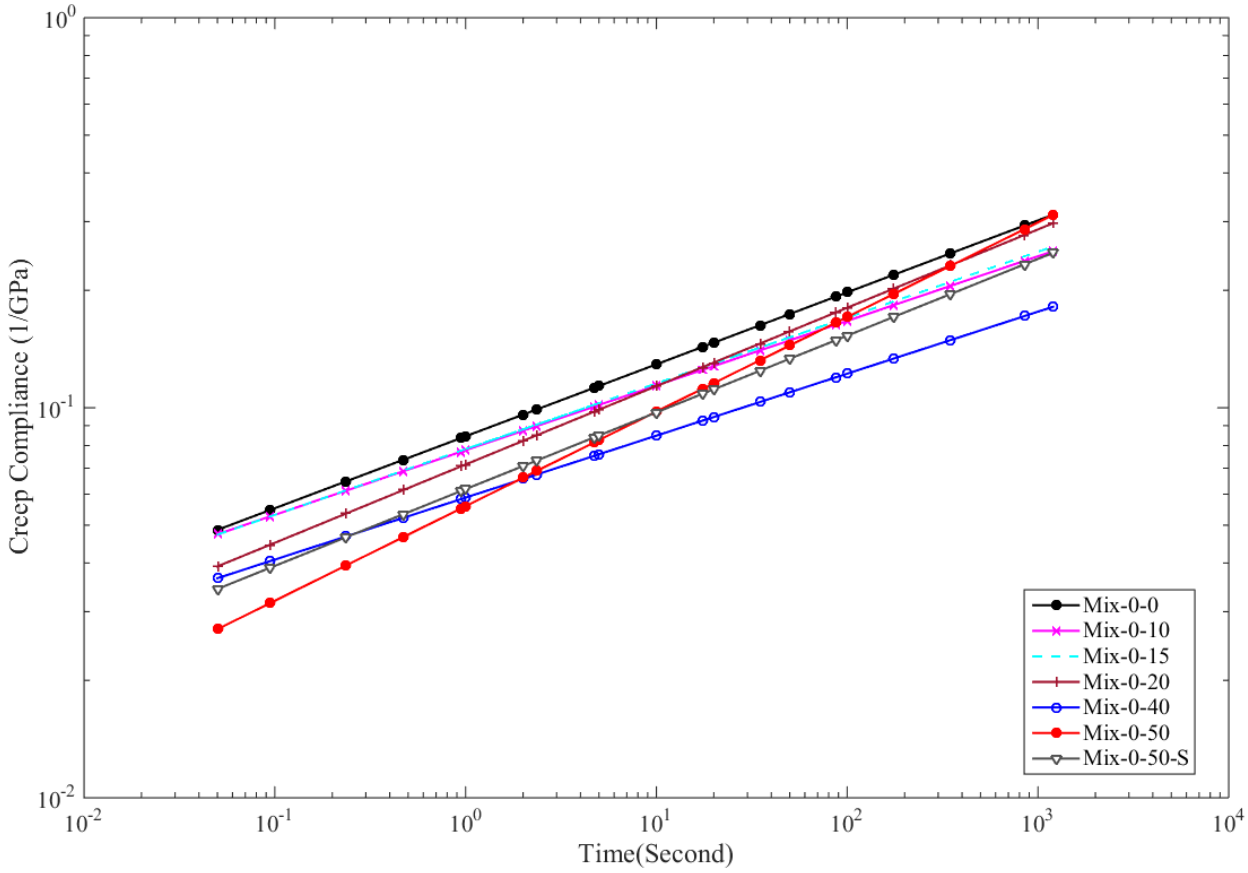

Figure 4.7: Creep compliance master curve of mixes from Source 1

Mixes containing 0%, 10%, and 15% RAP showed the same creep compliance at very low temperature (left side of the master curve). However, mix-0-0 showed slightly higher creep compliance values in comparison with mix-0-10 and mix-0-15 at high temperature (right side of the master curve). This implies that use of RAP up to 15% did not impact the low temperature performance of AC mix. This finding is in agreement with NCHRP 495 where it is recommended

to use 15% RAP with no change in the typical virgin asphalt binder grade (NCHRP-495 2016). The creep compliance at low temperature began to decrease when 20% RAP was used in the mix.

Mix-0-50 showed the lowest creep compliance which indicates it has the lowest resistance to shrinkage among the mixes from Source 1. This mix was very prone to thermal cracking due to presence of high amounts of aged RAP binder in the mix.

Mix-0-40 (40% RAP), and Mix-0-50-S (50% RAP with softer PG) showed very similar behaviour at low temperature. However, creep compliance values of Mix-0-50-S were noticeably higher at higher temperature. Use of one grade softer asphalt binder showed improvement in creep compliance master curve. The creep compliance of Mix-0-50-S was found to be higher than Mix-0-50 at low temperature. However, one grade softer binder was not sufficient to provide creep compliance values close to Mix-0-0.

Figure 4.8 shows the comparison of creep compliance master curve of Mix-0-10_2 and Mix-3-10 from Source 2 and Mix-0-0 from Source 1. Mix-3-10 showed lower creep compliance when it was compared to Mix-0-10_2 and Mix-0-0.

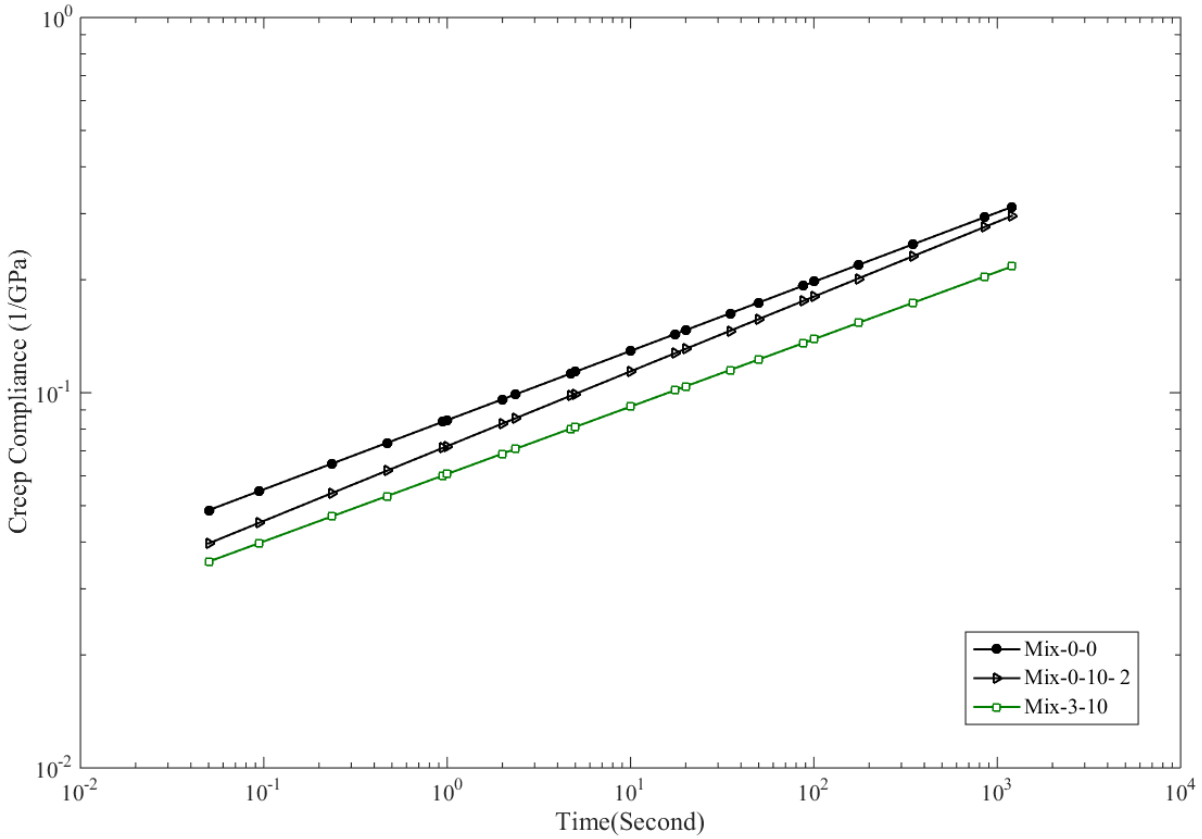

Figure 4.8: Creep compliance master curve of mixes from Source 2

Figure 4.9 compares the creep compliance master curve of laboratory produced mixes. Mix-5-10_lab showed very low creep compliance values at low temperature which may cause the mix to become very prone to thermal cracking. An increase of 2% RAS in the mix resulted in decrease in creep compliance of the mix. Although the difference of Mix-5-10_lab and Mix-3-10_lab was considerable at low temperature, the creep compliance values of those mixes was found to be very close at high temperature.

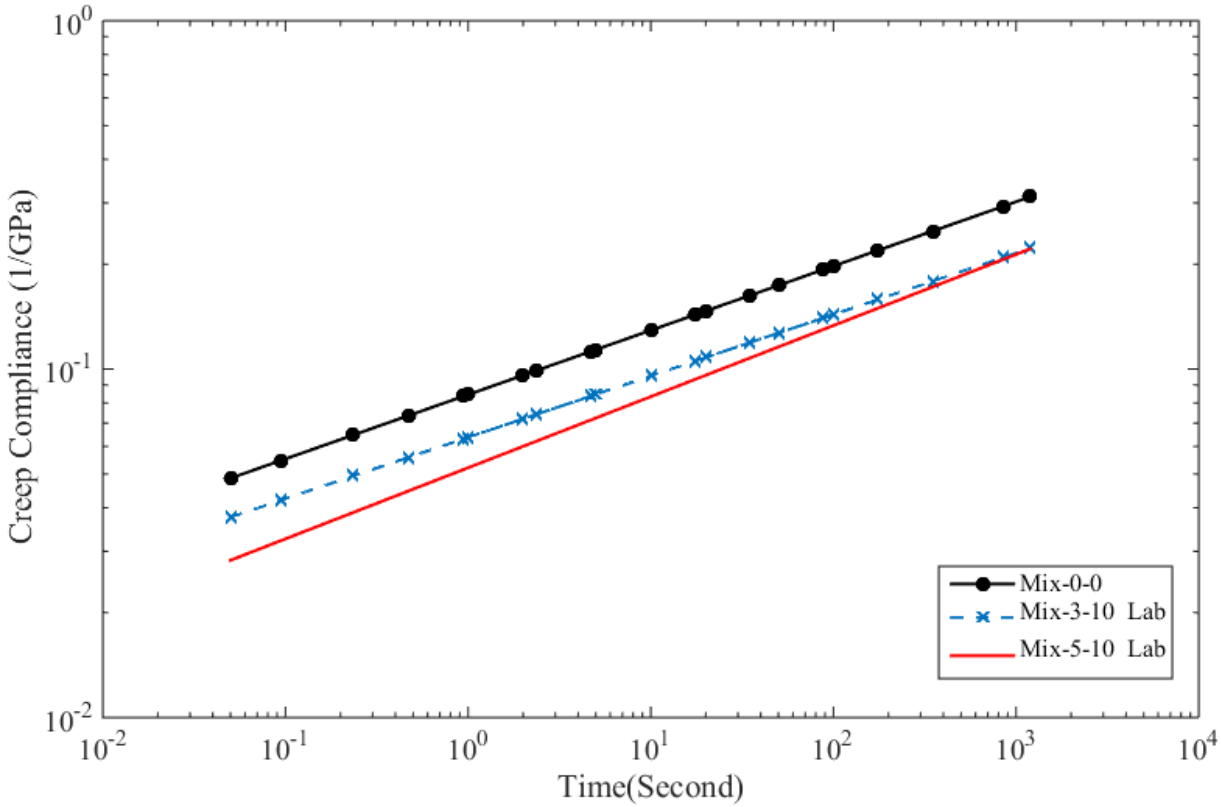

Figure 4.9: Creep compliance master curve of laboratory mixes

Figure 4.10 compares the creep compliance master curve of Mix-5-10_lab and Mix-0-50 with virgin Mix-0-0. Figure shows that the creep compliance of these two mixes were noticeably lower than Mix-0-0 at left side of the graph where it represents the creep compliance performance at -20°C and lower temperature. The creep compliance of mix-5-10_lab increased as the temperature increased. The creep compliance values of Mix-0-50 have similar values as Mix-0-0 at high temperature.

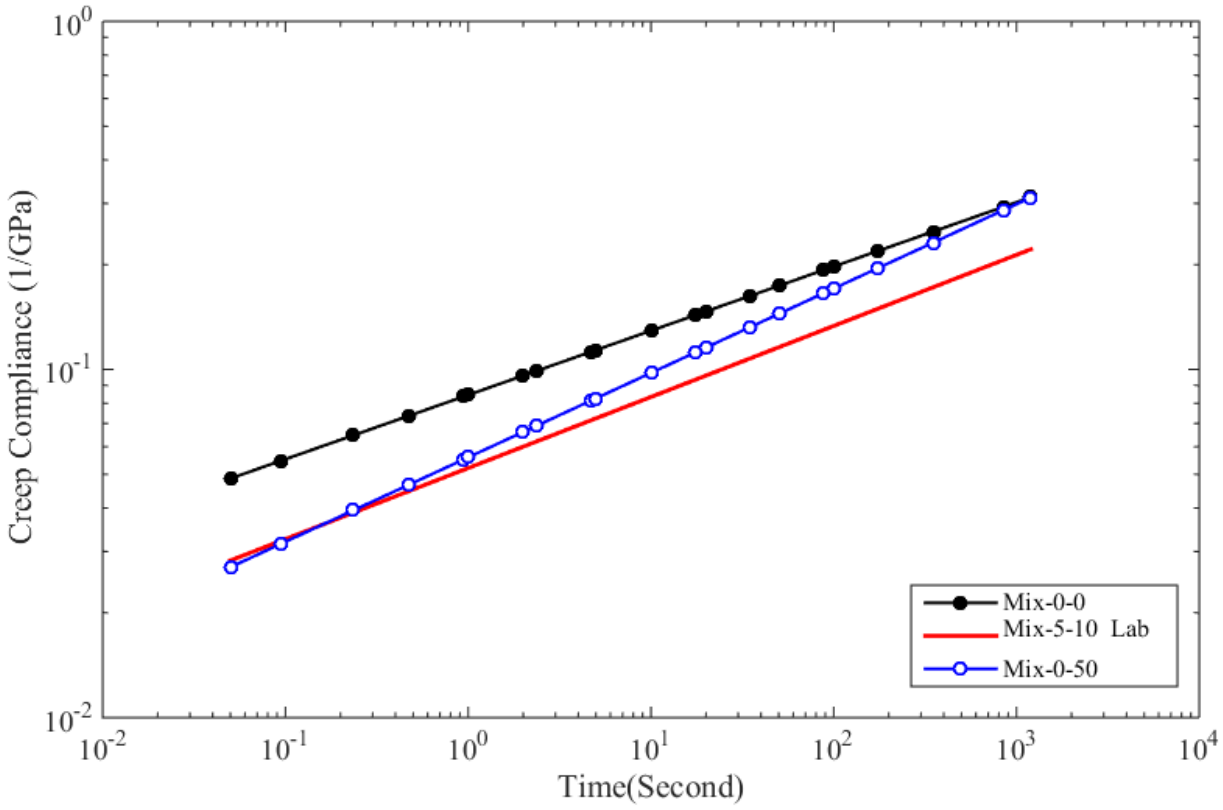

Figure 4.10: Creep compliance master curve of mix-5-10_lab and mix-0-50

In addition to creep compliance test, the indirect tensile strength test was performed at -10°C. The IDT strength test determines the stress at which the failure strength occurs for the first time in the mix (NCHRP 1-40D 2004). The IDT test was performed on the specimens right after the creep compliance test was completed. Figure 4.11 shows the IDT strength of the AC mixes.

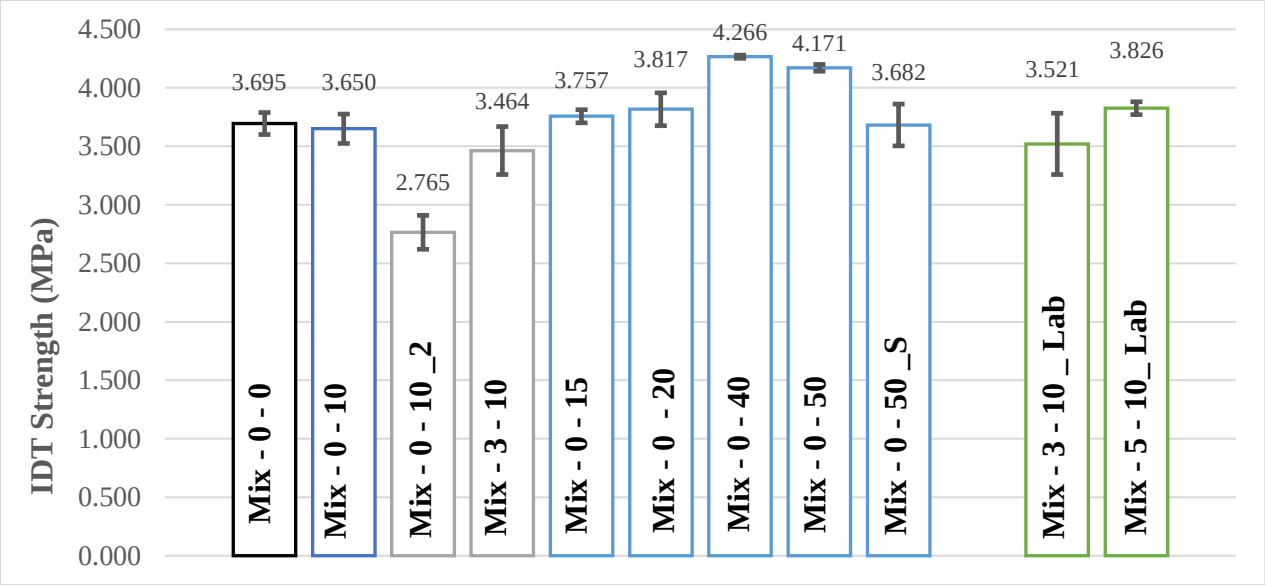

Figure 4.11 IDT strength test results of the mixes

The IDT strength of mixes increased as the percentage of RAP increased. Mix-0-10_2 and Mix-3-10 from Source 2 showed lower IDT strength. Use of RAS increased the IDT strength when it was compared to Mix-0-10_2 with no RAS. Use of softer binder in mix with 50% RAP resulted in reduction in stiffness of the mix. Mix-5-10_ lab with 2% more RAS compared to RAS content of Mix-3-10_lab showed higher strength as expected. This conceded with result of creep compliance test for laboratory mixes.

In addition to the laboratory tests, field evaluation of Mix-0-10_2 and Mix-3-10 was conducted. The field evaluation showed that the performance of these mixes are very comparable. The details of field evaluation can be found in Appendix A.

4.4 Summary

The dynamic modulus test was performed to evaluate the high temperature performance of the

mixes. Creep compliance and IDT strength tests were conducted to determine the performance of the mixes at low temperature.

- Results showed that the use of RAS and RAP increased the rutting resistance of the mixes. It was found that the dynamic modulus values of RAP mixes from Source 1 were different from Mix-0-0 (virgin mix). Moreover, it was found that the use of RAS in HMA can increase the rutting resistance of HMA mixes.
- University of Manitoba laboratory mix design showed lower stiffness at high temperature although the mix contains higher amounts of recycled materials (10% RAP and 5% RAS) in comparison with Minnesota mix (5% RAS) and Ontario mix (6% RAS). This implied that the University of Manitoba mix had lower rutting resistance when it was compared to other mixes with similar RAS content.
- Creep compliance results showed that the RAS and RAP directly affected the low temperature performance of the HMA mixes. The use of RAS and RAP increased the stiffness of the mixes at low temperature, as expected. IDT strength results agreed with creep compliance test results. It was found that utilizing RAS in HMA increased the IDT strength and reduced the creep compliance at low temperature.
- The stiffness of the mixes obtained from Source 2 showed variability at low temperature in creep compliance and dynamic modulus test results. This variability could be due to inconsistency in contribution of RAS and RAP binder in the sample mixes and lack of uniformity of RAS and RAP materials.
- Use of 15% RAP showed improvement in rutting resistance whereas it did not impact the low temperature performance. Therefore, 15% RAP can be used in an asphalt mix without changing the virgin asphalt binder grade when the design binder is PG 58-28. This finding

is in agreement with NCHRP 495 (NCHRP-495 2016).

- Mix-0-50 (50% RAP) and Mix-5-10 (5% RAS+10% RAP) showed excessive stiffness in creep compliance test which indicates that these mixes became brittle and prone to thermal cracking.
- Utilizing softer asphalt binder in a mix with high percentage of RAP was found beneficial. When one grade softer binder was added to the mix containing 50% RAP, the creep compliance improved. However, one grade softer was not sufficient for this mix to provide comparable creep compliance values as of Mix-0-0.

CHAPTER 5 - ALTERNATIVES FOR CALIBRATION OF E* PREDICTION MODELS OF ASPHALT CONCRETE CONTAINING RAP

5.1 Introduction

In Chapter 2, the NCHRP 1-37A and NCHRP 1-40D models, which have been incorporated into the MEPDG program to estimate E*, were reviewed and presented. In addition, it was shown that these models are inconsistent in predicting E* and required to be locally calibrated for local mixes and materials, particularly for mixes containing RAP. In this chapter, the E* models, presented in the final reports of NCHRP 1-37A and NCHRP 1-40D, shown by Equations 2.1 and 2.2, are used for calibration based on local materials.

This chapter presents two alternatives for conducting local calibration of mixes containing different amounts of RAP, and also evaluates the improvements obtained by local calibration over the globally calibrated models.

This chapter is part of the following paper: Esfandiarpour, S., Shalaby, A., 2016, Alternatives for Calibration of Dynamic Modulus Prediction Models of Asphalt Concrete., In press, International Journal of Pavement Research and Technology.

5.2 Asphalt Concrete Mixes Used in Evaluation of E* Predictive Models

As mentioned in previous chapters, the dynamic modulus test was conducted on laboratory samples prepared from Source 1 field mixes collected from highway paving projects in Manitoba, Canada. Source 2 mixes excluded from the evaluation of E* models since they were not available at the time of the evaluation. A total of 17 types of HMA mixes (51 specimens) from Source 1 were used for assessment of E* models. Three replicate specimens from each mix were prepared. The asphalt binder performance grade and aggregate gradations of the investigated mixes are shown in Table 5.1. The investigated mixes did not contain RAS. Table 5.2:shows the average and standard deviation of volumetric properties of mixes.

Table 5.1: Aggregate gradations of asphalt mixes

Mix ID	Aggregate Gradation									RAP %	Material Sources	Extracted Binder PG
	19 mm	16 mm	12.5 mm	9.5 mm	4.75 mm	2.0 mm	425 µm	180 µm	75 µm			
Mix-0-0	100	98.6	90.4	80.2	64.4	50.1	25.8	10.0	4.5	0	Source 1	58-28
Mix-0-0_2	100.	99.3	93.4	82.6	64.1	50.2	27.8	6.5	4.9	0	Source 1	58-28
Mix-0-0_3	100.	99.7	95.9	89.5	74.6	56.5	27.5	6.8	4.5	0	Source 1	58-28
Mix-0-0_4	100.	98.4	92.4	82.4	64.3	48.9	29.3	8.4	6.1	0	Source 1	58-28
Mix-0-0_5	100.	98.1	88.7	78.8	65.8	53.3	23.2	6.5	4.3	0	Source 1	58-28
Mix-0-0_6	100.	97.2	88.5	76.5	59.0	49.9	20.9	7.1	3.0	0	Source 1	52-34
Mix-0-0_7	100.	96.2	84.4	72.2	57.8	48.2	19.4	4.8	2.8	0	Source 1	58-28
Mix-0-0_8	100.	96.7	87.3	76.2	61.7	49.8	24.9	5.8	3.7	0	Source 1	58-28
Mix-0-10	100.	99.4	91.8	83.3	65.5	51.2	26.6	9.0	4.7	10	Source 1	58-28
Mix-0-10_3	100.	98.9	91.5	80.4	62.5	48.4	29.2	8.2	5.4	10	Source 1	58-28
Mix-0-10_4	100.	96.6	86.5	77.6	61.8	51.7	21.6	5.9	3.6	10	Source 1	58-28
Mix-0-10_5	100.	98.1	91.5	82.3	63.4	47.7	26.5	9.1	4.4	10	Source 1	58-28
Mix-0-15	100.	98.5	91.8	80.2	61.2	48.1	28.0	8.0	3.7	15	Source 1	58-28
Mix-0-15_2	100.	98.2	91.2	80.6	61.7	47.4	31.0	9.2	4.5	15	Source 1	58-28
Mix-0-15_3	100	96.2	86.7	76	59.5	48.4	19.6	6.7	4.5	15	Source 1	58-28
Mix-0-50	100.	98.8	94.2	83.3	66.3	50.7	27.7	9.6	6.7	50	Source 1	64-16
Mix-0-50_S	100.	98.6	93.6	84.4	68.5	52.1	28.1	10.3	7.1	50	Source 1	64-22

Table 5.2: Average and standard deviation of volumetric properties of mixes

Mix ID	AC %	Std.	VMA %	Std.	V_a %	Std.	VFA %	Std.	G_{mm}	Std.
Mix-0-0	6.0	0.2	15.2	0.5	4.2	0.5	72.7	2.9	2.445	0.009
Mix-0-0_2	5.5	0.4	14.5	0.6	4.0	0.8	72.4	4.9	2.501	0.012
Mix-0-0_3	6.3	0.2	16.5	2.6	6.6	2.4	60.6	8.4	2.491	0.016
Mix-0-0_4	5.5	0.3	14.3	0.5	4.0	0.3	72.0	2.3	2.496	0.014
Mix-0-0_5	6.9	0.2	16.2	0.5	3.3	0.5	79.7	2.8	2.417	0.012
Mix-0-0_6	5.3	0.3	14.7	1.3	4.0	0.6	73.3	5.7	2.446	0.012
Mix-0-0_7	6.3	0.3	14.8	0.4	4.2	0.5	71.8	3.0	2.428	0.007
Mix-0-0_8	6.4	0.3	14.3	0.6	4.1	0.6	71.0	4.6	2.432	0.011
Mix-0-10	6.3	0.5	14.5	0.3	3.7	0.3	74.8	2.2	2.435	0.008
Mix-0-10_3	5.4	0.2	14.1	1.0	3.7	0.6	73.6	4.6	2.486	0.016
Mix-0-10_4	6.7	0.3	15.2	0.4	3.5	0.4	76.9	2.4	2.410	0.009
Mix-0-10_5	5.4	0.2	14.4	0.5	4.1	0.5	71.8	2.8	2.485	0.007
Mix-0-15	5.9	0.2	13.7	0.7	3.8	0.9	72.3	4.9	2.437	0.007
Mix-0-15_2	6.1	0.3	14.5	0.3	3.1	0.6	78.5	4.0	2.457	0.061
Mix-0-15_3	5.4	0.1	14.9	0.7	4.7	0.5	68.3	5.8	2.501	0.012
Mix-0-50	5.0	0.2	12.2	0.4	3.6	0.6	70.6	3.7	2.516	0.008
Mix-0-50_S	5.1	0.2	12.0	0.3	3.6	0.3	69.8	2.9	2.526	0.011

AC=percent asphalt content; Std.= Standard deviation; VMA= voids in mineral aggregates; V_a = percent air voids; VFA= voids filled with asphalt; G_{mm}= maximum theoretical specific gravity.

Mixes used in Manitoba typically contain soft binders to resist thermal cracking under cold temperatures and resist rutting at high temperatures (up to 35°C). As a result, not all mixes could be tested at 54°C. Twenty-seven specimens were tested at all five temperatures (810 points) and 24 specimens were tested at four temperatures (576 points). In total, 1386 dynamic modulus measurements were used in this part of the study.

Figure 5.1 summarizes the research methodology used to predict E* values. Under Case 1, uncalibrated or globally calibrated models for both Levels 2 and 3 were used to estimate E* values. In Case 2, an exponential fit model was utilized to fit globally calibrated dynamic modulus outputs to local laboratory-obtained values. In Case 3, nonlinear regression model was utilized to update

the coefficients of NCHRP 1-37A and NCHRP 1-40 D models using local laboratory-obtained values. Finally, the accuracy of predicted E* by globally and locally calibrated NCHRP 1-37A and NCHRP 1-40D models for different RAP mixes were examined.

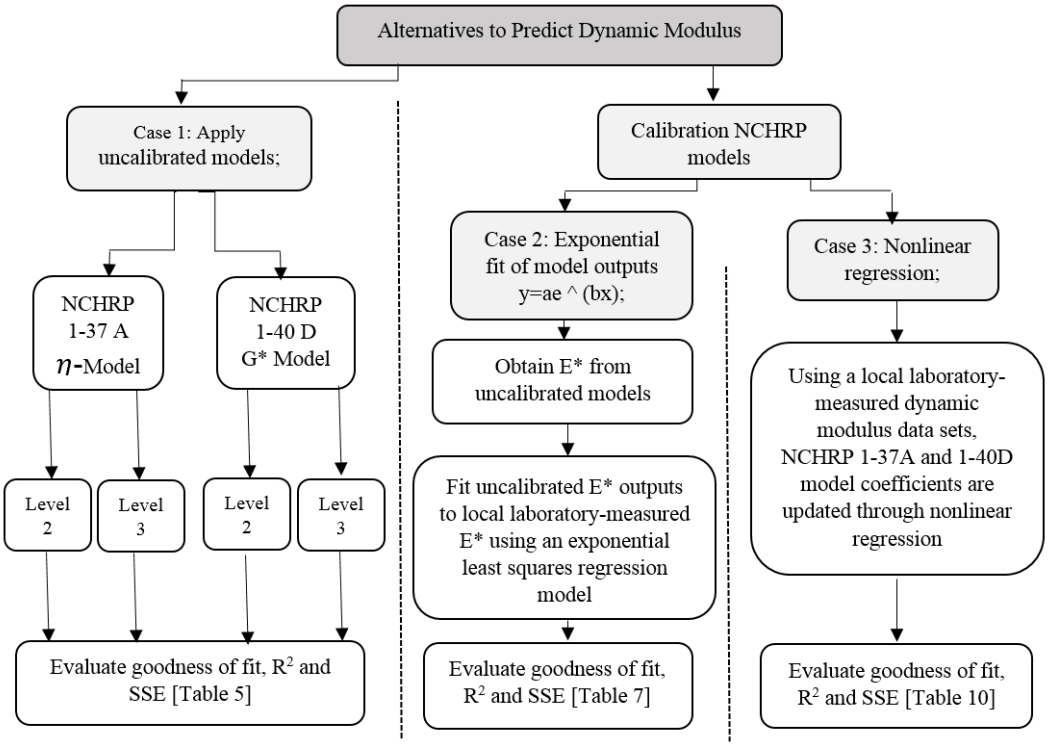

Figure 5.1. Research methodology

5.3 Prediction of Dynamic Modulus Values

For Level 3 inputs, default values of A and VTS parameters were determined based on asphalt binder performance grade for all the AC mixes. The G* and δ data were measured provided in the laboratory by MI for Level 2 input data. The viscosity-temperature parameters were calculated based on Equations 2.4 and 2.5. The viscosity-temperature parameters were computed and converted to G* and δ through Equations 2.6 to 2.11 to predict the E* using NCHRP 1-40D model. Table 5.3 shows the obtained A and VTS values along with the corresponding coefficient of

determination (R^2) for all the mixes in Level 2 and Level 3 asphalt binder input data. The A-VTS values obtained for Level 2 were determined from laboratory testing. The A-VTS values of asphalt binders with the same performance grade were found to vary depending on sources of the binders. Table 5.3 shows that the A-VTS values obtained from Level 2 were lower than the default A-VTS values for Level 3. Similar results were found by another study (El-Badawy et al. 2012).

Table 5.3. Asphalt binder viscosity-temperature parameters (A–VTS) for NCHRP 1-37A model

Mix ID	RAP %	Extracted Binder PG	Level 2			Level 3	
			A	VTS	R^2	A	VTS
Mix-0-0	0	58-28	10.782	-3.612	0.998	11.010	-3.701
Mix-0-0_2	0	58-28	11.209	-3.772	0.999	11.010	-3.701
Mix-0-0_3	0	58-28	10.117	-3.376	0.999	11.010	-3.701
Mix-0-0_4	0	58-28	10.110	-3.373	0.997	11.010	-3.701
Mix-0-0_5	0	58-28	10.231	-3.411	0.999	11.010	-3.701
Mix-0-0_6	0	52-34	10.691	-3.593	0.999	10.707	-3.602
Mix-0-0_7	0	58-28	10.273	-3.432	0.996	11.010	-3.701
Mix-0-0_8	0	58-28	8.092	-2.640	0.999	11.010	-3.701
Mix-0-10	10	58-28	9.923	-3.305	0.998	11.010	-3.701
Mix-0-10_3	10	58-28	10.142	-3.377	0.998	11.010	-3.701
Mix-0-10_4	10	58-28	10.493	-3.512	0.999	11.010	-3.701
Mix-0-10_5	10	58-28	10.237	-3.410	0.999	11.010	-3.701
Mix-0-15	15	58-28	10.051	-3.353	0.999	11.010	-3.701
Mix-0-15_2	15	58-28	9.972	-3.313	0.998	11.010	-3.701
Mix-0-15_3	15	58-28	10.051	-3.353	0.998	11.010	-3.701
Mix-0-50	50	64-16	10.530	-3.515	0.994	11.375	-3.822
Mix-0-50_S	50	64-22	10.940	-3.669	0.997	10.980	-3.68

5.3.1 Case 1: Apply Globally Calibrated Models

The dynamic modulus values were estimated using NCHRP 1-37A and NCHRP 1-40D for Level 2 and Level 3 for all asphalt mixes. In order to assess the reliability of predicted E*, actual measured laboratory dynamic modulus values were compared to predicted E*. Figures 5.2 and 5.3 show the comparison of laboratory-measured and predicted E* values by NCHRP 1-37A and NCHRP 1-40D for Level 2 and Level 3 on a logarithmic scale, respectively.

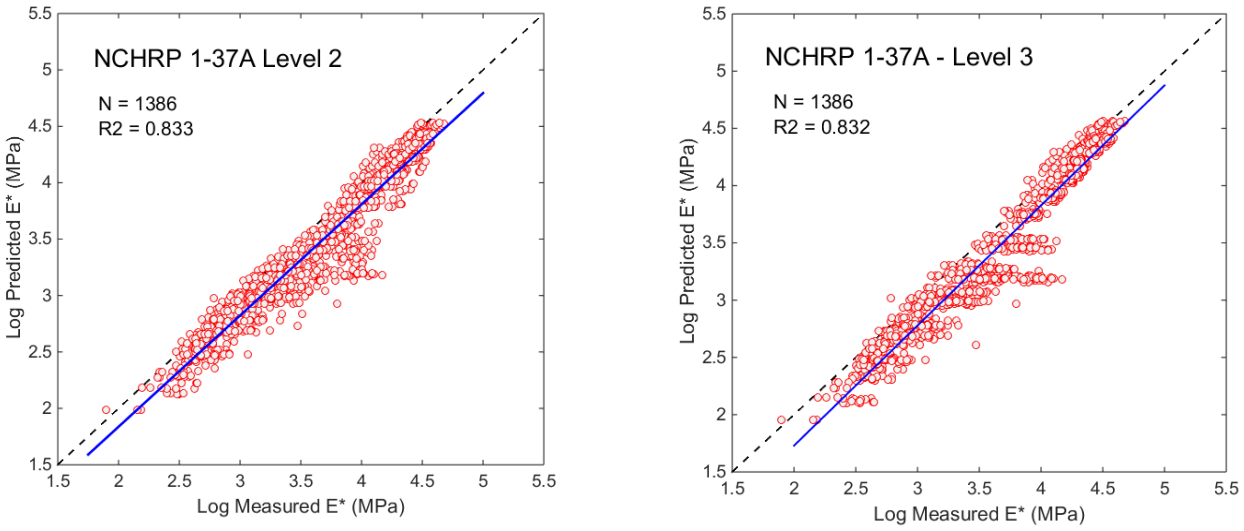

Figure 5.2. NCHRP 1-37A predicted E* values versus laboratory-measured E* for Level 2 and Level 3 asphalt binder inputs on a log-log scale

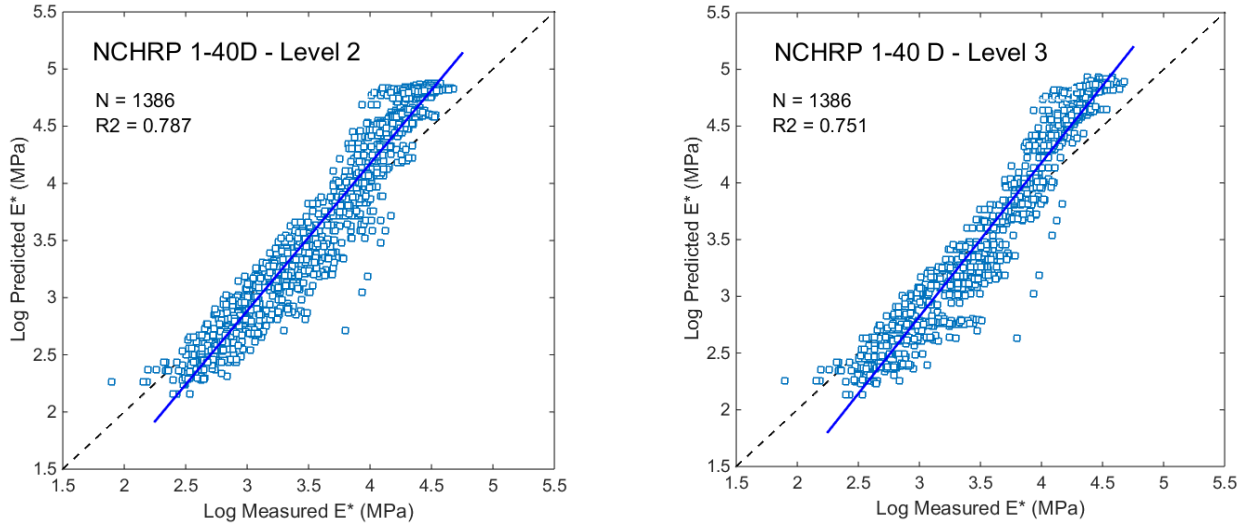

Figure 5.3. NCHRP 1-40D predicted E* values versus laboratory-measured E* for Level 2 and Level 3 asphalt binder inputs on a log-log scale

The majority of values predicted by NCHRP1-37A model appeared to be under the line of equality for both Level 2 and Level 3. This indicates that NCHRP 1-37A model underestimates the E* values at all temperature range. NCHRP 1-40D model showed bias in prediction of E* at low, and

high temperature and low bias at medium temperature. This model tends to overestimate the E* at low temperature and underestimate it at high temperature.

The accuracy of both models was evaluated based on the goodness of fit between the estimated and measured values with reference to the line of equality. Statistical parameters such as R^2 values, the standard error of predicted dynamic modulus (S_e), the standard deviation of the measured dynamic modulus (S_y), and the sum of squared errors (SSE) were calculated. The ratio Se/Sy is an indicator of the improvement of prediction and is a better indicator of prediction reliability for nonlinear models compared to R^2 (Kim et al. 2005). This shows that the R^2 and Se/Sy values of NCHRP 1-40D were lower and higher than those of NCHRP 1-37A, respectively. This indicates that NCHRP 1-37A model predicted E* values more accurately compared to NCHRP 1-40D. There are two potential reasons that can explain the lower accuracy of NCHRP 1-40D: a) estimating VTS and A from calculated G* and δ (Eq. 2.4 and 2.5), and b) conducting another set of equations (Equations 2.6 to 2.11) to convert the viscosity to G* and δ.

The SSE of NCHRP 1-37A is lower than NCHRP 1-40D that agrees with the corresponding R^2 and Se/Sy values. For NCHRP 1-37A model in Level 3, the R^2 and Se/Sy values were 0.832 and 0.410, respectively. These statistical parameters were found to be 0.833 and 0.409 in Level 2. The NCHRP 1-37A does not show significant difference in the prediction of E* between Level 2 and Level 3 asphalt binder input data. The R^2 and Se/Sy values of NCHRP 1-40D in Level 3 were 0.751 and 0.499, respectively. The predicted E* values were slightly improved in NCHRP 1-40D model for Level 2 input data with R^2 value of 0.787 and Se/Sy values of 0.461.

Slope and intercept of predicted E* were calculated as two additional indicators to present the bias

in predicted values. The variation of calculated slope and intercept of predicted E* conceded with the variation in other statistical parameters and shows that NCHRP 1-37A model generates more reliable E* than the NCHRP 1-40D model. Table 5.4 shows the summary statistics of predictive models in both levels.

Table 5.4: Summary statistics of Case 1: Globally calibrated E* prediction models

Scale	NCHRP 1-37A		NCHRP 1-40D	
	Level 2	Level 3	Level 2	Level 3
SSE (MPa)	90.322	90.561	114.493	134.178
R^2	0.833	0.832	0.787	0.751
Se/Sy	0.409	0.410	0.461	0.499
Slope	0.986	1.049	1.288	1.357
Intercept	-0.136	-0.368	-0.981	-1.250

SSE=Sum of squared errors

5.3.2 Local Calibration

In the previous section, it was shown that the investigated models depicted different performance in prediction of E*. El-Badawy et al. (2012) reported that the accuracy of predicted E* can have a significant impact on the predicted rutting and cracking performance by MEPDG software. Therefore, accurate E* is considered to be important for input in the MEPDG software.

To increase the accuracy of predicted E*, a local calibration of model is required. The purpose of local calibration is to minimize the sum of squared errors (SSE) between the predicted E* and laboratory-measured E*. Two alternative methods were applied to improve model predictions. An exponential fit was first applied to fit the outputs obtained from globally calibrated NCHRP 1-37A and NCHRP 1-40D models, to laboratory-measured E* values. Secondly, nonlinear multiple regression was used to update the coefficients of NCHRP 1-37A and NCHRP 1-40D.

5.3.2.1 Case 2: Exponential Fit of Model Outputs to Measured Values

Using the local laboratory-measured dynamic modulus data set, the globally calibrated dynamic modulus outputs were fitted to an exponential least squares regression model. NCHRP 1-37A and NCHRP 1-40D were first used to predict the E* values, then, an exponential regression was applied to fit those outputs to the measured E*. Table 5.5 shows the exponential fit of predicted E* for each model for Level 2 and Level 3.

Table 5.5: Exponential fit for each model in Level 2 and Level 3

Model	Level 2	Level 3
NCHRP 1-37A	$\log(E^*_{Calibrated}) = 0.938\log(E^*_{Predicted}) + 0.398$	$\log(E^*_{Calibrated}) = 0.893 \log(E^*_{Predicted}) + 0.563$
NCHRP 1-40D	$\log(E^*_{Calibrated}) = 0.727 \log(E^*_{Predicted}) + 0.947$	$\log(E^*_{Calibrated}) = 0.695 \log(E^*_{Predicted}) + 1.077$

The slope of exponential regression of NCHRP 1-37A model in both Levels was found higher than those in NCHRP 1-40D as shown in Table 5.5. Higher value of slope indicates this regression increases the predicted E* values. This is expected, since the NCHRP 1-37A model mostly tends to underpredict the E* values at low and high temperatures as it was discussed earlier. The slope and intercept of exponential fit of NCHRP 1-40D model in both Levels are lower and higher respectively, than those for calibrated NCHRP 1-37A. This is reasonable since the obtained predicted E* values from globally calibrated NCHRP 1-40D are not parallel to the line of equality.

Table 5.6 shows the summary of statistics of predicted E* after exponential regression was performed. The accuracy of calibrated NCHRP 1-37A and NCHRP 1-40D in both Levels significantly improved. Comparing the values of Table 5.6 with those of Table 5.4, it is noticed that the R^2 values are higher and SSE values are lower for both models in both Level 2 and Level 3. The slope and intercept of exponential fit of NCHRP 1-40D model showed improvement while

these values did not show significant improvement in calibrated NCHRP 1-37A when they compared to globally calibrated models. The performance of the model after local calibration is shown in Figures 5.4 and 5.5.

Table 5.6 Summary statistics of Case 2: Exponential fit of model outputs

Scale	NCHRP 1-37A		NCHRP 1-40D	
	Level 2	Level 3	Level 2	Level 3
SSE (MPa)	39.649	32.175	33.422	29.912
R^2	0.940	0.940	0.938	0.945
Se/Sy	0.271	0.244	0.249	0.235
Slope	0.932	0.940	0.938	0.945
Intercept	0.252	0.220	0.229	0.203

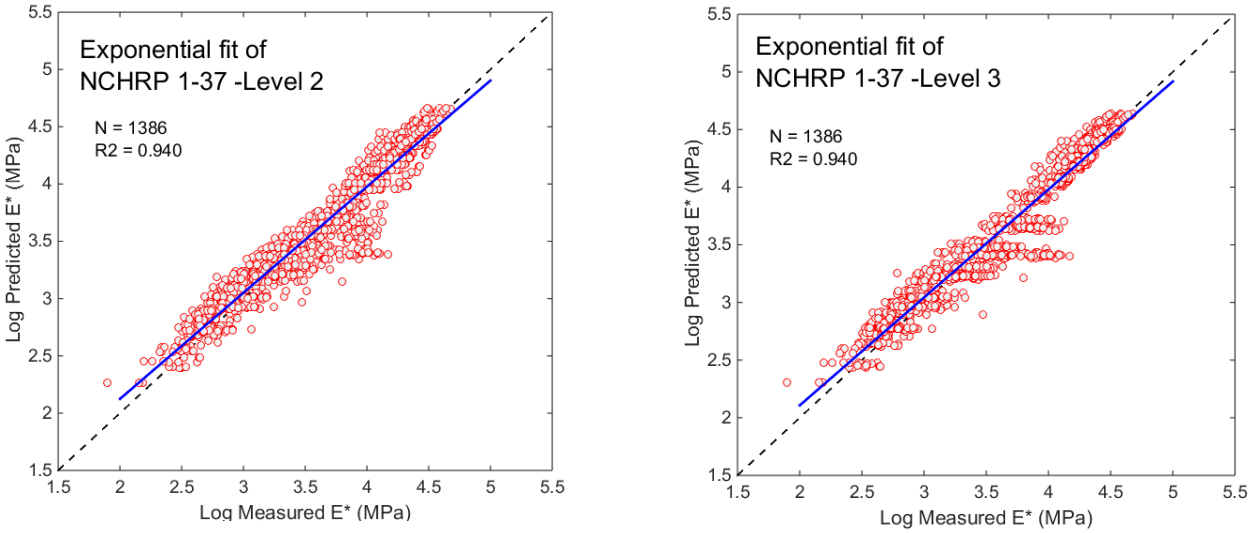

Figure 5.4: Exponential fit of NCHRP 1-37A predicted E* values versus laboratory-measured E* for Level 2 and Level 3 asphalt binder inputs on a log-log scale

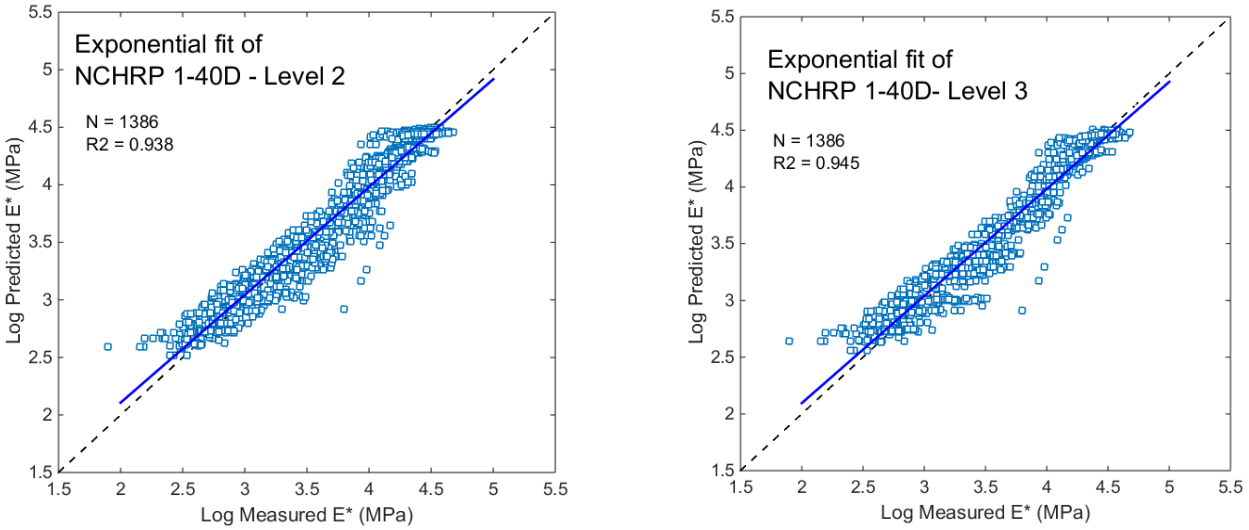

Figure 5.5: Exponential fit of NCHRP 1-40D predicted E* values versus laboratory-measured E* for Level 2 and Level 3 asphalt binder inputs on a log-log scale

5.3.2.2 Case 3: Update Model Coefficients Using Nonlinear Multiple Regression

The exponential fit can be used only after the E* values were predicted from NCHRP 1-37A and NCHRP 1-40D. One of the drawbacks of the exponential fit is that it does not provide a general model which can be used for both Levels and does not directly relates mix properties and asphalt binder inputs to E* values. A nonlinear multiple regression, on the other hand, retains the model form and only updates the coefficients to produce a better fit to locally obtained E* values. Nonlinear regression was conducted on E* predictive models to update the coefficients of the NCHRP 1-37A and NCHRP 1-40D models. There are 14 and 21 coefficients in NCHRP 1-37A and NCHRP 1-40D, respectively. The general models, which were subjected to nonlinear calibration, are given in Equations 5.1 and 5.2.

$$\text{Log}_{10}\ E^* = -(C1) + (C2)\rho_{200} - (C3)(\rho_{200})^2 - (C4)\rho_4 - (C5)V_a - (C6)\frac{V_{beff}}{V_{beff}+V_a} + \frac{(C7)-(C8)\rho_4+(C9)\ \rho_{38}-(C10)(\rho_{38})^2+(C11)\rho_{34}}{1+e^{(-(C12)-(C13)(logf)-(C14)(log\eta))}} \quad (5.1)$$

$$\text{Log}_{10} E^* = -(D1) + (D2)\,(|G_b^*|^{-D(3)})^*((D4) - (D5)\rho_{200} + (D6)(\rho_{200})^2 + (D7)\rho_4 - (D8)(\rho_4)^2 + (D9)\rho_{38} - (D10)(\rho_{38})^2 - (D11)V_a - (D12)(\frac{V_{beff}}{V_{beff}+V_a})) + \frac{(D13) + (D14)Va + (D15)\left(\frac{V_{beff}}{V_{beff}+V_a}\right) + (D16)\,\rho_{38} - (D17)(\rho_{38})^2 - (D18)\rho_{34}}{1+e^{(-(D19)-(D20)\left(\log\left(\left|G_b^*\right|\right)\right)+(D21)(log(\delta_b)))}}$$

(5.2)

The objective of nonlinear multiple regression was to update the coefficients for each model while minimizing sum of squared errors between the predicted E* and the laboratory-measured E* for both Levels, simultaneously. By optimizing the models for both Level 2 and Level 3 inputs, the models can be utilized regardless of the source and reliability of inputs. Equations 5.3 to 5.5 show the objectives of nonlinear multiple regression.

$$E^*_{Pr} = [E^*_{Pr\text{-}Level\ 3},\ E^*_{Pr\text{-}Level\ 2}] \quad (5.3)$$

$$E^*_{M} = [E^*_{M3},\ E^*_{M2}] \quad (5.4)$$

$$\text{Minimize } (E^*_{Pr} - E^*_{M})^2 \quad (5.5)$$

Where, $E^*_{Pr\text{-}Level\ 3}$ is a matrix of predicted E* in Level 3; $E^*_{Pr\text{-}Level\ 2}$ is a matrix of predicted E* in Level 2; E^*_{M3} is a matrix of measured E*; E^*_{M2} is a matrix of measured E* ; E^*_{Pr} is a matrix of predicted E* in both Level 2 and Level 3; E^*_{M} is a matrix of measured E*.

In each iteration, coefficients were selected such that to reduce the difference of predicted E* and laboratory-measured E* values in both Level 2 and Level 3 at the same time. Tables 5.7 and 5.8 show the original coefficients as well as updated coefficients after nonlinear multiple regression.

Table 5.7: Nonlinear multiple regression of NCHRP 1-37A predictive model

Parameter	NCHRP 1-37A coefficient	Calibrated coefficient
C1	1.249937	-4.81235
C2	0.029230	0.42905
C3	0.001767	0.05349
C4	0.002841	0.01998
C5	0.058097	0.43028
C6	0.822080	6.29353
C7	3.871977	4.15346
C8	0.002100	0.03492
C9	0.003958	-0.02127
C10	0.000017	-0.00168
C11	0.005470	0.00547
C12	0.603313	0.64591
C13	0.313351	0.45174
C14	0.393532	0.47811

Table 5.8: Nonlinear multiple regression of NCHRP 1-40D model

Parameter	NDHRP 1-40D coefficient	Calibrated coefficient
D1	0.34900	3.70917
D2	0.75400	2.80833
D3	0.00520	0.02046
D4	6.65000	2.00973
D5	0.03200	-0.24978
D6	0.00270	-0.03214
D7	0.01100	0.11355
D8	0.00010	0.00200
D9	0.00600	-0.05228
D10	0.00014	-0.00181
D11	0.08000	0.24776
D12	1.06000	3.87083
D13	2.55800	6.75482
D14	0.03200	-0.02249
D15	0.71300	-0.19306
D16	0.01240	-0.04551
D17	0.00010	-0.00123
D18	0.00980	0.09800
D19	0.78140	2.24101
D20	0.57850	-6.44E-08
D21	0.88340	0.01588

Table 5.9 shows the summary of statistics for nonlinear multiple regression. Comparing values of Table 5.9 with those of Table 5.4 and 5.6, it is observed that the SSE and Se/Sy values of nonlinear regression models are lower, and that R^2 is higher for both models in both Levels. The performance of nonlinear regression models was found to be similar or slightly better than the exponential fit technique.

Table 5.9. Summary statistics of Case 3: nonlinear regression prediction models

Scale	NCHRP 1-37A		NCHRP 1-40D	
	Level 2	Level 3	Level 2	Level 3
SSE (MPa)	26.863	24.332	30.280	30.072
R^2	0.950	0.955	0.943	0.944
Se/Sy	0.223	0.213	0.238	0.236
Slope	0.926	0.979	0.912	0.975
Intercept	0.277	0.074	0.341	0.076

The slope and intercept of fitted nonlinear regression model generally show improvement when they compared to those of globally calibrated and exponentially-fitted model results. Figures 5.6 and 5.7 show the performance of nonlinear regression of NCHRP 1-37A and NCHRP 1-40D for both Levels, respectively. Based on these results, it can be concluded that the nonlinear multiple regression of NCHRP 1-37A and NCHRP 1-40D models are the preferred technique for conducting local calibration. The nonlinear calibration of NCHRP 1-37A and NCHRP 1-40D can predict comparable E* values of laboratory E* values. Use of locally calibrated E* models instead of globally calibrated models can increase the reliability of the analysis and design of AC mixes using Pavement ME Design software.

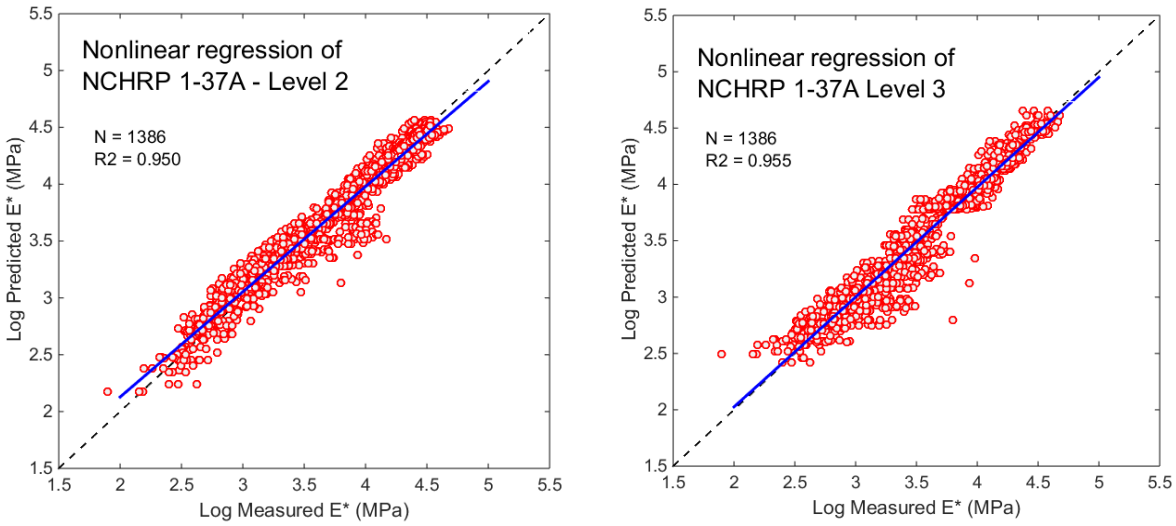

Figure 5.6: Nonlinear multiple regression of NCHRP 1-37A predicted E* values versus laboratory-measured E* for Level 2 and Level 3 asphalt binder inputs on a log-log scale

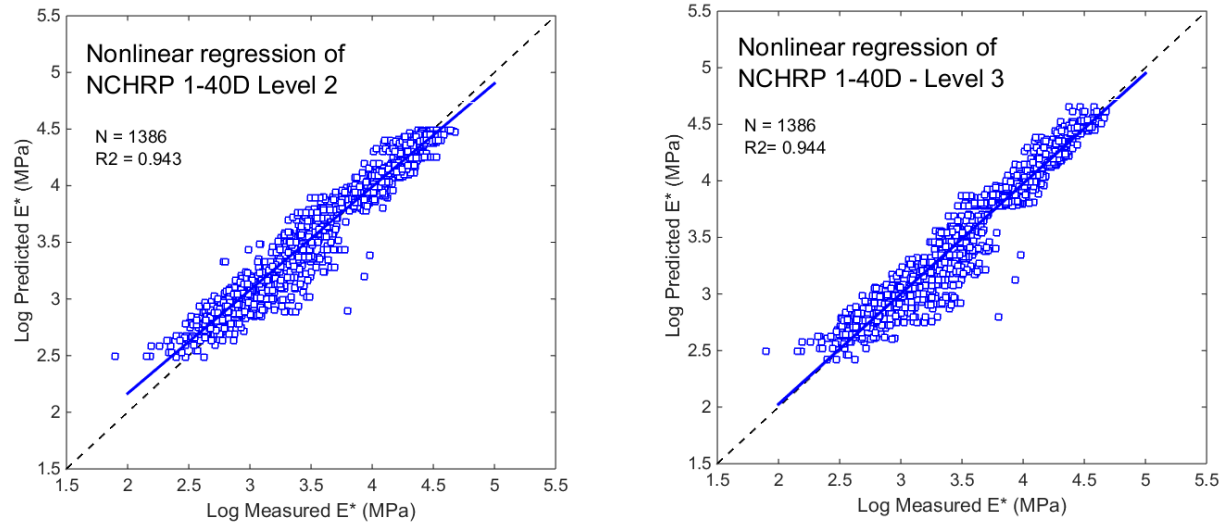

Figure 5.7: Nonlinear multiple regression of NCHRP 1-40D predicted E* values versus laboratory-measured E* for Level 2 and l 3 asphalt binder inputs on a log-log scale

5.4 Impact of Globally and Locally Calibrated E* Models on RAP Content

The effect of globally and locally calibrated NCHRP models on different RAP mixes for Level 3 inputs were evaluated. In this study, the accuracy of predicted E* for the developed database on log-log scale were evaluated. The scatter plots showing predictions of globally and locally calibrated models for RAP mixes are presented on arithmetic scale as well. Figure 5.8 shows that the globally calibrated NCHRP 1-37A models underestimate E* values for all mixes, as was mentioned previously. When locally calibrated models were used, the predicted values showed higher accuracy (i.e. less bias).

Figure 5.9 compares the predicted E* of RAP mixes from globally calibrated NCHRP 1-40D with exponential fit and nonlinear regression of NCHRP 1-40D. The globally calibrated NCHRP 1-40D overestimated the E* values for all RAP mixes. The locally calibrated models predicted E* values more accurately for all the RAP mixes when compared to the globally calibrated model.

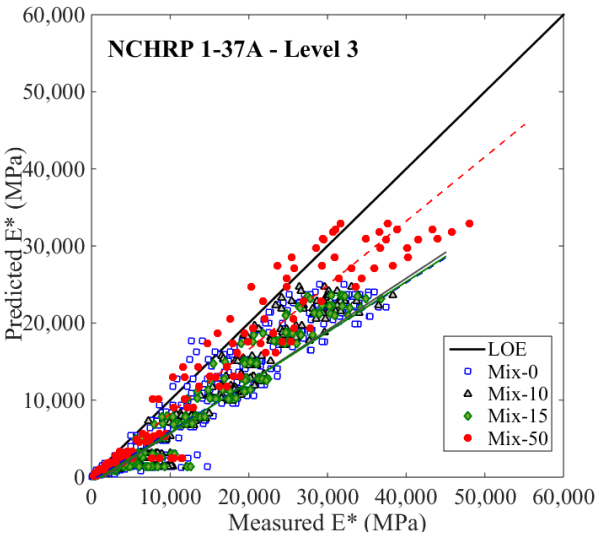

a) Globally calibrated NCHRP 1-37A

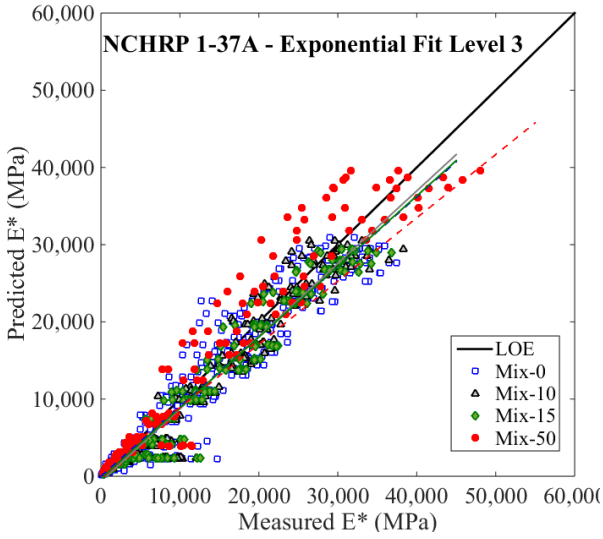

b) Exponential fit of NCHRP 1-37A

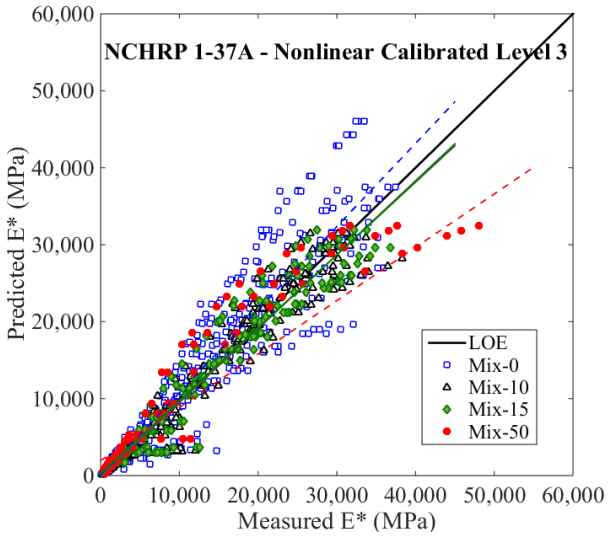

c) Nonlinear regression of NCHRP 1-37A

Figure 5.8: Globally and locally calibrated NCHRP 1-37A predicted E* values versus laboratory-measured E* for Level 3 for all RAP mixes on an arithmetic scale

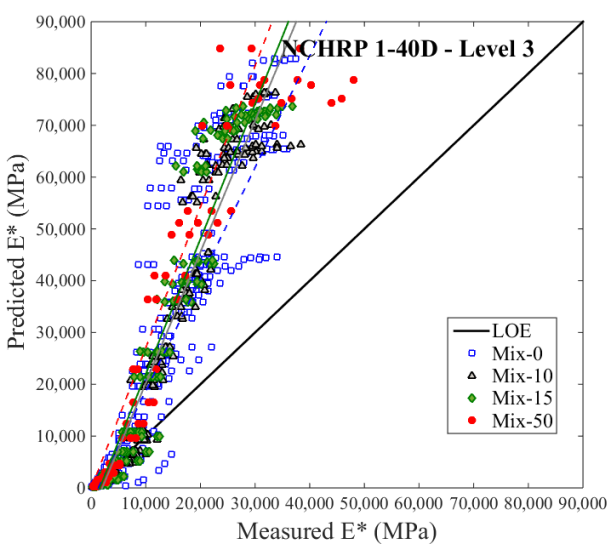

a) Globally calibrated NCHRP 1-40D

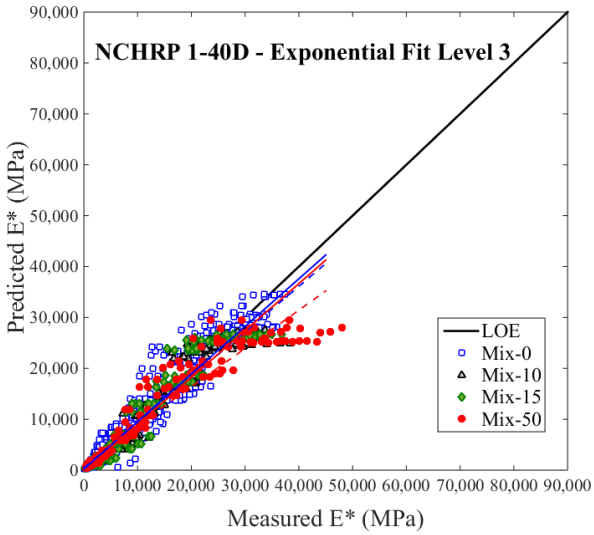

b) Exponential fit of NCHRP 1-40D

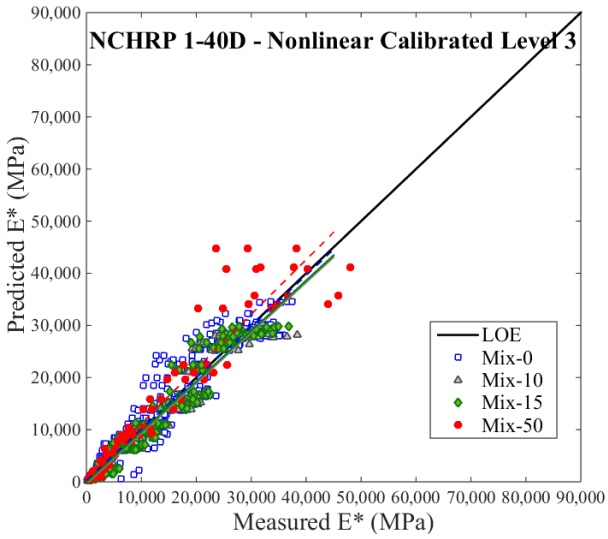

c) Nonlinear regression of NCHRP 1-40D

Figure 5.9: Globally and locally NCHRP 1-40D predicted E* values versus laboratory-measured E* for Level 3 for all RAP mixes on an arithmetic scale

Table 5.10 shows the summary statistics of globally and locally calibrated E* for RAP mixes. The slope and intercept of locally calibrated NCHRP 1-37A and NCHRP 1-40D are substantially closer to one and lower in comparison with globally calibrated models, respectively. This indicates both calibration alternatives showed improvement in prediction of E* for all RAP mixes.

Table 5.10: Summary statistics of globally and locally calibrated NCHRP 1-37A and NCHRP 1-40D models for Level 3

Prediction Models	Mix ID	N	% RAP	R^2	Slope	Intercept	SSE (MPa)
NCHRP 1-37A (Globally Calibrated)	Mix-0	666	0	0.932	0.722	-448	1.43E+10
	Mix-10	306	10	0.948	0.755	-1060	7.37E+09
	Mix-15	234	15	0.955	0.733	-726	5.47E+09
	Mix-50	180	50	0.941	0.832	-64	2.90E+09
Exponential fit of NCHRP 1-37A (Local calibration)	Mix-0	666	0	0.935	0.905	6	5.02E+09
	Mix-10	306	10	0.953	0.941	-682	2.05E+09
	Mix-15	234	15	0.958	0.915	-282	1.44E+09
	Mix-50	180	50	0.940	1.001	725	2.00E+09
Nonlinear calibration of NCHRP 1-37A (Local calibration)	Mix-0	666	0	0.902	1.08	-22	9.35E+09
	Mix-10	306	10	0.951	0.96	-114	1.66E+09
	Mix-15	234	15	0.946	0.946	301	1.36E+09
	Mix-50	180	50	0.924	0.835	1435	2.56E+09
NCHRP 1-40D (Globally Calibrated)	Mix-0	666	0	0.890	2.183	-2528	1.87E+11
	Mix-10	306	10	0.938	2.281	-4630	9.28E+10
	Mix-15	234	15	0.939	2.346	-3679	8.20E+10
	Mix-50	180	50	0.918	1.904	-786	5.17E+10
Exponential fit of NCHRP 1-40D (Local calibration)	Mix-0	666	0	0.906	0.891	463	6.60E+09
	Mix-10	306	10	0.951	0.922	-213	1.94E+09
	Mix-15	234	15	0.945	0.935	222	1.42E+09
	Mix-50	180	50	0.912	0.752	1375	3.90E+09
Nonlinear calibration of NCHRP 1-40D (Local calibration)	Mix-0	666	0	0.940	0.983	289	4.22E+09
	Mix-10	306	10	0.959	0.966	-398	1.48E+09
	Mix-15	234	15	0.956	0.968	-67	1.14E+09
	Mix-50	180	50	0.913	0.980	609	2.75E+09

However, the accuracy of predicted E* obtained from locally calibrated models for high RAP (50% RAP) mixes showed less improvement when they were compared to the other RAP mixes, particularly for globally calibrated NCHRP 1-37A. Figure 5.10 shows the percentage reduction in the sum of squared error of RAP mixes when SSE of exponential fit and nonlinear regression were

compared to SSE of the globally calibrated models. Locally calibrated NCHRP 1-40D models showed much higher improvement compared to locally calibrated NCHRP 1-37A. This result indicates that locally calibrated models successfully reduced the error of dynamic modulus prediction and improved the reliability of predicted E*.

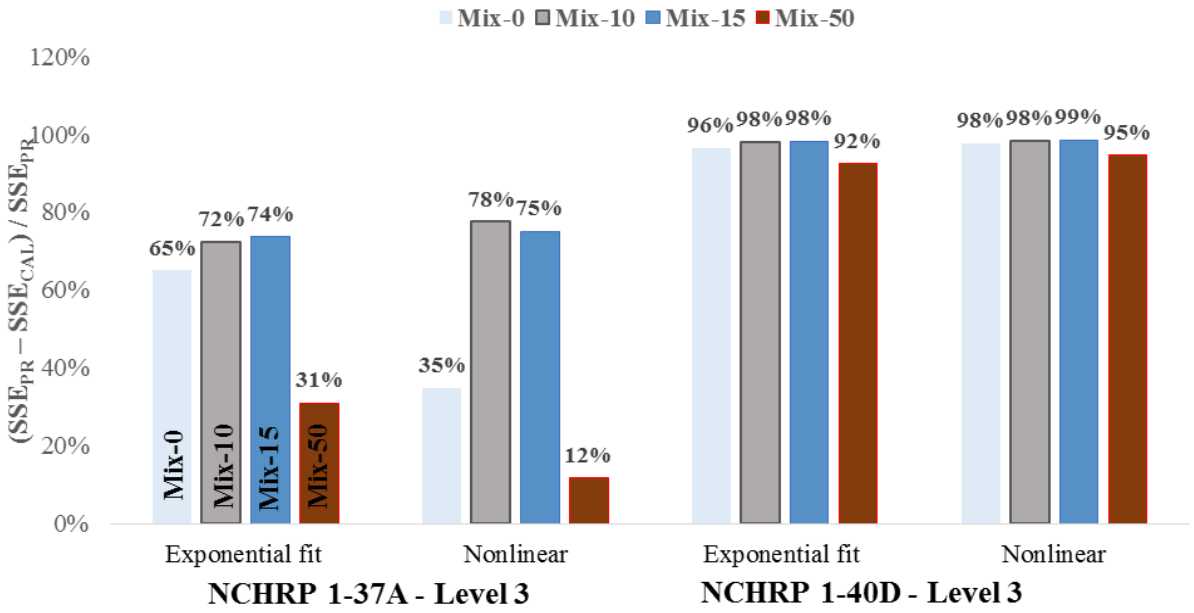

Figure 5.10: Percentage improvement of sum of squared error for RAP mixes

The mixes with 50% RAP showed the least improvement among RAP mixes for both locally calibrated NCHRP 1-37A and NCHRP 1-40D models. The prediction of high RAP mixes showed larger scatter (variability) compared to other RAP mixes. One reason for larger scatter of high RAP mixes is that the stiffness of these mixes are generally very high at low temperature due to the high amount of RAP. The large difference in the dynamic modulus of high RAP mixes in comparison with other mixes, particularly at low temperature, produces higher scatter and less reliable predictions. This implies that the existence of high RAP mixes in a database may reduce the

reliability of calibrated models.

5.5 Summary

This chapter presented alternatives for the prediction of dynamic modulus of AC mixes. Two predictive models NCHRP 1-37A and NCHRP 1-40D in two levels of asphalt binder inputs were used. In total, 1386 E* measurements from mixes with four different RAP contents were compared with predicted E* values. Exponential fit of model outputs and nonlinear multiple regression were applied to improve the reliability of E* predictions. The effect of RAP on locally and globally calibrated NCHRP models for Level 3 were evaluated. It was found that:

- Without local calibration, the NCHRP 1-37A model was found to predict E* more accurately in both Levels of asphalt binder inputs for all RAP mixes compared to NCHRP 1-40D model.
- The NCHRP 1-40D model over predicted the E* values at lower temperature and under predicted the E* at high temperature in both Levels of asphalt binder input data.
- The exponential fit of globally calibrated model outputs showed improvement in accuracy of E* prediction. The accuracy of E* values were more noticeable in NCHRP 1-40D model than NCHRP 1-37A model. The exponential fit does not provide a general model which can be used for both Levels.
- The nonlinear multiple regression of NCHRP 1-37A and NCHRP 1-40D were the preferred technique for local calibration. The results showed the highest degree of reliability in both Levels. The R^2 of nonlinear calibration models was found to be 95%.
- The nonlinear calibration of NCHRP 1-37A and NCHRP 1-40D can predict comparable

E* values of laboratory-measured E* values. Use of locally calibrated E* models instead of globally calibrated models can increase the reliability of the analysis and design of AC mixes using Pavement ME Design software.

- The exponential fit and nonlinear regression of NCHRP 1-37A and NCHRP 1-40D for Level 3 showed improvement in the prediction of E* in all RAP mixes. However, the mixes with 50% RAP showed the least improvement among RAP mixes for both locally calibrated NCHRP 1-37A and NCHRP 1-40D models.
- The existence of high RAP mixes in a database causes an adverse effect on the reliability of calibrated models.

CHAPTER 6 - LOCAL CALIBRATION OF CREEP COMPLIANCE MODELS OF ASPHALT CONCRETE

6.1 Introduction

In Chapter 2, the MEPDG creep compliance model used in Pavement ME Design software to estimate creep compliance was introduced. In addition, it was noted that there is a need to evaluate the accuracy of MEPDG creep compliance model and to calibrate based on local materials and mixes.

This chapter compares the reliability of predicted creep compliance values from the globally calibrated MEPDG model, as well as from two locally calibrated models that are based on properties of local mixes and conditions.

This Chapter is part of the following paper: Esfandiarpour, S., Shalaby, A., 2017, Local Calibration of Creep Compliance Models Of Asphalt Concrete, Journal of Construction and Building Materials, Volume 132, Pages 313–322.

6.2 Asphalt Mixes Used for Calibration of Creep Compliance Model

The creep compliance test was conducted on laboratory prepared samples obtained from Source 1 field mixes which were collected from highway paving projects in Manitoba, Canada. In total, 41 specimens from 14 types of AC mixes were used in the evaluation of creep compliance models. The asphalt binder performance grade and aggregate gradations of the investigated mixes are shown in Table 6.1. Average and standard deviations of the mix properties are shown in Table 6.2. The minimum and maximum values of the mix properties that will be used later for developing ANN model were also provided. Creep compliance test was performed at three temperatures (-20, -10, and 0°C). In total, 861 creep compliance measurements were used in this study.

Table 6.1: Volumetric properties and aggregate gradations of asphalt mixes

Mix ID	**Aggregate Gradation**										
	19 mm	16 mm	12.5 mm	9.5 mm	4.75 mm	2.0 mm	425 µm	180 µm	75 µm	RAP %	Extracted Binder PG
Mix-0-0	100.	98.6	90.4	80.2	64.4	50.1	25.8	10.0	4.5	0	58-28
Mix-0-0_4	100.	98.4	92.4	82.4	64.3	48.9	29.3	8.4	6.1	0	58-28
Mix-0-0_5	100.	98.1	88.7	78.8	65.8	53.3	23.2	6.5	4.3	0	58-28
Mix-0-0_7	100.	96.2	84.4	72.2	57.8	48.2	19.4	4.8	2.8	0	58-28
Mix-0-0_8	100.	96.7	87.3	76.2	61.7	49.8	24.9	5.8	3.7	0	58-28
Mix-0-10	100.	99.4	91.8	83.3	65.5	51.2	26.6	9.0	4.7	10	58-28
Mix-0-10_3	100.	98.9	91.5	80.4	62.5	48.4	29.2	8.2	5.4	10	58-28
Mix-0-10_4	100.	96.6	86.5	77.6	61.8	51.7	21.6	5.9	3.6	10	58-28
Mix-0-10_5	100.	98.1	91.5	82.3	63.4	47.7	26.5	9.1	4.4	10	58-28
Mix-0-15	100	98.5	91.8	80.2	61.2	48.1	28.0	8.0	3.7	15	58-28
Mix-0-15_2	100.	98.2	91.2	80.6	61.7	47.4	31.0	9.2	4.5	15	58-28
Mix-0-15_3	100	96.2	86.7	76	59.5	48.4	19.6	6.7	4.5	15	58-28
Mix-0-50	100.	98.8	94.2	83.3	66.3	50.7	27.7	9.6	6.7	50	64-16
Mix-0-50_S	100.	98.6	93.6	84.4	68.5	52.1	28.1	10.3	7.1	50	64-22

PG=performance grade; RAP= reclaimed asphalg pavement.

Table 6.2: Average, standard deviations, minimum and maximum of volumetric properties of mixes

Mix ID	AC %	Std.	VMA %	Std.	V_a %	Std.	VFA %	Std.	G_{mm}	Std.
Mix-0-0	6.0	0.2	15.2	0.5	4.2	0.5	72.7	2.9	2.445	0.009
Mix-0-0_4	5.5	0.3	14.3	0.5	4.0	0.3	72.0	2.3	2.496	0.014
Mix-0-0_5	6.9	0.2	16.2	0.5	3.3	0.5	79.7	2.8	2.417	0.012
Mix-0-0_7	6.3	0.3	14.8	0.4	4.2	0.5	71.8	3.0	2.428	0.007
Mix-0-0_8	6.4	0.3	14.3	0.6	4.1	0.6	71.0	4.6	2.432	0.011
Mix-0-10	6.3	0.5	14.5	0.3	3.7	0.3	74.8	2.2	2.435	0.008
Mix-0-10_3	5.4	0.2	14.1	1.0	3.7	0.6	73.6	4.6	2.486	0.016
Mix-0-10_4	6.7	0.3	15.2	0.4	3.5	0.4	76.9	2.4	2.410	0.009
Mix-0-10_5	5.4	0.2	14.4	0.5	4.1	0.5	71.8	2.8	2.485	0.007
Mix-0-15	5.9	0.2	13.7	0.7	3.8	0.9	72.3	4.9	2.437	0.007
Mix-0-15_2	6.1	0.3	14.5	0.3	3.1	0.6	78.5	4.0	2.457	0.061
Mix-0-15_3	5.4	0.1	14.9	0.7	4.7	0.5	68.3	5.8	2.501	0.012
Mix-0-50	5.0	0.2	12.2	0.4	3.6	0.6	70.6	3.7	2.516	0.008
Mix-0-50_S	5.1	0.2	12.0	0.3	3.6	0.3	69.8	2.9	2.526	0.011
Minimum value	5.0	-	12.0	-	3.1	-	68.3	-	2.410	-
Maximum value	6.9	-	16.2	-	4.7	-	79.7	-	2.526	-

AC=percent asphalt content; Std.= Standard deviation; VMA= voids in mineral aggregates; V_a = percent air voids; VFA= voids filled with asphalt; G_{mm}= maximum theoretical spesific gravity.

6.3 Globally Calibrated MEPDG Creep Compliance Model

The creep compliance values were predicted using MEPDG model for Level 3 for all asphalt mixes. The predicted penetration grades for different types of asphalt binder used in this study are shown in Table 6.3.

Table 6.3: A and VTS parameters and predicted penetration grade

Asphalt Binder performance grade	A	VTS	Pen_{77}
58-28	11.01	-3.701	92.1
64-16	11.38	-3.822	46.2
64-22	10.98	-3.680	53.8

In order to assess the reliability of the predicted creep compliance values, actual laboratory-measured creep values were compared to predicted ones. Figure 6.1 shows the comparison of laboratory-measured and predicted creep compliance values for Level 3 input data in arithmetic scale and logarithmic scale. Creep compliance values in all three temperatures were shown as one set of data in Figure 6.1.

The accuracy of the MEPDG model was evaluated based on the goodness of fit between the estimated and measured values with reference to the line of equality. A linear regression was fitted on plotted creep compliance data. The slope and intercept of predicted creep compliance values were calculated to show the possible underprediction or overprediction of the estimated values.

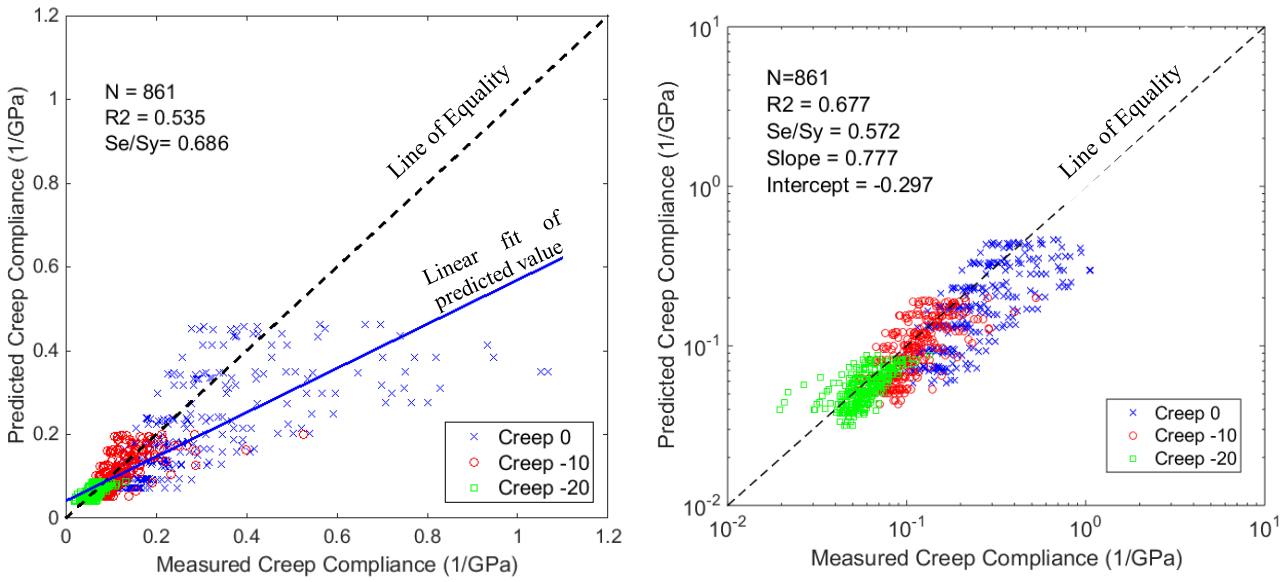

a) Arithmetic scale b) Logarithmic scale

Figure 6.1: MEPDG predicted creep compliance versus laboratory-measured values

The R^2 and Se/Sy of the MEPDG predictive model was 0.535 and 0.686, respectively. The SSE of the model was found as high as 8.297 (1/GPa) which implies high bias in predictions. The slope

and intercept were 0.500 and 0.041, which indicate the MEPDG model tends to underpredict the creep compliance.

Figure 6.2 shows the performance of MEPDG creep compliance predictive model at three test temperatures. The majority of predicted values at 0°C appears to be below the line of equality. This indicates that the models underestimate the creep values at 0°C. The R^2 and Se/Sy were 0.183 and 0.922 at this temperature, respectively. The predicted values at -20°C showed the best goodness of fit among the tested temperatures. The R^2 and Se/Sy at -20°C were 0.334 and 0.833, respectively. The SSE at 0°C had the highest value since the creep compliance values are much larger at this temperature when they were compared to -20°C.

Table 6.4 shows the summary of statistics of the overall MEPDG creep compliance prediction model, as well as at each test temperature. These results indicate that the MEPDG creep model is not reliable to predict creep compliance values.

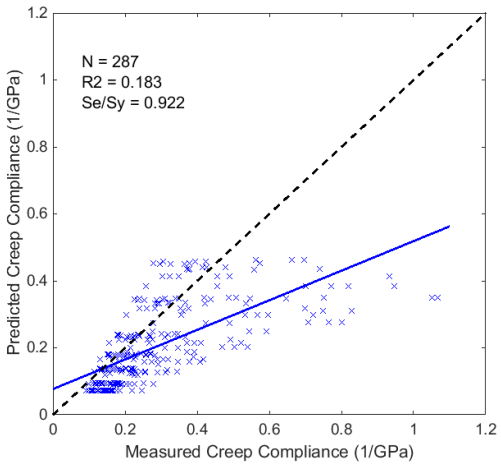

a) MEPDG model (0°C)

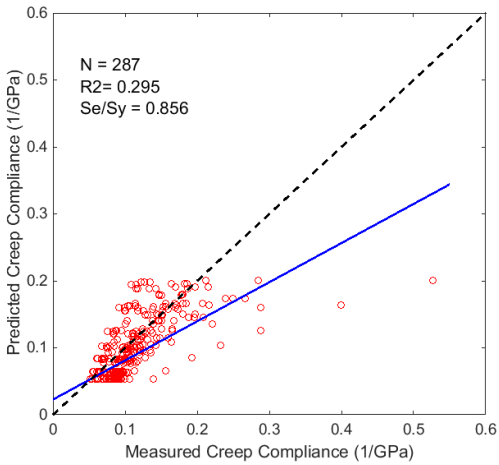

b) MEPDG model (-10°C)

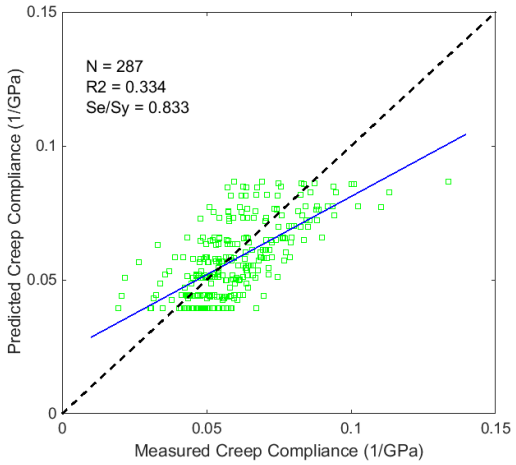

c) MEPDG model (-20°C)

Figure 6.2: MEPDG creep compliance predictive model

Table 6.4: Summary statistics of MEPDG creep compliance predictive model

Test Temperatures	R^2	Se/Sy	SSE (1/GPa)	slope	Intercept (1/GPa)
Overall	**0.535**	**0.686**	**8.297**	**0.500**	**0.041**
0°C	0.183	0.922	7.691	0.408	0.079
-10°C	0.295	0.856	0.558	0.513	0.043
-20°C	0.334	0.833	0.049	0.573	0.021

6.4 Local Calibration Alternatives

In the previous section, it was shown that the MEPDG model, without local calibration, performed poorly in prediction of creep compliance at all three temperatures. Previous studies reported that inaccurate creep compliance values can significantly impact thermal cracking model used in MEPDG software (Yin et al. 2009, Solanki et al. 2014). The thermal cracking model predicts the length of low temperature cracks and their rate of progression with time. Accurate creep compliance predictions can improve the accuracy of thermal cracking prediction and low temperature performance. The purpose of calibration is to minimize the error between the predicted values and laboratory-measured values.

Two alternative methods of calibration are used. First, the coefficients of MEPDG creep compliance model were independently updated for each temperature by using a nonlinear multiple regression model. In the second alternative method, an artificial Neural Network (ANN) is used to predict creep compliance values using a feed forward network.

6.4.1 Nonlinear Multiple Regression

A nonlinear multiple regression was conducted to update the coefficients for MEPDG creep compliance model. The objective of nonlinear multiple regression was to update the coefficients of the model while minimizing sum of squared errors between the predicted creep compliance and the laboratory-measured creep compliance values. Pavement ME Design uses a general creep compliance model as it was described in Equations 2.12 to 2.14. First, a general model was attempted to update the coefficients of the existing model using all three temperatures of creep

compliance, simultaneously. In the second attempt, temperature as an independent variable in Equations 2.13 and 2.14 were eliminated and creep compliance model was calibrated for each temperature, separately. When the nonlinear multiple calibration was separately attempted for each temperature, the results showed approximately 15% improvement in predicting creep compliance values compared to prediction of one general nonlinear model. The same approach was documented in NCHRP 704, where the temperature was removed from the creep compliance equation and a separate model was optimized for each temperature (NCHRP-673 2011).

Two main parameters of general creep compliance model in Equation 2.12, m and D_1, were replaced with existing Equations 2.13 and 2.14. The general expression of the model, where coefficients were replaced with b1 to b12, is shown in Equation 6.1. Twelve coefficients in this equation are required to be replaced with the new model coefficients. A numerical method was used to obtain the new coefficients while minimizing sum of squared errors between the predicted creep compliance from the model and the laboratory-measured creep compliance values. The general model that was used for calibration of each temperature is given in Equation 6.1.

$$D(t) = 10^{-\text{b1} + \text{b2 T} + \text{b3 log(Va)} + \text{b4 log(VFA)} - \text{b5 log(A)}}\, t^{\text{b6} - \text{b7 T} - \text{b8 Va} - \text{b9 VFA} + \text{b10 Pen77} + \text{b11 Pen77 (b12) T}} \quad (6.1)$$

The sum of square error between log of predicted values and log of measured values was minimized for each temperature separately as shown in Equation 6.2.

$$\text{Minimize} \sum (\log (CR_{Pr}) - \log (CR_M))^2 \quad (6.2)$$

Where: CR_{Pr} = is a matrix of predicted creep compliance values and CR_M = is a matrix of

laboratory-measured creep compliance values.

Table 6.5 shows the original coefficients as well as updated coefficients for each temperature after nonlinear multiple regression was completed.

Table 6.5: Globally calibrated and updated nonlinear regression of MEPDG model

Parameter	Original coefficient	Updated coefficient for 0°C	Updated coefficient for -10°C	Updated coefficient for -20°C
b1	-8.5240	15.9607	-8.4431	-2.5344
b2	0.0131	19.4842	-0.7962	0.1810
b3	0.7957	-1.9350	-0.1614	-0.3353
b4	2.0103	-3.7781	-0.8346	0.0129
b5	-1.9230	-13.2820	-3.9940	-0.1763
b6	1.1628	-1.4878	1.0927	1.1595
b7	-0.0019	28.7711	0.6952	0.0929
b8	-0.0460	0.1484	0.2249	0.0295
b9	-0.0113	0.0221	0.0272	0.0001
b10	0.0025	-0.0049	-0.1146	-0.0086
b11	0.0016	1.7498	-0.0657	-0.0092
b12	0.4605	2.0298	0.6717	0.4629

The reliability of nonlinear regression model was evaluated for each temperature, separately. Figure 6.3 shows the performance of nonlinear regression of MEPDG creep compliance predictive model at three test temperatures.

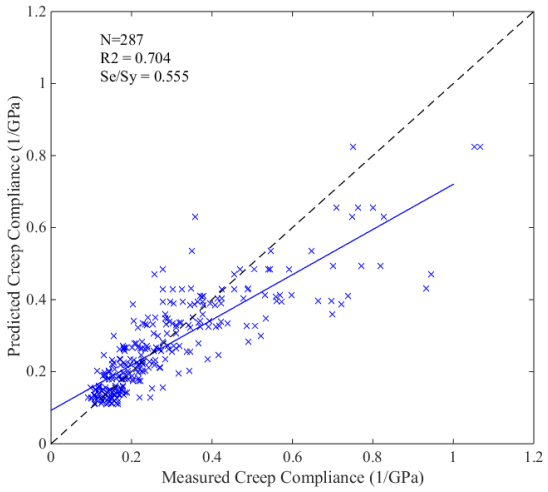

a) Nonlinear regression (0°C)

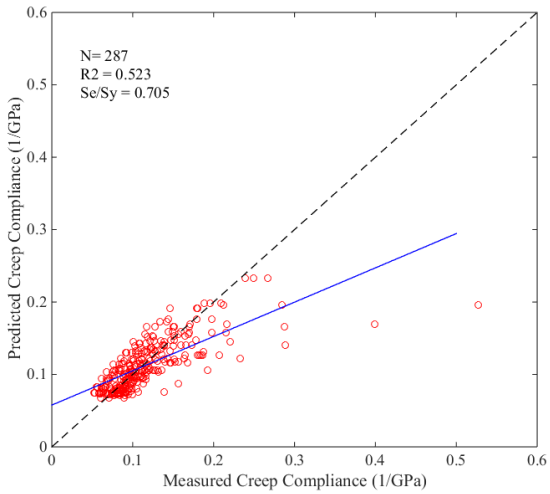

b) Nonlinear regression (-10°C)

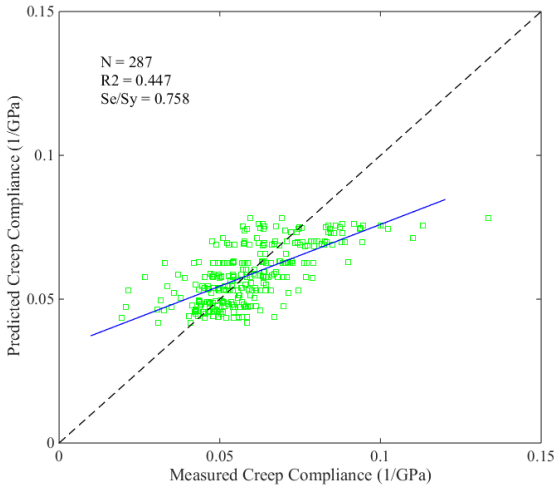

c) Nonlinear regression (-20°C)

Figure 6.3: Nonlinear regression of MEPDG creep compliance model at three test temperatures

Figure 6.4 compares the actual measured-laboratory creep compliance values with predicted creep values obtained from nonlinear multiple calibration model. The R^2 and Se/Sy of overall nonlinear regression model were 0.830 and 0.463, respectively. The SSE of nonlinear regression model was found to be 3.128 (1/GPa) which is less than half the value of SEE of globally calibrated model.

The slope and intercept of nonlinear regression model were 0.759 and 0.031, respectively.

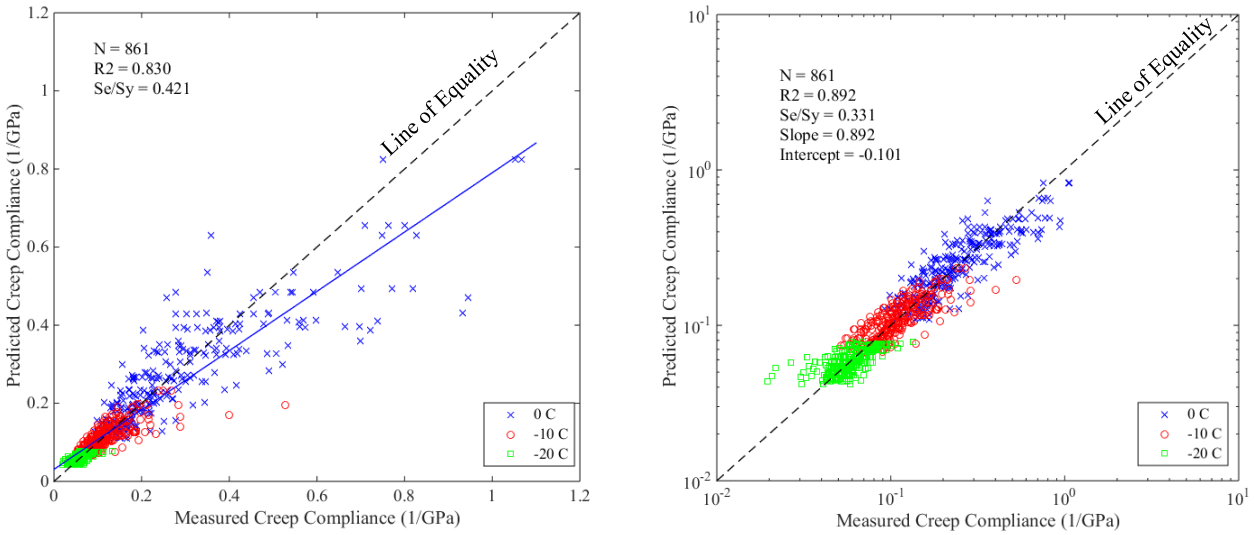

a) Arithmetic scale b) Logarithmic scale

Figure 6.4: Calibration of MEPDG creep compliance model using nonlinear regression

Table 6.6 shows the summary of statistics of the overall nonlinear prediction model and each separated temperature. Comparing the statistical parameters in table 6.6 with those in Table 6.4, it is observed that nonlinear regression at all three temperatures showed significant improvements. Therefore, it can be concluded that the nonlinear regression of MEPDG model is more reliable in prediction of creep compliance than the globally calibrated MEPDG model.

Table 6.6: Summary statistics of nonlinear regression of MEPDG creep compliance model

Test Temperatures	R^2	Se/Sy	SSE (1/GPa)	Slope	Intercept (1/GPa)
Overall	**0.830**	**0.421**	**3.128**	**0.759**	**0.031**
0°C	0.704	0.555	2.721	0.628	0.093
-10°C	0.523	0.705	0.368	0.474	0.058
-20°C	0.447	0.758	0.039	0.429	0.033

It should be noted that nonlinear regression is sensitive to seed coefficient values. Depending on the nonlinearity of the data, it is possible for regression to converge to local minima as opposed to the global minima, or to fail to converge.

6.4.2 Artificial Neural Network (ANN)

An artificial neural network is a mathematical model that consists of many interconnected elements called neurons. ANN is developed using a training data set to learn the relationship between input parameters and targets, and then generalize the learned relationship to new unseen data. Typically, three operations are required in ANN modeling; training, testing and validation. During training inputs along with desired targets are introduced to the network. The weights and biases for each neuron are iteratively calculated to generate the desired outputs (Lingireddy and Brion 2005). Testing is performed using an independent data set to ensure that the training and testing errors are both minimized. The validation is used to evaluate the performance of the model for new unseen data.

When a complex nonlinear relationship exists among input and output sets, use of two hidden

layers or more is preferred. For creep compliance model, it was found that one hidden layer provided reasonably acceptable results due to the limited range of mixes. Based on trial and error, a typical three-layered feed-forward back propagation ANN was developed.

The network includes one input layer, one hidden layer having seven neurons, and one output layer. A tan-sigmoid transfer function was used in the input layer, and a linear transfer function was used for the output layer. A feed forward error back propagation was performed, since back propagation is able to obtain the nonlinear relationship between input parameters and desired outputs (Pekcan et al. 2006).

Figure 6.5 shows the architecture of the neural network that was used in this study. Several attempts were made to select suitable input parameters. Only five parameters (voids in mineral aggregates, percent air voids, temperature, VTS and A and, slope and intercept of viscosity temperature) showed significant impact on predicting the desired outputs. Other parameters either did not have a significant impact, or reduced the network performance. To increase the efficiency of ANN model, preprocessing and postprocessing approach, known as network scaling, was conducted on both inputs and outputs.

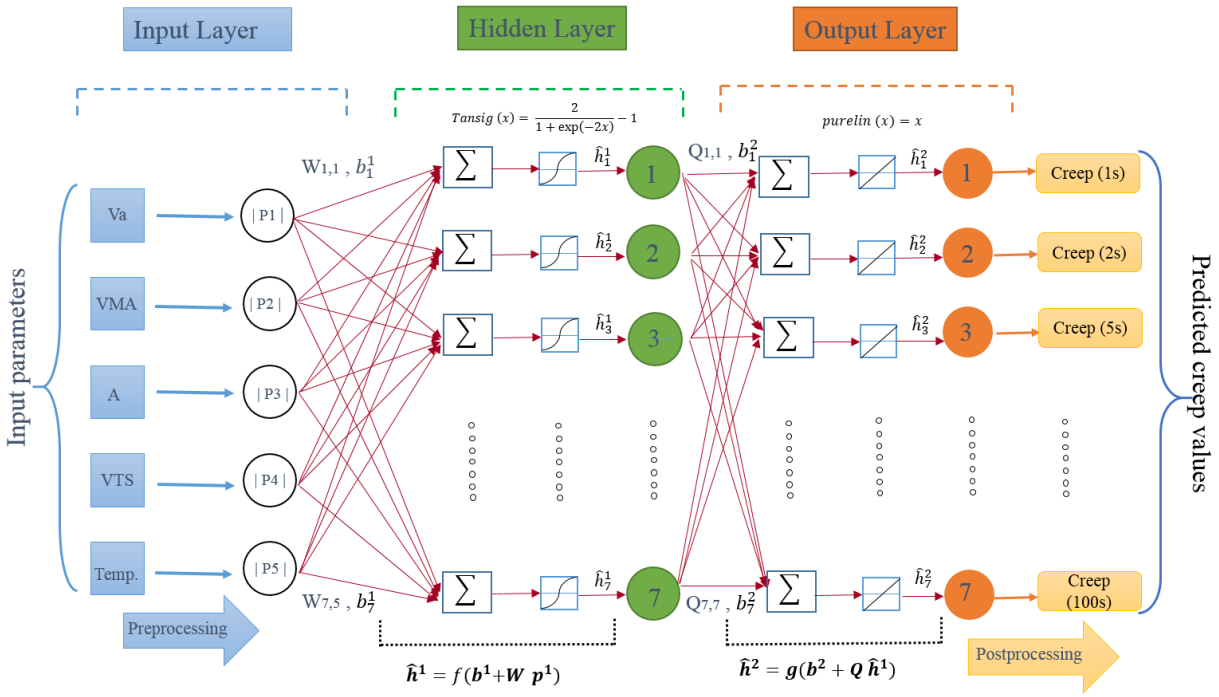

Figure 6.5: Architecture of the neural network

An ANN model provides the predictions based on training data set and the determined input ranges, therefore the model is recommended to be used for the mixes that fall within its inference space. If mixes that are outside the determined input ranges are to be used, the model should be retrained using data for their mix properties.

Generally, a large number of neurons or additional hidden layers provide more flexibility, since the network has more parameters that can be optimized. However, the purpose is to find the lowest number of neurons that provide the best performance. Excessive training and larger than necessary networks can result in overfitting of the training data. Overfitting results in minimizing the error in the training set, but not in the validation set. To avoid overfitting, the analysis ensured that the error in fitting the training set was approximately equal to the error in the validation set. In each

iteration, a randomized 70% (602 points) of the database was used for training, and the remaining 30% (259 points) of the data was used for validation. The verification data was independent from training data set. The calculated weights and biases in layers were extracted from neural network. The hidden layer weights (**W**), hidden layer biases ($\boldsymbol{b^1}$)**,** output layer weights (**Q**)**,** output layer biases ($\boldsymbol{b^2}$) of the developed ANN model coefficients are as follows:

$$\mathbf{W} = \begin{bmatrix} 2.458 & 0.092 & 0.130 & -0.640 & 0.799 \\ -0.102 & 0.043 & 0.050 & -0.018 & 0.294 \\ 0.019 & 0.066 & -0.022 & 0.090 & 0.354 \\ 2.410 & 0.040 & 0.305 & -0.230 & 0.124 \\ -0.416 & 0.018 & -0.049 & -0.057 & 0.289 \\ -0.873 & 0.096 & 0.001 & 0.306 & -1.365 \\ -0.729 & -0.784 & 0.385 & 0.490 & 1.356 \end{bmatrix} \tag{6.3}$$

$$\boldsymbol{b^1} = \begin{bmatrix} 0.298 \\ 0.064 \\ -0.012 \\ -0.323 \\ 0.427 \\ 0.088 \\ -2.281 \end{bmatrix} \tag{6.4}$$

$$\mathbf{Q} = \begin{bmatrix} -0.410 & 0.179 & 0.215 & 0.337 & 0.082 & -0.444 & 0.285 \\ -0.461 & 0.173 & 0.197 & 0.392 & 0.099 & -0.466 & 0.380 \\ -0.546 & 0.164 & 0.157 & 0.493 & 0.140 & -0.492 & 0.536 \\ -0.618 & 0.137 & 0.118 & 0.577 & 0.187 & -0.526 & 0.670 \\ -0.664 & 0.079 & 0.061 & 0.639 & 0.238 & -0.545 & 0.773 \\ -0.707 & 0.001 & -0.012 & 0.712 & 0.329 & -0.561 & 0.874 \\ -0.744 & 0.012 & -0.104 & 0.771 & 0.389 & -0.588 & 0.921 \end{bmatrix} \tag{6.5}$$

$$\boldsymbol{b^2} = \begin{bmatrix} -0.031 \\ 0.047 \\ 0.176 \\ 0.273 \\ 0.315 \\ 0.335 \\ 0.367 \end{bmatrix} \tag{6.6}$$

The bias ($\boldsymbol{b^1}$) is added to the multiplication of weight matrix (**W**) and input data ($\boldsymbol{P^1}$). Then, the tan-sigmoid transfer function is performed to obtain the outputs $(\hat{\boldsymbol{h}}^1)$ for hidden layer using Equations 6.7 and 6.8. The outputs of hidden layer are used as inputs for the output layer. The bias ($\boldsymbol{b^2}$) of output layer is added to the multiplication of weight matrix (**Q**) and input data $(\hat{\boldsymbol{h}}^1)$. Next, the purelin transfer function is perform using Equations 6.9 and 6.10. Finally, the postprocessing is performed on outputs to obtain the creep compliance values.

$$\hat{\boldsymbol{h}}^{\boldsymbol{1}} = f(\boldsymbol{b^1} + \boldsymbol{W}\ \boldsymbol{p^1}) \tag{6.7}$$

$$f\ (x) = \frac{2}{1+\exp(-2\ x)} - 1 \tag{6.8}$$

$$\hat{\boldsymbol{h}}^{\boldsymbol{2}} = g\ (\boldsymbol{b^2} + \boldsymbol{Q}\ \hat{\boldsymbol{h}}^{\boldsymbol{1}}) \tag{6.9}$$

$$g\ (x) = x \tag{6.10}$$

Where, x = variables (inputs); f = tan-sigmoid transfer function; g = purelin transfer function; $\boldsymbol{p}^1$ = postprocessed input variables; $\hat{\boldsymbol{h}}^1$ = transferred value at the hidden layer; $\hat{\boldsymbol{h}}^2$ = transferred value at the output layer; $\boldsymbol{W}$ = matrix of weight factors for the hidden layer; $\boldsymbol{Q}$ = matrix of weight factors for the output layer.

Figure 6.6 shows the comparison of the measured and predicted creep compliance values obtained from ANN model.

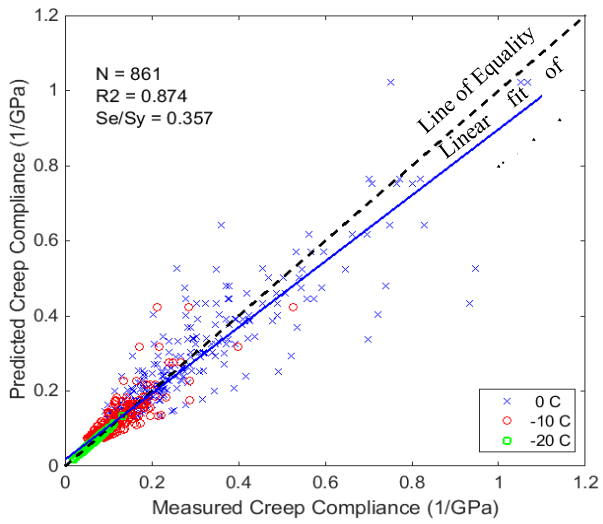

a) Arithmetic scale

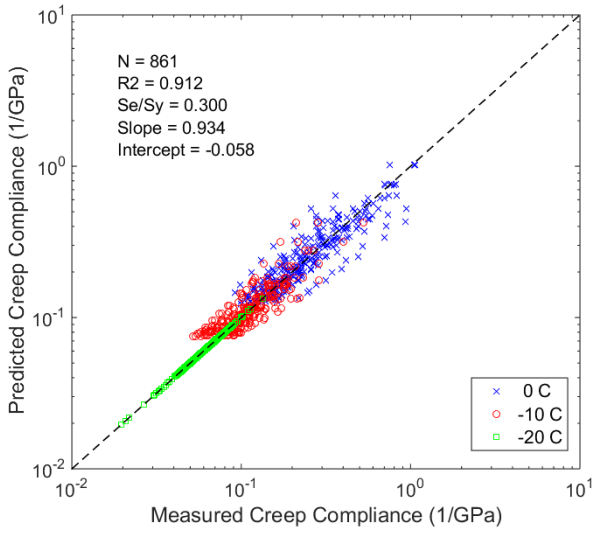

b) Logarithmic scale

Figure 6.6: Comparison of measured and predicted creep compliance values obtained from ANN model

The statistical results showed that the ANN model has a R^2 of 0.874 and Se/Sy of 0.357. The overall SSE of this model was found to be 2.243 (1/GPa). These results confirmed that the ANN model predicts the creep compliance values more accurately. The R^2, Se/Sy, and SSE of ANN model showed significant improvement compared to the globally calibrated MEPDG model. Figure 6.7 shows the performance of ANN model for each temperature. The predicted creep compliance values showed low bias at all three temperatures.

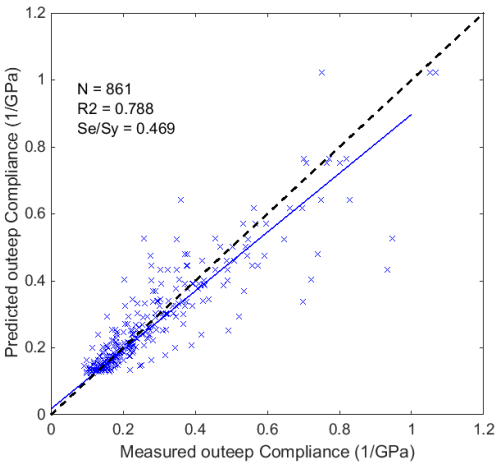

a) ANN model (0°C)

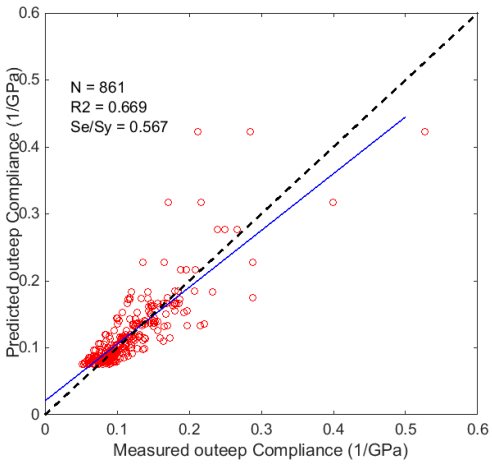

b) ANN model (-10°C)

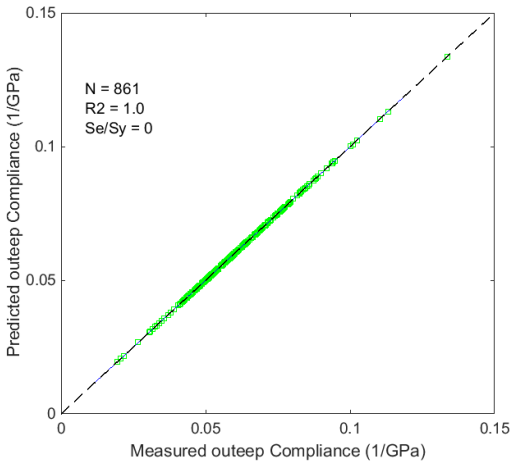

c) ANN model (-20°C)

Figure 6.7: ANN creep compliance predictive model performance at each test temperatures

The slope and intercept of ANN model are in agreement with the goodness of fit parameters. The majority of data is evenly distributed along the line of equality. These results show that ANN

model is a better alternative to calibrate the creep compliance model. Table 6.7 shows the summary of statistics for ANN creep compliance predictive model.

Table 6.7: Summary statistics of ANN creep compliance prediction model

Test Temperature	R^2	Se/Sy	SSE (1/GPa)	Slope	Intercept (1/GPa)
Overall	**0.874**	**0.357**	**2.243**	**0.890**	**0.017**
0°C	0.788	0.469	1.943	0.797	0.054
-10°C	0.669	0.587	0.255	0.849	0.021
-20°C	1.000	0.000	0.000	1.000	0.000

6.5 Comparison of Globally-Calibrated and Locally-Calibrated MEPDG Models

The reliability of models in predicting creep compliance values were evaluated based on goodness of fit statistics as well as slope and intercept of plotted data. In the assessment of goodness of fit statistics, R^2 and Se/Sy, and SSE were compared. The slope and intercept of plotted data were calculated by fitting a linear regression on plotted data to illustrate the potential for underprediction or overprediction of the model. The performance of the alternatives for predicting creep compliance is summarized in Table 6.8. The Nonlinear regression model and ANN predictive model produced higher accuracy and lower bias in comparison with the globally-calibrated MEPDG model. The ANN predictive model was found to be more reliable in prediction of creep compliance values at low temperature such as -20°C. Based on these results, it can be concluded that the ANN creep compliance model is able to produce creep compliance values that are close to laboratory-measured values. This can increase the accuracy of long-term performance prediction of AC mixes using Pavement ME Design program.

Table 6.8: Performance of globally-calibrated and locally-calibrated creep compliance models

Predictive model	R^2	Se/Sy	SSE (1/GPa)	slope	Intercept (1/GPa)
Globally-calibrated MEPDG model	0.535	0.686	8.297	0.500	0.041
Local-calibration using nonlinear regression	0.830	0.421	3.128	0.759	0.031
Local calibration using ANN	0.874	0.357	2.243	0.890	0.017

6.6 Summary

Local calibration can be used to improve the performance of the MEPDG creep compliance model for local materials, environment, and practices. This chapter presented two alternatives for local calibration of creep compliance of AC mixes: nonlinear multiple regression and artificial neural network. The performance of the MEPDG creep compliance predictive models was evaluated, and the following conclusions were drawn:

- This study showed that the MEPDG creep compliance model is a generic model. This model is not able to accurately predict creep values, particularly for mixes used in cold climates, in part because these mixes constituted only a small fraction of the mixes used to develop the creep compliance MEPDG model.
- For the particular dataset used in this analysis, the globally-calibrated MEPDG model, in general, underpredicted creep compliance. The model is less reliable for predicting creep compliance values at low temperatures (-20°C) than at other temperatures. The R^2 and Se/Sy of this model were 0.535 and 0.686, respectively.

- Nonlinear regression and ANN may be used as two alternatives to predict creep compliance values more reliably. The local-calibration can lead to better quantification of thermal cracking as well as other distresses such as roughness and the overall service life.
- Nonlinear multiple regression showed significant improvement in accuracy of creep compliance prediction at each individual test temperature.
- ANN model showed the highest reliability in prediction of creep compliance values at each test temperature.
- The ANN model was able to produce creep compliance values that were close to laboratory-measured values. This can increase the accuracy of long-term performance prediction of AC mixes using Pavement ME Design program.

CHAPTER 7 - EFFECT OF GLOBALLY AND LOCALLY CALIBRATED E* AND CREEP COMPLIANCE MODELS ON PREDICTED DISTRESSES FOR AC MIXES

7.1 Introduction

In the previous two chapters (Chapters 5 and 6), it was shown that globally calibrated (uncalibrated) models are not reliable to predict creep compliance and dynamic modulus values of local mixes for Level 3 input data. This chapter evaluates the impact of globally and locally calibrated creep compliance and dynamic modulus on predicted distresses using Pavement ME Design software.

In this chapter, predicted distresses for three Levels called; Manitoba default Level 3, Manitoba calibrated Level 3, and Manitoba Level 1 are compared. The differences between Manitoba default Level 3 and Manitoba calibrated Level 3 were in the dynamic modulus and creep compliance input

values. In Manitoba calibrated Level 3 input data, the creep compliance and dynamic modulus values are predicted by using the localized predictive models that were developed for the mixes in previous chapters. Updated nonlinear NCHRP 1-37A dynamic modulus predictive model and ANN creep compliance model were used to predict E* and creep compliance values for Manitoba calibrated Level 3 input data, respectively. For Manitoba default Level 3, globally calibrated creep compliance and dynamic modulus values were used. The measured-laboratory values were used for Manitoba Level 1 input data.

Three mixes Mix-0-0, Mix-0-15, and Mix-0-50 were selected to evaluate their long-term performance using Pavement ME Design program. Mix-0-0 and Mix-0-50 were selected as these two mixes had the lowest and highest amounts of RAP content. Mix-0-15 was selected since this mix showed the optimal laboratory low and high temperature performance as presented in Chapter 4 and is the maximum allowable amount of RAP for use in surface layer in Manitoba highways.

The goal of this chapter is to evaluate the long-term performance of asphalt mixes containing RAP and to assess the possible difference in performance of the abovementioned mixes for three Levels; Manitoba default Level 3, Manitoba calibrated Level 3, and Manitoba Level 1.

A section of Provincial Truck Highway 1 (PTH 1) located at west of the city of Winnipeg in Manitoba was selected as the design example presented in this chapter. This section is a four-lane two-way highway with annual average daily truck traffic (AADTT) of 1660. It was assumed that 50% of total trucks is in the design direction and 100% trucks of each direction is on the design lane. The design life of the pavement is assumed to be 20 years. Winnipeg was selected as the project environmental condition and its historical climate data was used in all analysis. The typical Manitoba structural thicknesses were estimated based on subgrade strength and traffic level and used in this analysis. In order to evaluate the asphalt mix performance, the thicknesses for all layers

were kept unchanged.

Table 7.1 shows the required asphalt mix and asphalt binder inputs data for Level 1 and Level 3. For Level 1 input data, all the tests and properties are required except the aggregate gradation. However, in Level 3, basic properties of the mix such as mix design properties and aggregate gradation and performance grade of asphalt binder should be entered into to the software. Other laboratory properties of mixes were estimated based on models and default data.

Table 7.1: Required asphalt mix and asphalt binder inputs data for Level 1 and Level 3

Input data	Test measurement	Levels of input	
		Level 1	Level 3
Asphalt mix	Mix Design (VMA %, Va %, and asphalt content percentages)	√	√
	Aggregate Gradation	x	√
	Dynamic modulus	√	x
	Creep Compliance (-20°C,-10°C, and 0°C)	√	x
	Indirect Tensile (-10°C)	√	x
Asphalt binder	Performance Grade	x	√
	Complex Shear Modulus (G*)	√	x
	Phase angle (δ)	√	x

7.2 Materials Properties

7.2.1 Unbound Materials Inputs

Typical properties of Manitoba unbound materials were used for all the analyzed Levels. Table 7.2 shows the subgrade, subbase and base material properties and their layer thicknesses.

Table 7.2: Unbound materials properties

Properties	Subgrade	Subbase	Base
Materials Type	A-7-6	Crushed lime stone C-base	Crushed lime stone A-base
Thickness (mm)	-	300	200
Resilient Modulus (MPa)	30	120	140
Moisture Content (%)	29	8	10.8
Liquid limit	75	6	6
Plasticity index	42	1	1
Maximum Dry Density (Kg/m^3)	1410	2220	2170

7.2.2 Asphalt Binder and Asphalt Mix Inputs

The thickness of asphalt mix layer was 150 mm for all the mixes. Complex shear modulus (G*) and phase angle (δ) for three mixes were measured by using DSR. Binder performance grade inputs are shown in Table 7.3 which was provided by MI. The volumetric properties and aggregate gradations of these mixes are shown in Tables 7.4 and 7.5, respectively.

Table 7.3: Binder complex shear modulus (G^*) and phase angle (δ)

Mix design	Temperature (degree C)	Complex shear modulus G^* (Pa)	Phase angle δ (degree)
Mix-0-0	15	3000000	57
	35	116000	71
	58	3550	82
	64	1700	85
Mix-0-15	15	3640000	58
	35	130000	71
	58	3570	83
	64	1680	85
Mix-0-50	15	7580000	44
	35	331000	63
	64	3690	81
	70	1640	84

Table 7.4: Volumetric properties of the mixes

Mix ID	Mix Properties						Extracted Binder PG
	AC, %	VMA, %	V_a %	V_{be} %	VFA, %	Gmm	
Mix-0-0	6.0	15.2	4.2	11.0	72.7	2.445	58-28
Mix-0-15	5.9	13.7	3.8	9.9	72.3	2.437	58-28
Mix-0-50	5.2	12.2	3.6	8.6	70.6	2.516	64-16

AC=percent asphalt content; VMA= voids in mineral aggregates; V_a = percent air voids; V_{be} = effective Asphalt Content by Volume; VFA= voids filled with asphalt binder; G_{mm}= maximum theoretical spesific gravity

Table 7.5: Aggregate gradation of the mixes

Mix ID	Aggregate Gradation								
	19 mm	16 mm	12.5 mm	9.5 mm	4.75 mm	2.0 mm	425 µm	180 µm	75 µm
Mix-0-0	100.0	98.6	90.4	80.2	64.4	50.1	25.8	10.0	4.5
Mix-0-15	100.0	98.5	91.8	80.2	61.2	48.1	28.0	8.0	3.7
Mix-0-50	100.0	98.8	94.2	83.3	66.3	50.7	27.7	9.6	6.7

The globally and locally calibrated creep compliance values and dynamic modulus values as well as laboratory-measured values used in the analysis of mixes are shown in Tables 7.6 and 7.7, respectively. Since the E* values at -10°C of Mix-0-50 exceeded the maximum allowable dynamic modulus input in this software, the dynamic modulus at -10°C of mixes was not used in Pavement ME Design software.

Table 7.6: Creep compliance values obtained from different Levels

Mix Type	Loading Time (s)	Globally Calibrated Model			Locally Calibrated Model			Measured Laboratory Creep Compliance		
		(- 20°C)	(-10°C)	(0°C)	(- 20°C)	(-10°C)	(0°C)	(- 20°C)	(-10°C)	(0°C)
Mix-0-0	1	0.0288	0.0424	0.0553	0.0498	0.0836	0.1336	0.0511	0.0812	0.1710
	2	0.0318	0.0500	0.0729	0.0514	0.0884	0.1459	0.0539	0.0853	0.1902
	5	0.0363	0.0621	0.1051	0.0552	0.0974	0.1697	0.0582	0.0932	0.2291
	10	0.0401	0.0732	0.1385	0.0588	0.1066	0.1958	0.0632	0.1020	0.2717
	20	0.0443	0.0863	0.1825	0.0642	0.1189	0.2316	0.0694	0.1131	0.3314
	50	0.0505	0.1072	0.2629	0.0753	0.1435	0.3040	0.0808	0.1352	0.4533
	100	0.0558	0.1264	0.3465	0.0884	0.1714	0.3867	0.0934	0.1586	0.5904
Mix-0-15	1	0.0284	0.0409	0.0528	0.0479	0.0756	0.1461	0.0461	0.0848	0.1392
	2	0.0313	0.0481	0.0694	0.0494	0.0802	0.1640	0.0479	0.0899	0.1521
	5	0.0356	0.0596	0.0997	0.0521	0.0889	0.2005	0.0516	0.0995	0.1771
	10	0.0393	0.0702	0.1311	0.0552	0.0978	0.2425	0.0551	0.1103	0.2054
	20	0.0433	0.0826	0.1723	0.0598	0.1091	0.3020	0.0599	0.1237	0.2448
	50	0.0493	0.1024	0.2475	0.0684	0.1307	0.4239	0.0687	0.1498	0.3228
	100	0.0543	0.1204	0.3255	0.0778	0.1540	0.5646	0.0773	0.1776	0.4098
Mix-0-50	1	0.0235	0.0349	0.0453	0.0488	0.0760	0.1576	0.0386	0.0567	0.1262
	2	0.0253	0.0400	0.0564	0.0503	0.0818	0.1806	0.0397	0.0600	0.1453
	5	0.0278	0.0478	0.0753	0.0533	0.0937	0.2289	0.0416	0.0664	0.1772
	10	0.0299	0.0548	0.0936	0.0561	0.1073	0.2869	0.0435	0.0737	0.2239
	20	0.0322	0.0627	0.1165	0.0591	0.1249	0.3704	0.0453	0.0834	0.3009
	50	0.0355	0.0750	0.1555	0.0646	0.1617	0.5461	0.0494	0.1059	0.4501
	100	0.0381	0.0859	0.1934	0.0704	0.2048	0.7533	0.0552	0.1327	0.6420

Table 7.7: Dynamic modulus values obtained from different Levels

	Mix	Dynamic Modulus (E*), MPa						
		Temp., °C	0.1 Hz	0.5 Hz	1 Hz	5 Hz	10 Hz	25 Hz
Globally Calibrated Model	Mix-0-0	**-10**	16725	19665	20907	23678	24810	26240
		5	5667	7778	8804	11410	12609	14244
		25	970	1544	1873	2867	3407	4092
		40	301	490	604	979	1199	1558
	Mix-0-15	**-10**	16616	19533	20763	23510	24632	26050
		5	5641	7738	8757	11343	12534	14156
		25	968	1541	1868	2857	3395	4070
		40	302	490	604	977	1196	1554
	Mix-0-50	**-10**	27428	30473	31697	34316	35345	36615
		5	11262	14422	15860	19298	20794	22759
		25	2003	3087	3680	5389	6274	7396
		40	560	910	1119	1783	2163	2769
Locally Calibrated Model	Mix-0-0	**-10**	21691	24960	26225	28805	29763	30895
		5	8582	12021	13617	17409	19023	21088
		25	1520	2636	3299	5340	6442	8043
		40	481	844	1079	1900	2405	3245
	Mix-0-15	**-10**	22672	25960	27228	29807	30762	31890
		5	9270	12831	14470	18339	19976	22065
		25	1746	2969	3687	5866	7030	8748
		40	575	990	1255	2166	2718	3629
	Mix-0-50	**-10**	26605	28807	29615	31196	31762	32417
		5	13410	17038	18575	21948	23286	24927
		25	2679	4398	5349	8041	9386	11467
		40	769	1347	1710	2916	3621	4745
Measured Laboratory E*	Mix-0-0	**-10**	19285	23299	24807	28174	29857	32265
		5	7609	10899	12424	16222	17990	20267
		25	1922	3149	3940	6232	7438	9457
		40	400	647	829	1550	1957	3016
	Mix-0-15	**-10**	18565	22234	23707	26883	28287	29813
		5	7540	10553	12026	15547	17131	19314
		25	2530	4052	4944	7485	8937	10695
		40	638	981	1201	2028	2547	3479
	Mix-0-50	**-10**	29227	33806	35585	39420	41210	42866
		5	10170	13858	15395	19680	21283	23827
		25	2486	4026	4875	7688	9085	10954
		40	786	1223	1512	2599	3298	4308

7.3 Predicted Distresses of the Asphalt Mixes For Different Levels

For all of the three mixes, the same subgrade, subbase and base properties and thickness were used to evaluate the impact of asphalt binder and mix properties in Manitoba Level 1, Manitoba default Level 3, and Manitoba calibrated Level 3. The reliability for each distress was selected to be 90% for 20 years pavement design life. The distress criteria of predicted distresses were selected based on MEPDG manual of practice recommendation and Manitoba specification. Tables 7.8 through 7.10 summarized the comparison of distress prediction among Manitoba Level 1, Manitoba default Level 3, and Manitoba calibrated Level 3 input data.

The limits of international roughness index (IRI) and AC thermal cracking were chosen as 2.5 m/Km and 200 m/km, respectively. The maximum value of AC surface down cracking (longitudinal cracking) and AC bottom up cracking (alligator cracking) were selected as 380 m/km and 15%, respectively. The limits for permanent deformation (AC only), and permanent deformation (total pavement rutting) were selected as 12 mm and 19 mm, respectively. The main focus of this study is on AC rutting, thermal cracking, and fatigue cracking, although other distresses were evaluated.

As it can be seen from Tables 7.8 to 7.10, the Manitoba calibrated Level 1 input data showed a better predicted performance when it was compared to Manitoba default Level 3 input data for all mixes regardless of RAP content.

Table 7.6: Predicted performance of Mix-0-0 for Level 1, Manitoba default Level 3, and Manitoba calibrated Level 3

Distresses		Input Data		
		Manitoba Default Level 3	Manitoba Calibrated Model	Manitoba Level 1
Terminal IRI	Target (m/Km)	2.5	2.5	2.5
	Predicted (m/Km)	2.8	2.53	2.53
	Reliability (%)	78.1	88.8	88.8
	Acceptance	**Fail**	**Fail**	**Fail**
	Predicted life at 90% reliability (yrs)	16	19	19
AC Surface Down Cracking	Target (m/Km)	380	380	380
	Predicted (%)	506.2	64	50.8
	Reliability (%)	82.3	100	100
	Acceptance	**Fail**	Pass	Pass
	Predicted life at 90% reliability (yrs)	10	>20	>20
AC Bottom Up Cracking	Target (%)	15	15	15
	Predicted (%)	11.6	1.6	1.7
	Reliability (%)	95.86	100	100
	Acceptance	Pass	Pass	Pass
	Predicted life at 90% reliability (yrs)	>20	>20	>20
AC Thermal Fracture	Target (m/Km)	200	200	200
	Predicted (m/Km)	608.6	491	491
	Reliability (%)	11	0.2	0.2
	Acceptance	**Fail**	**Fail**	**Fail**
	Predicted life at 90% reliability (yrs)	< 2	< 2	< 2
Permanent Deformation (AC Rutting only)	Target (mm)	12	12	12
	Predicted (mm)	6.8	0.84	0.9
	Reliability (%)	100	100	100
	Acceptance	Pass	Pass	Pass
	Predicted life at 90% reliability (yrs)	>20	>20	>20
Permanent Deformation (Total Pavement Rutting)	Target (mm)	19	19	19
	Predicted (mm)	19.9	12	11.8
	Reliability (%)	81.9	100	100
	Acceptance	**Fail**	Pass	Pass
	Predicted life at 90% reliability (yrs)	17	>20	>20

Table 7.7: Predicted performance of Mix-0-15 for Level 1, Manitoba default Level 3, and Manitoba calibrated Level 3

Distresses		Input Data		
		Manitoba Default Level 3	Manitoba Calibrated Model	Manitoba Level 1
Terminal IRI	Target (m/Km)	2.5	2.5	2.5
	Predicted (m/Km)	2.8	2.53	2.53
	Reliability (%)	78.1	88.8	88.8
	Acceptance	**Fail**	**Fail**	**Fail**
	Predicted life at 90% reliability (yrs)	16	19	19
AC Surface Down Cracking	Target (m/Km)	380	380	380
	Predicted (%)	468.5	62.1	50.3
	Reliability (%)	84.6	100	100
	Acceptance	**Fail**	Pass	Pass
	Predicted life at 90% reliability (yrs)	12	>20	>20
AC Bottom Up Cracking	Target (%)	15	15	15
	Predicted (%)	6.2	1.62	1.6
	Reliability (%)	99.9	100	100
	Acceptance	Pass	Pass	Pass
	Predicted life at 90% reliability (yrs)	>20	>20	>20
AC Thermal Fracture	Target (m/Km)	200	200	200
	Predicted (m/Km)	608.6	491	491
	Reliability (%)	11	0.2	0.2
	Acceptance	**Fail**	**Fail**	**Fail**
	Predicted life at 90% reliability (yrs)	< 2	< 2	< 2
Permanent Deformation (AC Rutting only)	Target (mm)	12	12	12
	Predicted (mm)	6.8	0.8	0.9
	Reliability (%)	100	100	100
	Acceptance	Pass	Pass	Pass
	Predicted life at 90% reliability (yrs)	>20	>20	>20
Permanent Deformation (Total Pavement Rutting)	Target (mm)	19	19	19
	Predicted (mm)	19.9	11.9	11.8
	Reliability (%)	82.9	100	100
	Acceptance	**Fail**	Pass	Pass
	Predicted life at 90% reliability (yrs)	17	>20	>20

Table 7.8: Predicted performance of Mix-0-50 for Level 1, Manitoba default Level 3, and Manitoba calibrated Level 3

Distresses		Input Data		
		Manitoba Default Level 3	Manitoba Calibrated Model	Manitoba Level 1
Terminal IRI	Target (m/Km)	2.5	2.5	2.5
	Predicted (m/Km)	2.7	2.6	2.6
	Reliability (%)	81.5	87.7	87.6
	Acceptance	**Fail**	**Fail**	**Fail**
	Predicted life at 90% reliability (yrs)	17	19	19.5
AC Surface Down Cracking	Target (m/Km)	380	380	380
	Predicted (%)	316.7	51.3	51.7
	Reliability (%)	93.9	100	100
	Acceptance	Pass	Pass	Pass
	Predicted life at 90% reliability (yrs)	>20	>20	>20
AC Bottom Up Cracking	Target (%)	15	15	15
	Predicted (%)	3.1	1.8	1.8
	Reliability (%)	100	100	100
	Acceptance	Pass	Pass	Pass
	Predicted life at 90% reliability (yrs)	>20	>20	>20
AC Thermal Fracture	Target (m/Km)	200	200	200
	Predicted (m/Km)	608.6	491	491
	Reliability (%)	11	0.2	0.2
	Acceptance	**Fail**	**Fail**	**Fail**
	Predicted life at 90% reliability (yrs)	< 1	< 1	< 1
Permanent Deformation (AC Rutting only)	Target (mm)	12	12	12
	Predicted (mm)	5	1.3	1.4
	Reliability (%)	100	100	100
	Acceptance	Pass	Pass	Pass
	Predicted life at 90% reliability (yrs)	>20	>20	>20
Permanent Deformation (Total Pavement Rutting)	Target (mm)	19	19	19
	Predicted (mm)	17.7	12.9	13
	Reliability (%)	96.5	100	100
	Acceptance	Pass	Pass	Pass
	Predicted life at 90% reliability (yrs)	>20	>20	>20

When Manitoba default Level 3 was used for Mix-0-0 and Mix-0-15, all the predicted distresses failed to meet the distress criteria except AC permanent deformation. In contrast, when Manitoba Level 1 or calibrated Level 3 were used as input data, only IRI and AC thermal cracking failed to meet the distress criteria. AC thermal cracking failed to meet the specified target 200 m/km for all mixes. This indicated that the binder type used in these mixes might not be adequate for Manitoba weather.

The predicted life at 90% reliability for each distress was higher for Manitoba Level 1 and calibrated Level 3 asphalt mix data compared to the Manitoba default Level 3 asphalt mix data, regardless of the distress prediction passed or failed to meet the target criterion. In other words, the amounts of predicted distresses were lower for Manitoba Level 1 and Manitoba calibrated Level 3 asphalt data compared to the Manitoba default Level 3 asphalt mix data.

All the predicted distresses from each Level were normalized by dividing the predicted distress values obtained from Manitoba default Level and Manitoba calibrated Level to corresponding predicted distress values obtained from Manitoba Level 1. Figures 7.1 to 7.3 show a relative difference in predicted distresses of each mix for three Levels of input data.

The predicted performance of Manitoba default Level 3 showed higher normalized number in predicted rutting and fatigue distresses compared to calibrated Level 3. This indicates that Manitoba default Level 3 overpredicts the distresses of the asphalt mix. The predicted performance of Manitoba calibrated Level 3 was found similar to Level 1 input data for all three mixes. This implies that utilizing locally calibrated models improve the reliability of MEPDG prediction.

Therefore, Manitoba calibrated Level 3 asphalt mix input data can be used for the analysis and design of Manitoba mixes with comparable accuracy of Level 1 input data. This can save

tremendous time and cost since it is time consuming and expensive to provide laboratory asphalt testing for each mix.

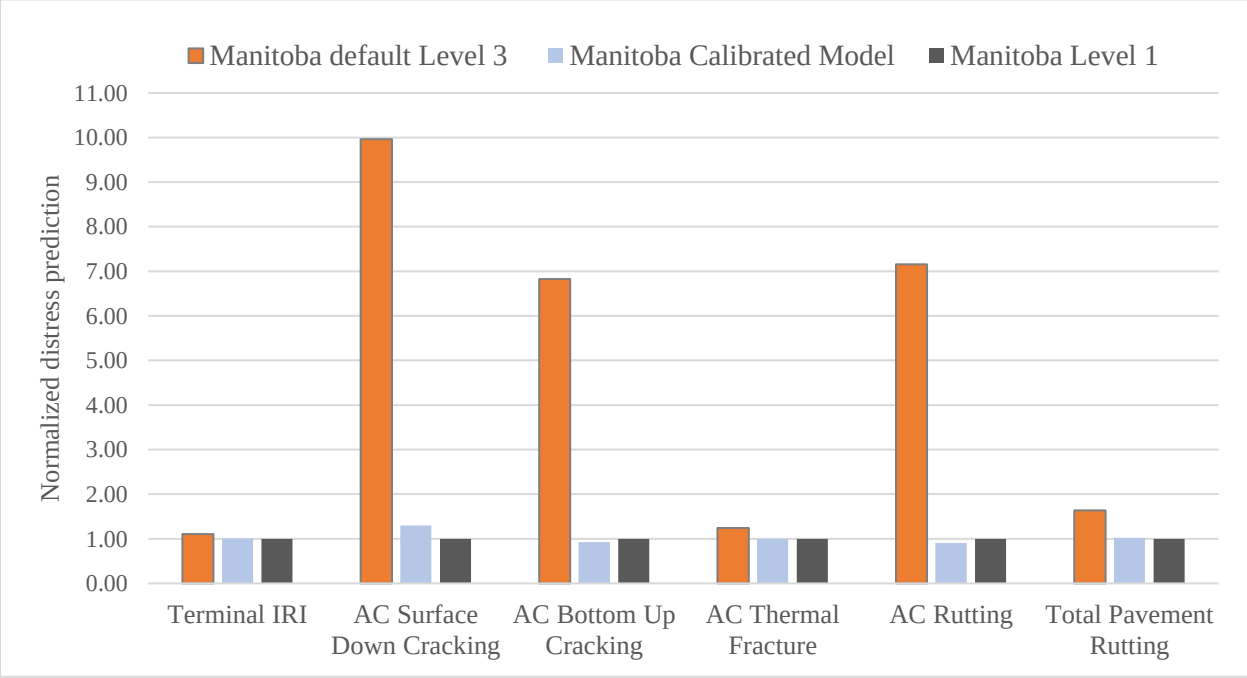

Figure 7. 1: Long-term performance of Mix-0-0 for three Levels of input

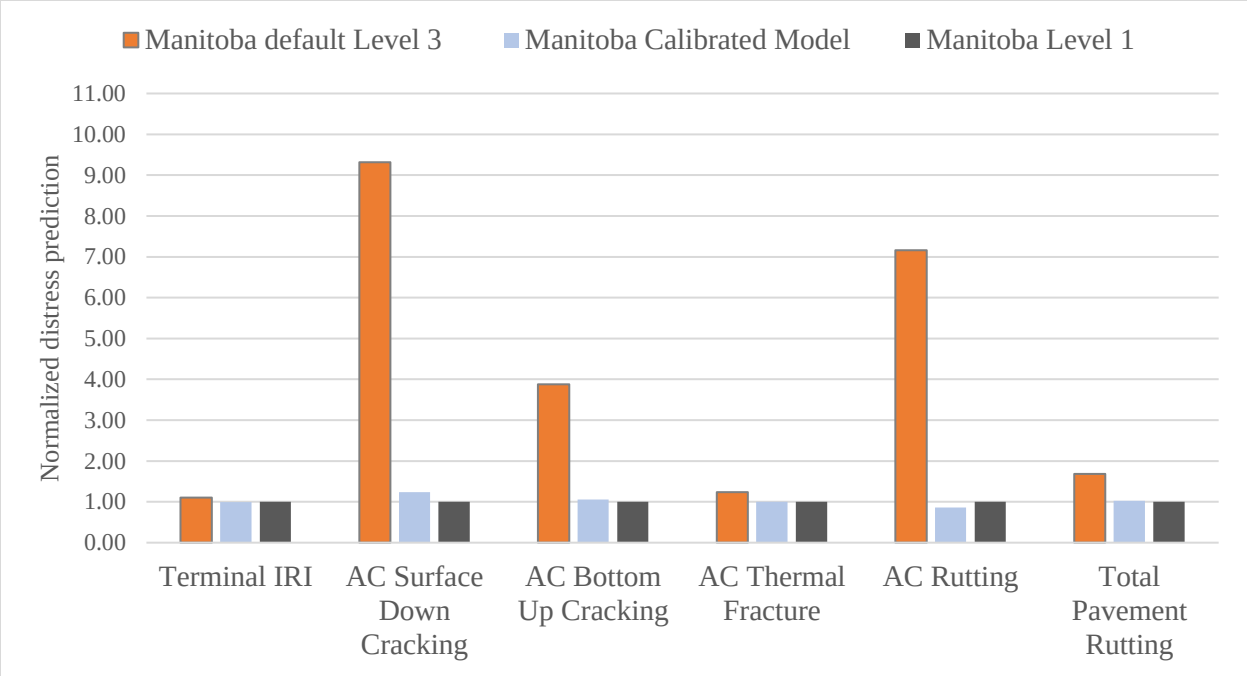

Figure 7.2: Long-term performance of Mix-0-15 for three Levels of input

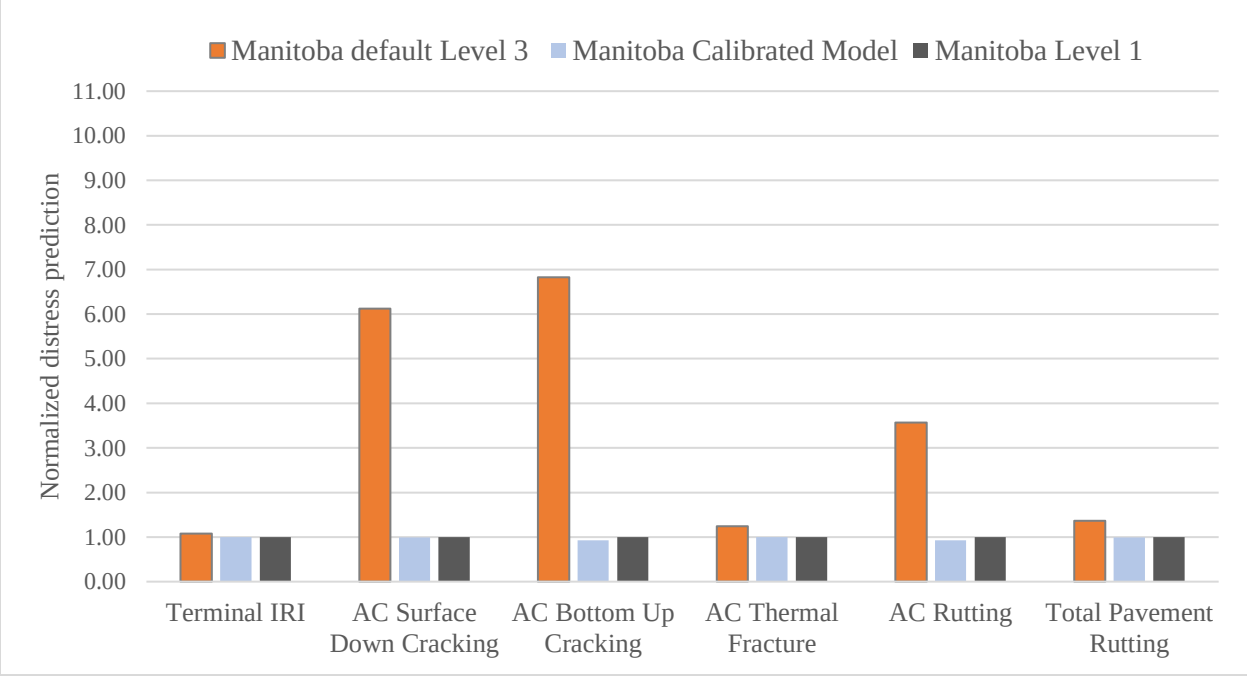

Figure 7.3: Long-term performance of Mix-0-50 for three Levels of input

It should be noted that the predicted AC rutting and AC thermal cracking for Level 1 agreed with

the laboratory findings. In Chapter 4, it was found that Mix-0-0 and Mix-0-15 have similar low and high temperature performance. The predicted AC rutting and AC thermal cracking of Mix-0-0 and Mix-0-15 were found to be very similar for Manitoba Level 1 input data. Alternatively, laboratory results of Mix-0-50 showed very high stiffness (low creep compliance) at low temperature which agreed with the predicted AC thermal cracking by Pavement ME Design software.

7.4 Long-Term Performance of Mixes Containing Different Amounts of RAP for Manitoba Calibrated Level 3 Analysis

The predicted distresses of mixes for Manitoba calibrated Level 3 were plotted. Figure 7.4 shows the IRI performance of the mixes. The terminal IRI of all three mixes were slightly more than 2.5 at the end of 20 years pavement design life. It should be noted that MEPDG roughness prediction can be affected by the predicted cracking and other distresses. It is expected that if the design meets thermal cracking criterion, it will change the predicted roughness as well.

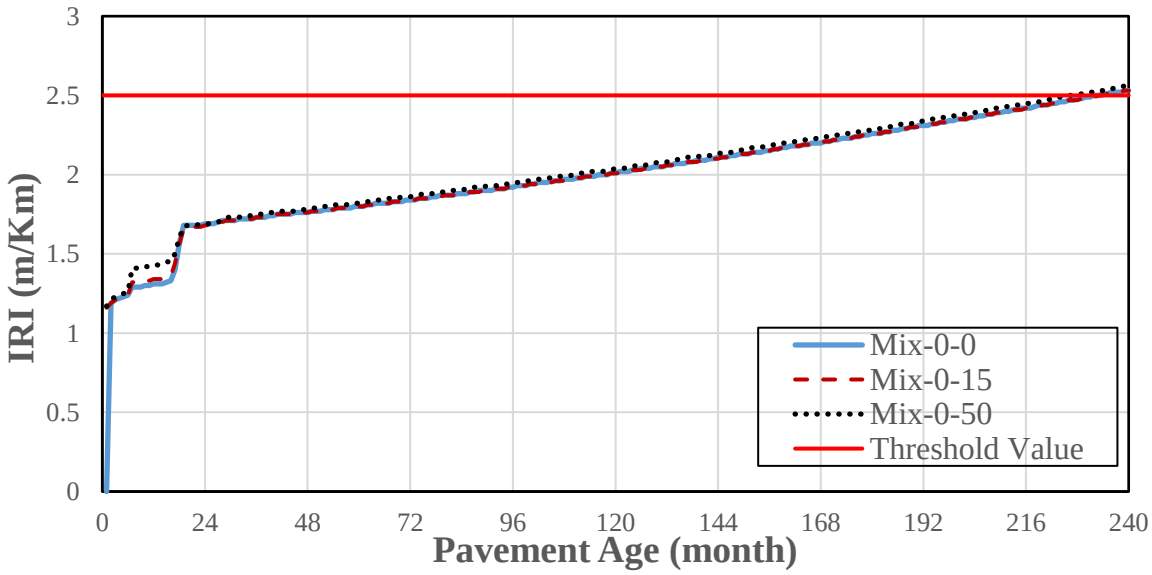

Figure 7.4: Predicted IRI and pavement life for mixes

Two figures are presented for each distresses to show a better comparison between the mixes. The first figure presents the performance of the mixes as compared to threshold values and the second figure shows more detail of the distresses for better comparison of predicted performance between mixes.

Figure 7.5 shows the predicted alligator cracking of three mixes and pavement life. All the mixes successfully met the specified alligator cracking criterion. Figure 7.5-b shows that Mix-0-50 has higher amounts of alligator cracking compared to Mix-0-0 and Mix-0-15 although the difference is very low. This could be due to higher the dynamic modulus values at intermediate temperatures.

Figure 7.6 shows the predicted longitudinal cracking of three mixes and pavement life. Mix-0-50 shows lower predicted longitudinal cracking in comparison to the other mixes.

Predicted thermal cracking of the mixes are shown in Figure 7.7. It should be noted that the PG 58-28 is a common asphalt binder performance grade used in Manitoba and the city of Winnipeg mixes. The binder performance grade of Mix-0-0 and Mix-0-15 was PG 58-28 and the binder performance grade of Mix-0-50 was PG 64-16.

Figure 7.7 shows that all the mixes failed to meet the thermal cracking criterion. Figure 7.7-b shows the thermal cracking resistance of the mixes up to the second year of pavement life. Mix-0-50 exceeded the thermal criterion before the first year of pavement life. The results of this prediction showed that PG 58-28 is not sufficient for Manitoba cold season.

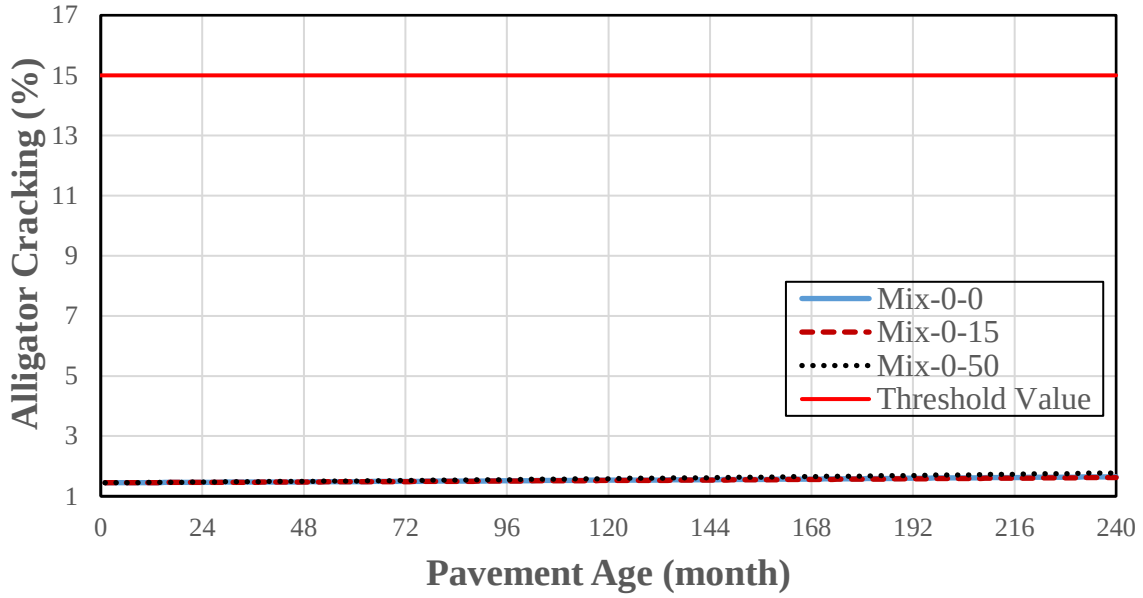

a) Alligator cracking of the mixes with respect to target value

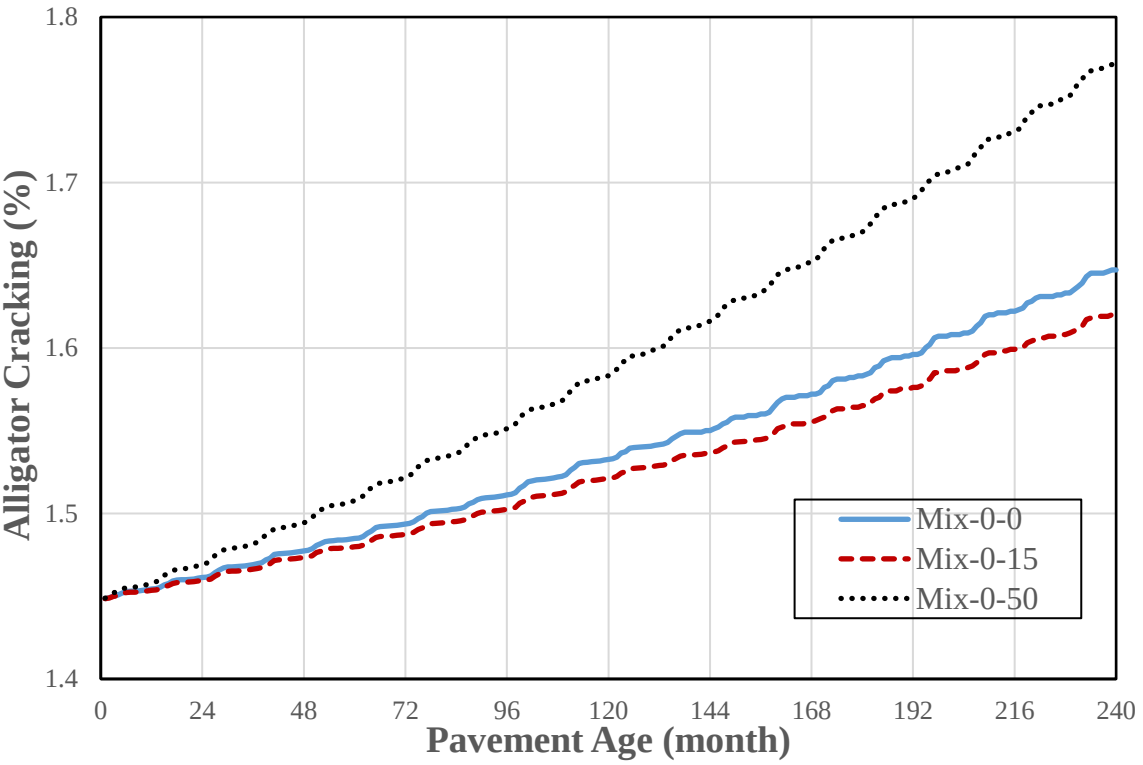

b) Comparison of alligator cracking of the mixes

Figure 7.5: Predicted alligator cracking and pavement life of mixes

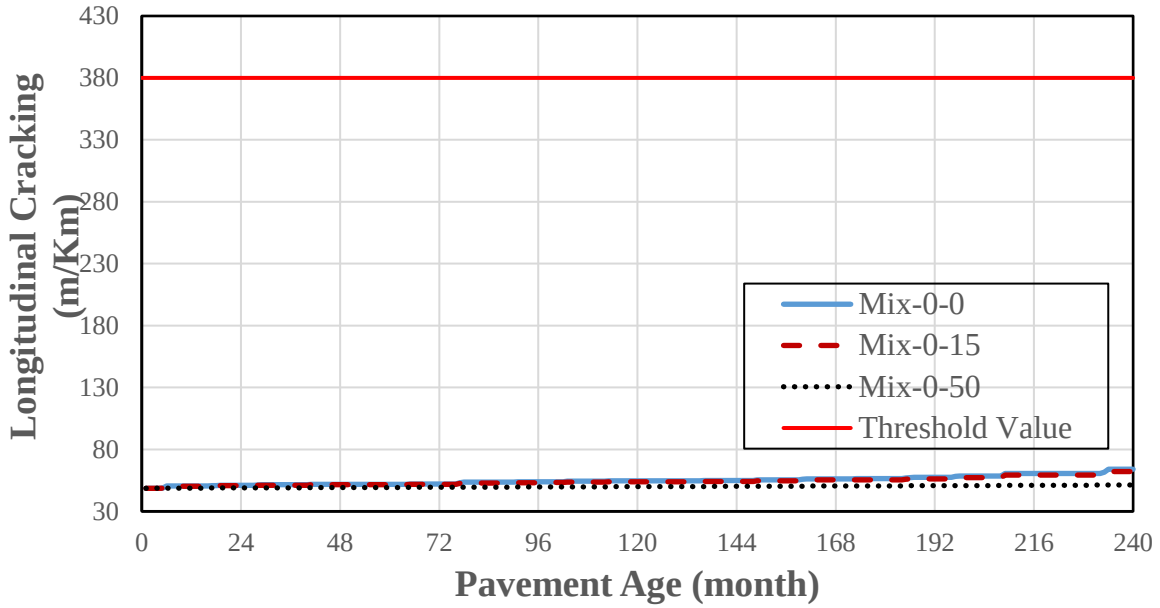

a) Longitudinal cracking of the mixes with respect to target value

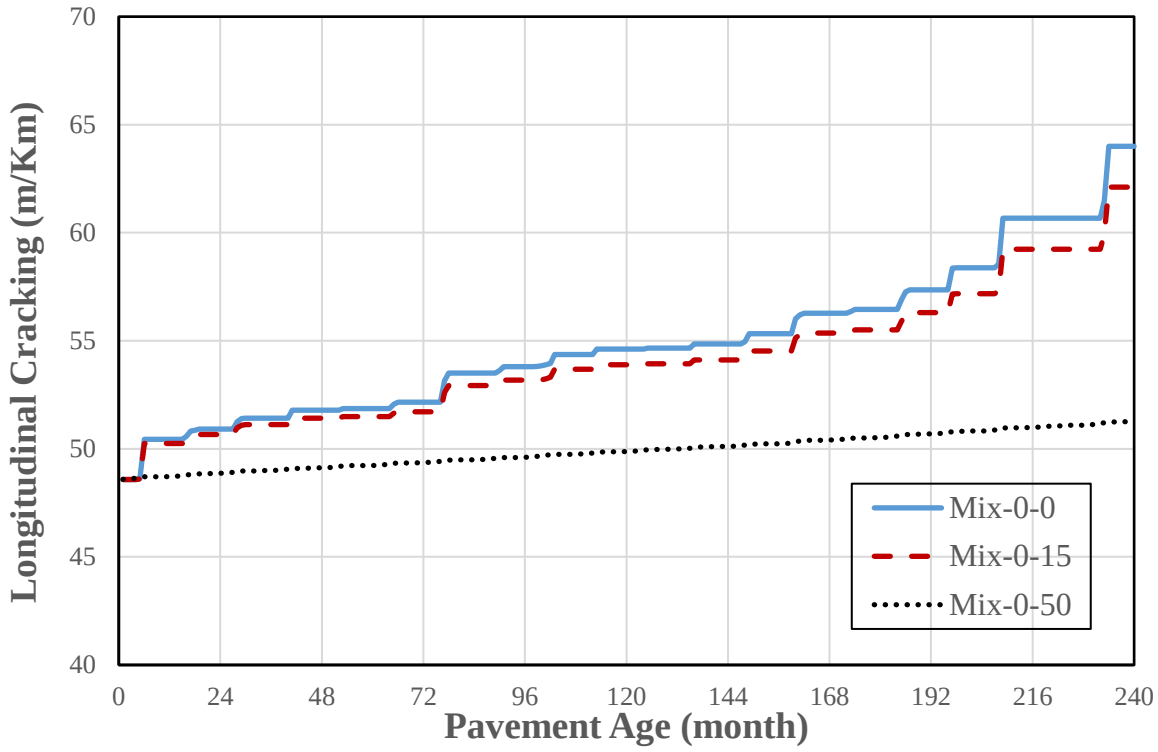

b) Comparison of longitudinal cracking of the mixes

Figure 7.6: Predicted longitudinal cracking and pavement life of mixes

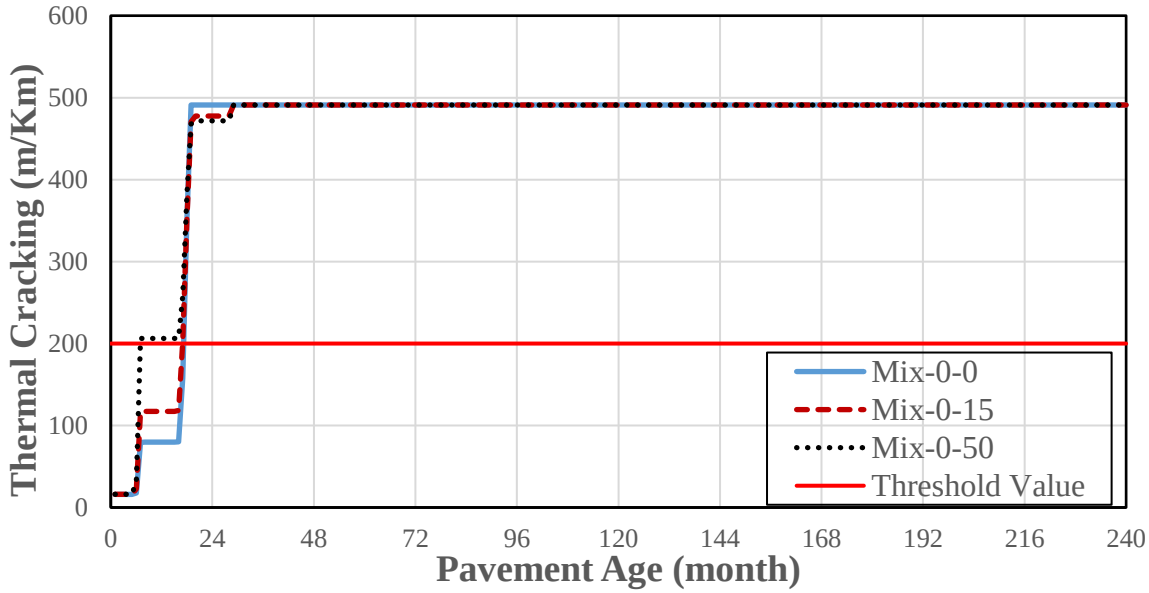

a) Thermal cracking of the mixes respect to target value

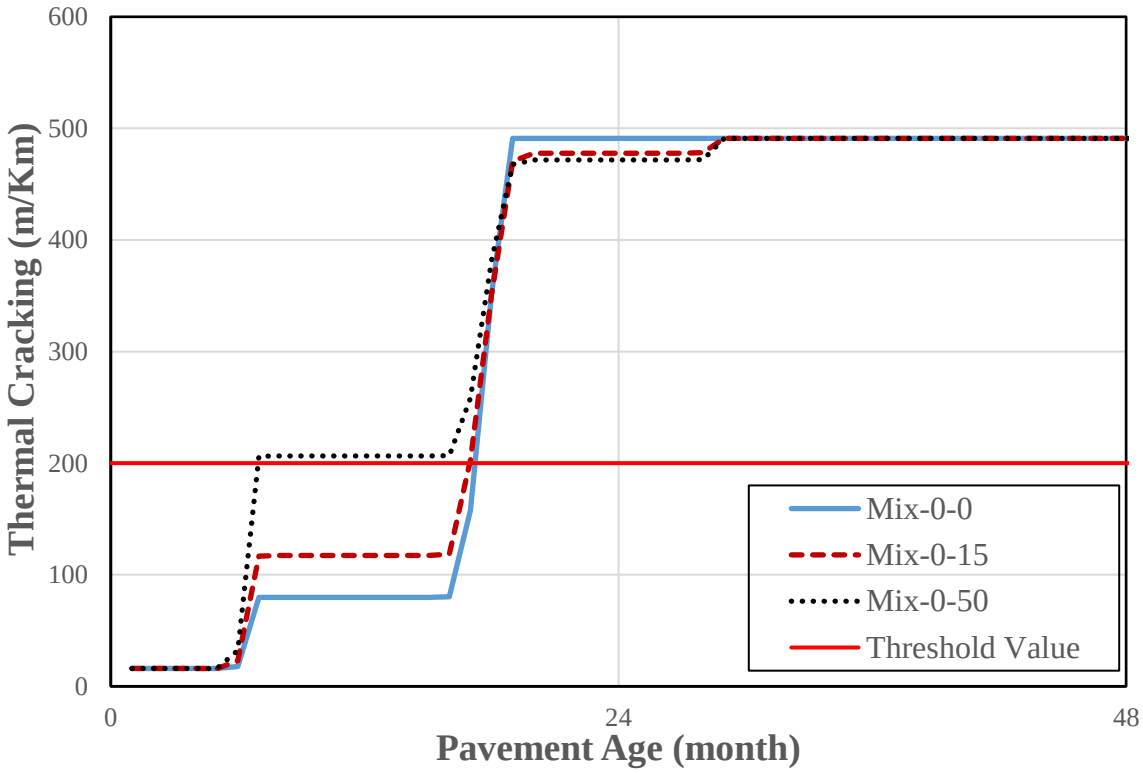

b) Comparison of thermal cracking of the mixes

Figure 7.7: Predicted thermal cracking and pavement life of mixes

Figures 7.8 and 7.9 show the predicted AC rut and total rut for the mixes, respectively. All the mixes successfully met the distress rut criteria. The AC rut for all mixes was noticeably low which is possibly due to the AC thickness and the uncalibrated rut prediction model used in the MEPDG software. The AC rut of Mix-0-50 was slightly higher than Mix-0-0 and Mix-0-15, which was not expected.

When a type of distress occurs in a pavement, it will cause the deterioration of the asphalt pavement to accelerate. It seems Pavement ME Design does not fully consider the possible interactions between distresses. For instance, when the AC thermal cracking failed to meet the target value, it was expected to affect the other distresses such as rutting and fatigue cracking. However, the AC rut and total rut as well as longitudinal and alligator cracking were predicted without consideration of the predicted AC thermal distress.

Based on the results in this study, the AC thermal cracking was predicted to be 491 meters per kilometer by year 2 for Mix-0-0 (Figure 7.7-b), while no corresponding impact or acceleration in prediction trends of other distresses can be observed at the second year of pavement life or after that. It was noted that all distresses were predicted independently and excessive thermal cracking was not considered in prediction of other distresses. This indicated that MEPDG program may be required improving the interactions between predicted distresses in the future.

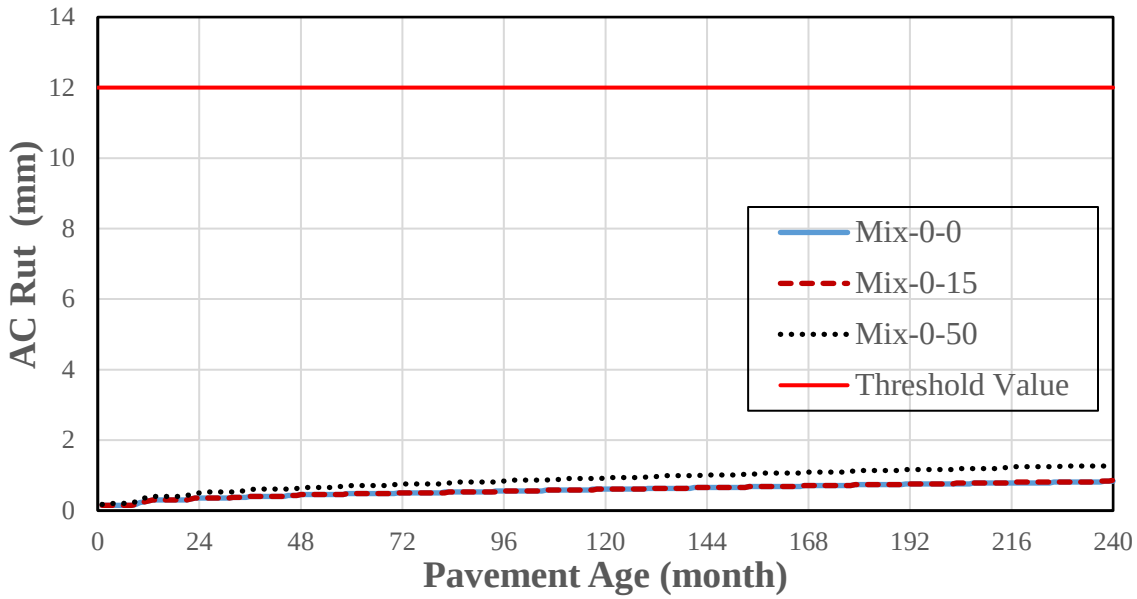

a) AC layer rutting of the mixes with respect to target value

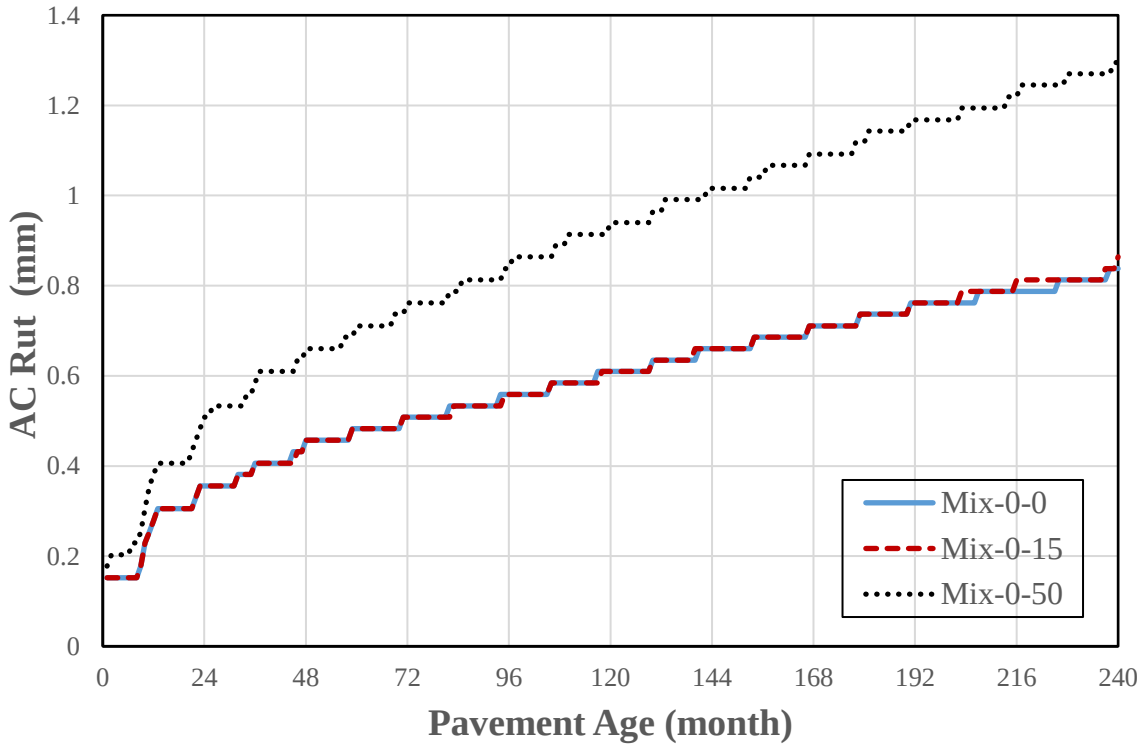

b) Comparison of rutting of AC mixes

Figure 7.8: Predicted AC rutting and pavement life of mixes

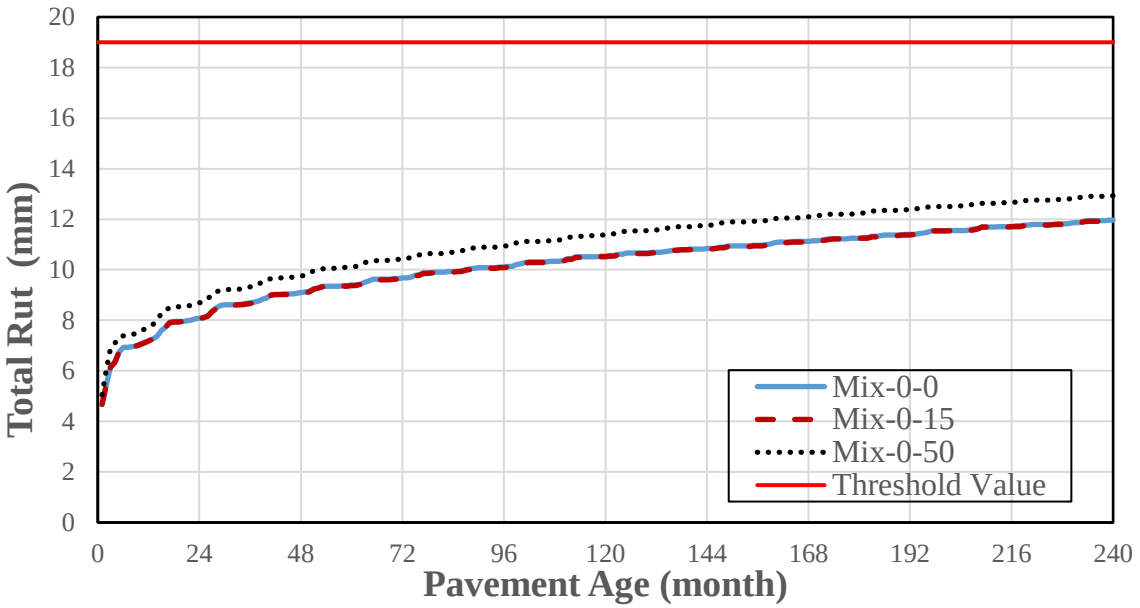

a) Total rut of the mixes with respect to target value

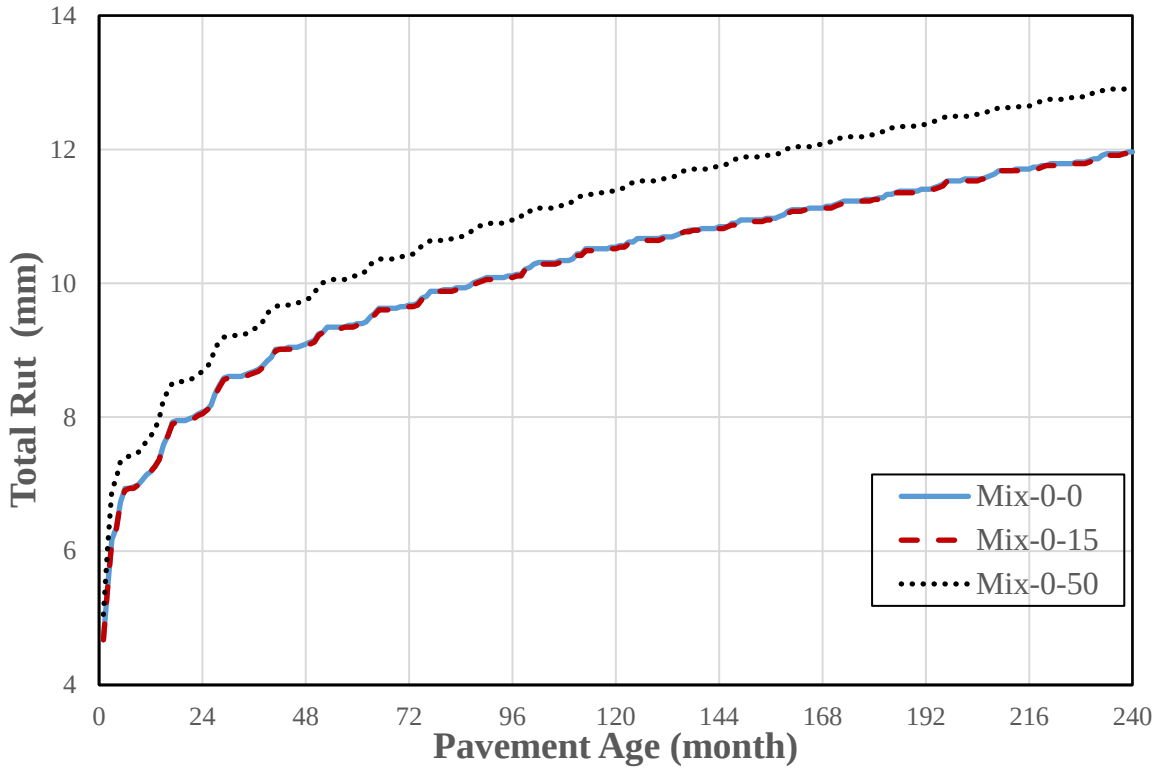

b) Comparison of total rut of the mixes

Figure 7.9: Predicted total rut and pavement life of mixes

7.5 Summary

Pavement ME Design program was used to predict distresses of the asphalt mixes. The predicted distresses include roughness or IRI, AC bottom up fatigue cracking (alligator cracking), AC surface down fatigue cracking (longitudinal cracking), AC thermal cracking, AC rut, and total rut. The targets of distresses were determined based on MEPDG recommendations and Manitoba specification. Manitoba default Level 3, Manitoba calibrated Level 3, and Manitoba Level 1 were used as three Levels of asphalt mix input data. Long-term performance of the three mixes: Mix-0-0, Mix-0-15, and Mix-0-50 for those three Levels of input data were evaluated and compared.

- The Pavement ME Design analysis results showed that the predicted AC rut and AC thermal cracking for Level 1 agreed with the laboratory findings. The predicted AC rut and AC thermal cracking of Mix-0-0 and Mix-0-15 were found to be very similar for Manitoba Level 1 input data. In addition, laboratory results of Mix-0-50 showed very high stiffness (low creep compliance) at low temperature that agreed with the predicted AC thermal cracking by MEPDG software.
- Results showed that all the mixes exceeded the specified maximum value of AC thermal cracking for all the Manitoba Levels. Considering the binder performance grade of Mix-0-0 and Mix-0-15 which was PG 58-28 and performance grade of Mix-0-50 which was PG 64-16, the common asphalt binder with PG 58-28 used in Manitoba is not sufficient for Manitoba weather.
- The predicted terminal roughness of the mixes were slightly higher than IRI target. The predicted roughness can be influenced by the predicted cracking. It is expected that if the design meets the distresses targets, it will reduce the predicted roughness as well.
- The predicted performance of Manitoba default Level 3 showed higher normalized number

compared to calibrated Level 3 which implied that Manitoba default Level 3 overpredicted the distress predictions of the asphalt mix.

- The Manitoba calibrated Level 3 asphalt mix input showed similar results to Manitoba Level 1. This result showed that the use of Manitoba calibrated Level 3 input data instead of Manitoba default Level 3 increases the accuracy of predicted distresses. This implies that calibrated Level 3 Manitoba asphalt mix input data can be used for the design and analysis of Manitoba mixes with comparable accuracy with Level 1 input data. This can save a tremendous amount of time and enormous amount of cost of operating and testing. Since it is time consuming and expensive to provide laboratory asphalt testing for each mix.
- It was noted that Pavement ME Design did not fully consider the possible interactions between distresses. When excessive thermal cracking occurred at early age of pavements, no corresponding impact was observed in prediction of other distresses.

CHAPTER 8 - CONCLUSIONS AND RECOMMENDATIONS

The study undertaken for this thesis applied the sustainability practices by (1) integrating recycled and reclaimed materials such as RAS and RAP in new asphalt pavements; and (2) developing a local database of measured-laboratory values to perform calibration on Level 3 MEPDG creep compliance and dynamic modulus prediction models to achieve higher reliability in design and analysis of the pavements.

Performance of different amounts of RAS and RAP in HMA were evaluated through laboratory asphalt testing. The MEPDG creep compliance and dynamic modulus prediction models were calibrated based on local mixes and materials. Finally, the impact of local calibration on predicted pavement distresses were evaluated using Pavement ME Design program. The findings and conclusions from the research are as follows:

8.1 Mechanistic Characteristics of Asphalt Mixes

In this thesis, mixes with different amounts of RAS and RAP were prepared. The low and high

temperature performance of the mixes were evaluated. The creep compliance and IDT strength tests were performed to determine the low temperature performance of the mixes and dynamic modulus tests were carried out to examine the high temperature performance. The findings and conclusions from laboratory tests are as follows:

1. The dynamic modulus test results showed that the use of RAS and RAP increased the dynamic modulus at high temperature which resulted in improvement of the potential rutting resistance of the mixes.

2. Creep compliance test results showed that RAS and RAP directly impact the low temperature performance of the HMA mixes. The use of RAS and RAP increased the stiffness of the mixes at low temperature, as expected. IDT strength test results agreed with creep compliance test results. It was found that utilizing RAS in HMA increased the IDT strength and decreased creep compliance values at low temperature.

3. Use of 15% RAP showed improvement in rutting resistance while it did not impact the low temperature performance. Therefore, 15% RAP can be used in an asphalt mix containing a design asphalt binder of PG 58-28 without changing the virgin binder grade.

4. Mix-0-50 (50% RAP) and Mix-5-10 (5% RAS+10% RAP) showed excessive stiffness in creep compliance which indicates these mixes are more prone to thermal cracking.

5. Utilizing soft asphalt binder in a mix with high percentage of RAP was found beneficial. When one grade softer binder was added to the mix containing 50% RAP, the creep

compliance increased. However, one grade softer was not sufficient for this mix to provide comparable creep compliance values as of Mix-0-0.

6. University of Manitoba laboratory mix showed lower stiffness at high temperature although the mix contained higher amounts of recycled materials (10% RAP and 5% RAS) in comparison with laboratory mixes of Minnesota (5% RAS) and Ontario (6% RAS). This implied that the Manitoba mix has lower rutting resistance when it is compared to other mixes with almost similar RAS content.

8.2 Local Calibration of the MEPDG Prediction Models

Local calibration was needed to optimize the MEPDG creep compliance model and NCHRP 1-37A and NCHRP 1-40D dynamic modulus prediction models for local materials, environment and conditions.

Two predictive models, NCHRP 1-37A and NCHRP 1-40D, for Level 2 and Level 3 of asphalt binder inputs were used to predict the E* values. Exponential fit of model outputs and nonlinear multiple regression were applied to improve the reliability of E* predictions. Based on the results, the following conclusions were drawn:

1. Without local calibration, the NCHRP 1-37A model was found to predict E* more accurately in both Levels of asphalt binder inputs for all RAP mixes compared to NCHRP 1-40D model.

2. The NCHRP 1-40D model overpredicted the E* values at lower temperature and underpredicted the E* at high temperature in both Levels of asphalt binder input data.

3. The exponential fit of uncalibrated model outputs showed improvement in accuracy of E* prediction. The accuracy of the predicted E* values were more noticeable in NCHRP 1-40D model than NCHRP 1-37A model. The exponential fit does not provide a general model that can be used for both Levels.

4. The nonlinear multiple regression of NCHRP 1-37A and NCHRP 1-40D were the preferred technique for local calibration. The results showed the highest degree of reliability in both Levels. The R^2 of nonlinear regression models was found to be 95%.

5. The exponential fit and nonlinear regression of NCHRP 1-37A and NCHRP 1-40D for Level 3 showed improvement in prediction of E* for all RAP mixes. However, the mixes with 50% RAP showed the least improvement among RAP mixes for both local calibrated NCHRP 1-37A and NCHRP 1-40D models.

6. The existence of high RAP mixes in a database caused an adverse effect on reliability of calibrated models.

Furthermore, two alternatives for local calibration of creep compliance of AC mixes: nonlinear multiple regression and artificial neural network were performed. Based on the results, the following conclusions were drawn:

1. The MEPDG creep compliance model is a generic model. This model was not able to accurately predict creep compliance values, particularly for mixes used in cold climates, in part because these mixes constituted only a small fraction of the mixes used to develop the MEPDG creep compliance model.

2. For the particular dataset used in this analysis, the globally-calibrated MEPDG model underpredicted creep compliance. The model was less reliable for predicting creep compliance values at low temperatures (-20°C) than that of at other temperatures.

3. Nonlinear regression and ANN can be used as two alternatives to predict creep compliance values more reliably. The local-calibration will lead to better quantification of thermal cracking as well as other distresses such as roughness and the overall service life.

4. Nonlinear multiple regression showed significant improvement in the accuracy of creep compliance prediction. However, the ANN model showed the highest reliability in prediction of creep compliance values at each test temperature.

8.3 Impact of Globally and Locally Calibrated E* and Creep Values on Long-Term Performance of the Asphalt Mixes

Pavement ME Design program was used to predict distresses of asphalt mixes. The predicted distresses include roughness or IRI, AC bottom up fatigue cracking (Alligator cracking), AC surface down fatigue cracking (longitudinal cracking), AC thermal cracking, AC rut, and total rut. The targets of distresses were determined based on MEPDG recommendations and Manitoba

practice.

The laboratory-measured values were used for Manitoba Level 1 inputs data. For Manitoba calibrated Level 3 input data, the creep compliance and dynamic modulus values were predicted by using the localized predictive models. Whereas, for Manitoba default Level 3 the globally calibrated values were used.

Long-term performance of the three asphalt mixes namely Mix-0-0, Mix-0-15, and Mix-0-50 for Manitoba default Level 3, Manitoba calibrated Level 3, and Manitoba Level 1 were evaluated. The findings and conclusions were as follows:

1. Manitoba default Level 3 asphalt mix data provided a high estimate of the predicted distresses of the asphalt mixes. The amounts of predicted distresses were found to be lower for Manitoba Level 1 and Manitoba calibrated Level 3 asphalt mix data compared to the Manitoba default Level 3 asphalt mix data.

2. When Manitoba default Level 3 was used for Mix-0-0 and Mix-0-15, all the predicted distresses failed to meet the targets except AC permanent deformation. In contrast, when Manitoba Level 1 or calibrated Level 3 were used as input data, only IRI and AC thermal cracking failed to meet the targets.

3. Results showed that all the mixes exceeded the specified maximum value of AC thermal cracking for all the Manitoba Levels. It was found that the dominant asphalt binder used in Manitoba (PG 58-28) was not soft enough for Manitoba weather.

4. The predicted terminal roughness of the mixes were slightly higher than the IRI target. The predicted roughness can be influenced by the predicted cracking. It is expected that if the design meets the distresses targets, it will reduce the predicted roughness as well.

5. The predicted performance of Manitoba default Level 3 showed higher normalized number compared to calibrated Level 3 which confirmed that Manitoba default Level 3 overpredicted the distress predictions of the asphalt mix.

6. It was found that the Pavement ME Design program does not fully consider the possible interactions between the predicted distresses. When excessive thermal cracking occurred at early age of pavements, no impact was observed in prediction of other distresses. It was expected that when a type of distress occurs in a pavement, it would have impacted the other distresses and caused the deterioration of asphalt pavements to accelerate.

7. The calibrated Level 3 Manitoba asphalt mix input showed very similar results to Manitoba Level 1. These results showed that use of calibrated Level 3 Manitoba input data instead of Manitoba default Level 3 can increase the accuracy of predicted distresses. This implied that calibrated Level 3 Manitoba asphalt mix input data can be used for the design and analysis of the Manitoba mixes with comparable accuracy with the Manitoba Level 1 input data. This can save an enormous amount of time and cost of operating and testing. Since it is time consuming and expensive to provide laboratory asphalt testing for the analysis and design of the mixes.

8.4 Limitations and Recommendation for Future Work

Although all the goals of this thesis have been reached, there were some limitations. For instance, the first limitation of this study is lack of variability in asphalt binder performance grades. Most of the mixes used in this study contained one type of asphalt binder performance grade due to limited material availability. The second limitation is lack of field performance evaluation. The long-term field performance of the mixes containing RAS and RAP was not fully evaluated and considered due to the time limit. Based on these limitations the following future research is proposed:

1. It is recommended to extend and update the dataset for validation of the calibrated MEPDG models in the future, as dataset used for local calibration of the models appears to be of sufficient size. It is recommended to extend the dataset and repeat the calibration should additional binder types be used or should mix parameters exceed their range of values presented in this research.

2. Pavement ME Design program utilizes predictive models to estimate the amounts of pavement distresses. In order to increase the accuracy of distress prediction, it is recommended to use a field section and calibrate the distress prediction models such as rutting models, fatigue models, and thermal cracking model for Manitoba flexible pavements. This will increase the reliability of predicted distresses by the Pavement ME Design program.

3. It is recommended to evaluate and possibly calibrate other inputs prediction models used in the MEPDG software. For instance, the accuracy of IDT strength predictive model can be evaluated and local calibration may be performed to increase the reliability of predictions.

4. In this study, a few mixes containing both RAS and RAP were prepared and analyzed through laboratory testing. More mixes containing RAS and RAP are required to be tested and analyzed to be used as part of the local calibration process. In addition, it is suggested that the effect of mixes containing both RAS and RAP on the predicted distresses using Pavement ME Design software are to be evaluated.

5. In this research, field performance of only two mixes were evaluated since field performance of mixes was out of the scope of this thesis. Field evaluation can assist to consider unknown factors that have not been considered in laboratory evaluation. Therefore, it is recommended to conduct the field performance evaluation of mixes containing reclaimed and recycled materials, particularly mixes containing high RAP such Mix-0-50 and Mix-0-40.

REFERENCES

AASHTO (American Association of State Highway and Transportation Officials), 2015, Mechanistic-Empirical Pavement Design Guide: A Manual of Practice. AASHTO Designation: MEPDG-1. Washington, D.C.

AASHTO (American Association of State Highway and Transportation Officials), 2008, Mechanistic-Empirical Pavement Design Guide: A Manual of Practice. AASHTO Designation: MEPDG-1. Washington, D.C.

AASHTO (American Association of State Highway and Transportation Officials), 2010. Guide for the Local Calibration of the Mechanistic-Empirical Pavement Design Guide, Washington, D.C.

AASHTO PP62 (American Association of State Highway and Transportation Officials), 2010, Standard Practice for Developing Dynamic Modulus Master Curves for Hot Mix Asphalt (HMA). Washington, D.C.

AASHTO R35 (American Association of State Highway and Transportation Officials), 2012, Standard Practice for Superpave Volumetric Design for Hot-Mix Asphalt (HMA), Washington D.C.

AASHTO T 342 (American Association of State Highway and Transportation Officials), 2011, Determining Dynamic Modulus of Hot Mix Asphalt (HMA), Washington D.C.

AASHTO T313 (American Association of State Highway and Transportation Officials), 2012, Determining the Flexural Creep Stiffness of Asphalt Binder Using the Bending Beam Rheometer (BBR), Washington D.C.

AASHTO T315 (American Association of State Highway and Transportation Officials), 2012, Determining the Rheological Properties of Asphalt Binder Using a Dynamic Shear Rheometer (DSR), Washington, D.C.

AASHTO T322 (American Association of State Highway and Transportation Officials), 2007, Standard Method of Test for Determining the Creep Compliance and Strength of Hot Mix Asphalt (HMA) Using the Indirect Tensile Test Device, Washington D.C.

Abbas, A.R., Mannan, U.A., Dessouky, S., 2013, Effect of Recycled asphalt Shingles on Physical and Chemical Properties of Virgin Asphalt Binders, Journal of Construction and Building Materials. Volume 45, Pages 162–172.

Abu Abdo, A., Bayomy, F., Nielsen, R., Weaver, T., Jung, S.J., and Santi, M., 2009, Prediction of the Dynamic Modulus of Superpave Mixes. Bearing Capacity of Roads, Railways, and Airfields, Taylor & Francis, London, 305–314.

ASTM D2493M (American Society for Testing Materials), 2009, American Society for Testing and Materials Miscellaneous, Standard viscosity-temperature chart for asphalts. West Conshohocken, PA.

Awed, A., El-Badawy, S., and Bayomy, F, Santi, M., 2011, Influence of the MEPDG Binder Characterization Input Level on the Predicted Dynamic Modulus for Idaho Asphalt Concrete Mixtures. 90th Annual Meeting of the Transportation Research Board, Washington D.C.

Bari, J., Witczak, M.W., 2006, Development of A New Revised Version of The Witczak E* Predictive Model for Hot Mix Asphalt Mixtures, Journal of Association Asphalt Paving Technologists, 75, 381–424.

Baus, R. L. and Stires, N. R., 2010, Mechanistic-Empirical Pavement Design Guide Implementation, Department of Civil and Environmental Engineering, University of South Carolina, Report No. GT06-10.

Biligiri, K.P., Way, G.B., 2014, Predicted E* Dynamic Moduli of the Arizona Mixes using Asphalt Binders Placed over a 25-Year Period. Construction and Building Materials, 54, pp. 520-532.

Birgisson, B., Sholar, G., Roque, R., 2005, Evaluation of a Predicted Dynamic Modulus for Florida Mixtures, 84th Annual Meeting of the Transportation Research Board Washington D.C.

Bonaquist, R., 2011, Effect of Recovered Binders from Recycled Shingles and Increased RAP Percentages on Resultant Binder PG, Report submitted to Wisconsin Highway Research Program.

Ceylan, H., Schwartz, C.W., Sunghwan Kim, S., Gopalakrishnan, K., 2009, Accuracy of Predictive Models for Dynamic Modulus of Hot-Mix Asphalt. Journal of Materials in Civil Engineering. Vol. 21, No. 6, 286-293.

Clyne, T.R., Li, X., Marasteanu, M.O., Skok, E.L., 2009, Dynamic and Resilient Modulus of MN/DOT Asphalt Mixtures, University of Minnesota, Minneapolis, MN, United States.

Copeland, A., 2011, Reclaimed Asphalt Pavement in Asphalt Mixtures: State of the Practice. Report FHWA-HRT-11-021. Federal Highway Administration, McLean, Virginia.

Daniel J.S. and Lachance A., 2005, Mechanistic and Volumetric Properties of Asphalt Mixtures with Recycled Asphalt Pavement, Transportation Research Record, No. 1929, pp. 28-36, Transportation Research Board of the National Academies, Washington, D.C.

Ddamba, S., Tighe, S., Essex, R., and Hanasoge, N., 2012, Evaluation of the Effect of Recycled Asphalt Shingles on Ontario Hot Mix Pavement, Canadian Technical Asphalt Association (CTAA) Conference.

Ddamba, S.J., 2011, Evaluation of the Effect of Recycled Asphalt Shingles on Ontario Hot Mix Pavement MSc Thesis, University of Waterloo, Ontario, Canada.

Diefenderfer, S., Nair, H., 2014, Evaluation of High RAP Mixture Production, Construction, and

Properties, Transportation Research Board (TRB) Annual Meeting, Washington, D.C.

El-Badawy, S., Bayomy, F., and Awed, A., 2012, Performance of MEPDG Dynamic Modulus Predictive Models for Asphalt Concrete Mixtures: Local Calibration for Idaho. Journal of Materials in Civil Engineering, 1412-1421.

Esfandiarpour, S., Ahammed, M.A., Shalaby, A., Liske, T., Kass, S., 2015, An Evaluation of Pavement ME Design Dynamic Modulus Prediction Model for Asphalt Mixes Containing RAP. The 2015 Conference of the Transportation Association of Canada.

Esfandiarpour, S., Shalaby, A., 2016, Alternatives for Calibration of Dynamic Modulus Prediction Models of Asphalt Concrete., In press, International Journal of Pavement Research and Technology.

Esfandiarpour, S., Shalaby, A., 2017, Local Calibration of Creep Compliance Models of Asphalt Concrete, Journal of Construction and Building Materials, Volume 132, Pages 313–322.

Far, M., Underwood, B., Ranjithan, S., Kim, R., and Jackson, N., 2009, Application of Artificial Neural Networks for Estimating Dynamic Modulus of Asphalt Concrete. Transportation Research Record 2127, Transportation Research Board, Washington, D.C., 173–183.

FHWA (Federal Highway Administration), 2015, Van Dam, T.J., Harvey, J.T., Muench, S.T., Smith, K.D., Snyder, M.B., Al-Qadi, I.L., Ozer, H., Meijer, J., Ram, P.V., Roesler, J.R., Kendall, A., Towards Sustainable Pavement Systems: A Reference Document. Federal Highway Administration, FHWA-HIF-15.

Flintsch, G., McGhee, K.K., 2009, Quality Management of Pavement Condition Data Collection-A Synthesis of Highway Practice, National Cooperative Highway Research Program Synthesis 401.

Galal, K. A., and Chehab, G. R. 2005, Implementing the Mechanistic Empirical Design Guide Procedure for a Hot-Mix Asphalt-Rehabilitated Pavement in Indiana, Transportation Research Record 1919, Transportation Research Board, Washington, DC, 121–131.

Georgouli, K., Loizos, A., Plati, C., 2016, Calibration of Dynamic Modulus Predictive Model.

Construction and Building Materials, 102, 65–75.

Goodrich, J.L., 1991, Asphaltic Binder Rheology, Asphalt Concrete Rheology And Asphalt Concrete Mix Properties, in Proceedings of the Association of Asphalt Paving Technologists, vol. 60, pp. 80–120.

Hajj, E. Y., Sebaaly, P. E., Loria, L., Kass, S., Liske, T., 2011, Impact of High RAP Content on the Performance Characteristics of Asphalt Mixtures in Manitoba, Transportation Association of Canada (TAC), Edmonton, Alberta.

Hansen K. R. and A. Copeland, 2013, Asphalt Pavement Industry Survey on Recycled Materials and Warm-Mix Asphalt Usage: 2009–2012. Information Series 138. National Asphalt Pavement Association, Lanham, MD. (Web Link).

Hansen K. R. and A. Copeland, 2014, Annual Asphalt Pavement Industry Survey on Recycled Materials and Warm-Mix Asphalt Usage: 2009-2013. National Asphalt Pavement Association. Lanham, MD.

Harran, G., and Shalaby, A., 2009, Improving The Prediction Of The Dynamic Modulus Of Fine-Graded Asphalt Concrete Mixtures At High Temperatures. Canadian Journal of Civil Engineering. 36(2), 180–190.

Indiana DOT 2010 Standard Specifications Sections 401 & 402 - http://www.in.gov/dot/div/contracts/standards/book/sep09/sep.htm

Islam, M.R., Mannan, U.A., Rahman, ASM.A., Tarefder, R.A., 2014, Effects of Recycled Asphalt Pavement on Mix and Binder Properties and Performance in the Laboratory. Transportation Research Board (TRB) Annual Meeting, Washington, D.C.

Jamrah, A., Kutay, M.E., 2015, An investment of Different Methods for Obtaining Asphalt Mixture Creep Compliance for Use in Pavement ME Design Software. 94th Transportation Research Board Annual Meeting, Washington, D.C.

Jeong, M. G., 2010, Implementation of a Simple Performance Test Procedure in a Hot Mix Asphalt Quality Assurance Program. PhD Thesis, Arizona State University, Arizona, United States.

Johnson, E., Johnson, G., Dai, S., Linell, D., Mcgraw, J., Watson, M., 2010, Incorporation of Recycled Asphalt Shingles in Hot Mixed Asphalt Pavemetn Mixtures, Minnesota Department of Transportation.

Khattab, A.M., El-Badawy, S.M., Al-Hazmi, A., Elmwafi, M., 2014, Evaluation of Witczak E* Predictive Models for The Implementation of AASHTOWare-Pavement ME Design in the Kingdom of Saudi Arabia. Construction and building Materials, 360-369.

Kim, Y.R., Momen, M., King, M., 2005, Typical Dynamic Moduli for North Carolina Asphalt Concrete Mixtures, North Carolina State University, Raleigh, FHWA/NC.

Lingireddy, S., and Brion, G. M., 2005, Artificial neural Networks in Water Supply Engineering, American Society of Civil Engineers (ASCE): Publisher, Reston, VA.

Martinez, F.O., Angelone, S.M., 2009, Evaluation of Different Predictive Dynamic Modulus Models of Asphalt Mixtures Used in Argentina, in 88th Annual Meeting of the Transportation Research Board Washington D.C.

Massachusetts Department of Transportation (Mass Dot), Highway Division, 2010, supplemental specifications, Retrieved July 26 2016, from URL
http://www.massdot.state.ma.us/Portals/8/docs/construction/SSP022510MetEng.pdf

Material Specification for Hot Mix Asphalt, (2010), Ontario Provincial Standard Specification, OPSS 1150.

Maupin, G.W., 2010, Investigation of the Use of Tear-Off Shingles in Asphalt Concrete. Final Report VTRC 10-R23, Virginia Transportation Research Council, Charlottesville, VA.

McDaniel, R.S., Shah, A., Huber, G., 2012, Investigation of Low- and High-Temperature Properties of Plant-Produced RAP Mixtures, Submitted to Federal Highway Administration (FHWA-HRT-11-058).

McDaniel, R.S., Soleymani, H., Anderson, R.M., Turner, P., Peterson, R., 2000, Recommended Use of Reclaimed Asphalt Pavement in the Superpave Mix Design Method, National Cooperative Highway Research Program (NCHRP), Washington D.C.

Minnesota Department of Transportation (MnDOT), MnDOT Plant Mixed Asphalt Pavement 2360, St. Paul, 2013, update [Online]. Available: http://www.dot.state.mn.us/pre-letting/prov/order/2360-2013.pdf.

Mo DOT Engineering Policy Guide RSS, 2011, Category: 403 asphaltic concrete pavement, Retrieved July 26 2016, from URL http://epg.modot.org/index.php?title=Category:403_asphaltic_concrete_pavement

Momin, S. A., 2011, Local Calibration of Mechanistic Empirical Pavement Design Guide for North Eastern United States, Master of Science in Civil Engineering. University Of Texas at Arlington.

NAPA (national asphalt pavement association), 2016, Newcomb, D.E., Epps, J.A., Zhou, F., Use of RAP & RAS in High Binder Replacement Asphalt Mixtures: A Synthesis, Special Report 213.

NCHRP 1-37A (National Cooperative Highway Research Program), 2004, Guide for Mechanistic-Empirical Design of New and Rehabilitated Pavement Structures. NCHRP 1-37A Final Report. Washington, D.C.

NCHRP 452 (National Cooperative Highway Research Program) 2001, McDaniel, R., Anderson, R.M, Recommended Use of Reclaimed Asphalt Pavement in the Superpave Mix Design Method: Technician's Manual, Washington, D.C.

NCHRP 495(National Cooperative Highway Research Program) SYNTHESIS, 2016, Use of Reclaimed Asphalt Pavement and Recycled Asphalt Shingles in Asphalt Mixtures. NCHRP 495. Washington, D.C.

NCHRP 673(National Cooperative Highway Research Program), 2011, A Manual for Design of Hot Mix Asphalt with Commentary, NCHRP 673. Washington, D.C.

NCHRP 702 (National Cooperative Highway Research Program), 2011 A Performance-Related Specification for Hot-Mixed Asphalt. NCHRP 702. Washington, D.C.

NCHRP 9-12 (National Cooperative Highway Research Program), 2000 Incorporation of Reclaimed Asphalt Pavement in the Superpave System. Washington, D.C., Transportation

Research Board.

Nguyen, V.H., 2009, Effects of Laboratory Mixing Methods and RAP Materials on Performance of Hot Recycled Asphalt Mixtures, Doctor of Philosophy thesis, University of Nottingham, England.

Obulareddy, S., 2006, Fundamental characterization of Louisiana HMA Mixtures for the 2002 mechanistic-empirical design Guide (Master's Thesis), Louisiana State University, Louisiana, United States.

Ozer, H., Al-Qadi, I. L., Kanaan, A.I., Lippert, D. L., 2013, Performance Characterization of High Asphalt Binder Replacement With Recycled Asphalt Shingles (RAS) for a Low N-Design Mixture, Transportation Research Board (TRB) Annual Meeting.

Pekcan, O., Tutumluer, E., Thompson, M.R., 2006, Nondestructive Flexible Pavement Evaluation Using ILLI-PAVE Based Artificial Neural Network Models. GeoCongress. Atlanta, Georgia, United States.

Pellinen, T.K., witczak, M.W., and Bonaquist, R.F., 2004, Asphalt Mix Master Curve Construction Using Sigmoidal Fitting Function with Non-Linear Least Squares Optimization. Geotechnical special publication, v l23.

Robbins, M., and Timm, D., 2011, Evaluation of Dynamic Modulus Predictive Equations for NCAT Test Track Asphalt Mixtures. Transportation Research Board 90th Annual Meeting Compendium of Papers (CD-ROM), Paper No. 11-4070, Washington, D.C.

Salari, S., 2012, Effect if Recycled Asphalt Shingle on the Rheological and Molecular Composition Properties of Asphalt Cement. M.S. Thesis, Louisiana State University and Agricultural and Mechanical College, Louisiana, United States.

Santero, N.J., 2009, Pavements and the Environment: A Life-Cycle Assessment Approach, A Ph.D. dissertation, University of California, Berkeley, California, United States.

Schwartz, C., 2007, Implementation of the NCHRP 1-37A Design Guide, Maryland State Highway Administration, Lutherville, MD, Report No.SP0077B41.

Sengoz, B., and Topal, A., 2004, Use of Asphalt Roofing Shingle Waste in HMA, Construction and Building Materials Journal, Volume 19, p. 337-346.

Shalaby, A., El Halm, A., Easa, S., 1996, Low-Temperature Stresses and Fracture Analysis of Asphalt Overlays. Washington, D.C.: Transportation Research Board, p. 132-139.

Shannon, C.P., 2012, Fractionation of Recycled Asphalt Pavement Materials: Improvement of Volumetric Mix Design Criteria for High-RAP Content Surface Mixtures, University of Iowa, M.s. Thesis, Iowa, United States.

Shu, X., B. Huang, and D. Vukosavljevic, 2008, Laboratory Evaluation of Fatigue Characteristics of Recycled Asphalt Mixture, Construction and Building Materials, Volume 22, Issue 7, 1323–1330.

Singh, D., Zaman, M., and Commuri, S., 2011a, Evaluation of Predictive Models for Estimating Dynamic Modulus of HMA Mixes Used In Oklahoma. Transportation Research Board 90th Annual Meeting Compendium of Papers (CD-ROM), Paper No. 11-3885, Washington.

Singh, D., Zaman, M., and Commuri, S., 2011b, Evaluation of Measured and Estimated Dynamic Moduli for Selected Asphalt Mixes. Journal of ASTM International, Vol. 8, No. 9.

Singh, D., Zaman, M., Commuri, S., 2012, Artificial Neural Network Modeling for Dynamic Modulus of Hot Mix Asphalt Using Aggregate Shape Properties. Journal of Materials in Civil Engineering., Vol. 25, No. 1, 54-62.

Singh, D., Zaman,M., Commuri, S., 2013, Effect Of Production And Sample Preparation Methods on Aggregate Shape Parameters, International Journal of Pavement Engineering, 14:2, 154-175.

Solanki, P., Zaman, M., Adje, D., Hossain, Z., 2014, Effect of Recycled Asphalt Pavement on Thermal Cracking Resistance of Hot-Mix Asphalt. International Journal of Geomechanics. Vol. 15, Issue 5., A4014001-1- A4014001-9.

University of California Pavement Research Center (UCPRC), 2010, UCPRC Pavement LCA Guideline. UCPRC-TM-2010-03. University of California Pavement Research Center, Davis, CA.

Uzarowski, L., Prilesky, H. Berube, E., Henderson, V., and Rizi, R., 2010, Evaluation of Mechanistic Properties of Hot Mix Asphalt Containing Recycled Asphalt Shingles for Use in the Pacific Northwest Coastal Region, Canadian Technical Asphalt Association (CTAA) Annual Conference, p.272-291.

VDOT, 2016, Division II – Materials, Special Provision and Supplemental Specifications, Retrieved July 26 2016, from URLhttp://www.virginiadot.org/business/resources/const/07RevDiv_II.pdf

Velasquez, R., Hoegh, K., Yut, I., Funk, N., Cochran, G., Marasteanu, M., and Khazanovich, L., 2009, Implementation of the MEPDG for New and Rehabilitated Pavement Structures for Design of Concrete and Asphalt Pavements in Minnesota, Minnesota Department of Transportation, St. Paul, MN, Report MN/RC 2009-06.

Watson, J.M., Mcgraw, J., Johnson, E., Linell, D., Dai, S., 2011, the Effect of Recycled Asphalt Materials on Hot Mixed Asphalt Pavement Performance, Green Streets and Highways, ASCE.

Williams, R., Cascione, A., Haugen, D., Buttlar, W., Bentsen, R., and Behnke, J., 2011 ,Characterization Of Hot Mix Asphalt Containing Post-Consumer Recycled Asphalt Shingles and Fractionated Reclaimed Asphalt Pavement, Final Report Submitted to Illinois State Toll Highway Authority, Iowa State University.

Witczak, M., El-Basyouny, M., and El-Badawy, S., 2006, Incorporation of the new, E* (2005) predictive model in the MEPDG. NCHRP 1-40D Inter-Team Technical Rep., Arizona State University, Tempe, AZ, United States.

Wu, Z., 2012, Evaluation of Current Louisiana Flexible Pavement Structure Using PMS Data and New Mechanistic-Empirical Pavement Design Guide, Louisiana Transportation research center, Louisiana, United States.

Yin, H., Chehab, G.R., Stoffels, S.M., Kumar, T., Premkumar, L., 2010, Use of Creep Compliance Interconverted from Complex Modulus for Thermal Cracking Prediction Using the M–E Pavement Design Guide. International Journal of Pavement Engineering. Vol. 11, 95-105.

You, Z., Goh, S.W., Dong, J., 2012, Predictive Models for Dynamic Modulus Using Weighted

Least Square Nonlinear Multiple Regression Model. Canadian Journal of Civil Engineering. 39(5): 589-597.

Yousefdoost, S., Vuong, B., Rickards, I., Armstrong, P., Sullivan, B., 2013, Evaluation of Dynamic Modulus Predictive Models for Typical Australian Asphalt Mixes. AAPA International Flexible Pavements Conference, 15th, Brisbane, Queensland, Australia.

Zborowski, A., Kaloush, K.E., 2011, A Fracture Energy Approach to Model the Thermal Cracking Performance of Asphalt Rubber Mixtures. Road Materials and Pavement Design. Vol 12, 377-395.

Zeghal, M., 2008, Modeling the Creep Compliance of Asphalt Concrete Using the Artificial Neural Network Technique. GeoCongress. Characterization, Monitoring, and, Modeling of Geosystems. New Orleans, Louisiana, United States. 910-916.

Zhao, S., Huang, B., Shu, X., Jia, X., Woods, M., 2012, Laboratory Performance Evaluation of Warm Mix Asphalt Containing High Percentages of RAP, Transportation Research Board Annual Meeting, Washington, D.C.

Zhou, F., Button, J.W., Epps, J., 2011, Best Practice for Using RAS in HMA, Texas Department of Transportation Research and Technology Implementation Office, Report, Texas, United States.

CONTRIBUTIONS TO KNOWLEDGE

This doctoral thesis is based on research performed during 2012 – 2016, at the Pavement Group Division, Department of Civil Engineering, University of Manitoba in Winnipeg, Canada.

The contributions of the thesis are summarized as follows:

1. Esfandiarpour, S., Shalaby, A., 2017, Alternatives for Calibration of Dynamic Modulus Prediction Models of Asphalt Concrete., In press, International Journal of Pavement Research and Technology.

2. Esfandiarpour, S., Shalaby, A., 2017, Local Calibration of Creep Compliance Models Of Asphalt Concrete, Construction and Building Materials, Volume 132, Pages 313–322.

3. Esfandiarpour, S., Ahammed, M.A., Shalaby, A., Liske, T., Kass, S., 2015, An Evaluation of Pavement ME Design Dynamic Modulus Prediction Model for Asphalt Mixes Containing RAP. The 2015 Conference of the Transportation Association of Canada.

4. Liu, Q., Esfandiarpour, S., Shalaby, A., 2015, Effect of Reclaimed Asphalt Pavement on 3-Dimensional Surface Texture, International Conference on Managing Pavement Assets (ICMPA9), Washington DC, USA.

5. Esfandiarpour, S., Shalaby, M.A., Ahammed, A., Liske, T., Kass, S., 2014, Effects of RAP

on the Mechanical Properties of Asphalt Mixes and Binder, and on the Predicted Pavement Performance, Transportation Association Canada, Montreal, Canada.

6. Esfandiarpour, S., Kavanagh, L., Shalaby, A., 2014, City of Winnipeg's experience with Recycled Asphalt Shingles (RAS) In Hot Mix Asphalt (HMA) Overlays, Canadian Technical Asphalt Association, Winnipeg, Canada.

7. Esfandiarpour, S., Shalaby, A., Ahammed, M.A., Liske, T., Kass, S., 2013, Sensitivity of Pavement ME Design Predicted Distresses To Asphalt Materials Inputs. Transportation Association Canada, Winnipeg, Canada.

Reports:

1. Esfandiarpour, S., Kavanagh, L., Shalaby, A., 2016, Mix Design Formulation and Lab Characterization of RAS Blends In Hot Mix Asphalt (HMA) for City of Winnipeg, Public Works Department, City of Winnipeg, Final Report #2.

2. Esfandiarpour, S., Kavanagh, L., Shalaby, A., 2014, City of Winnipeg RAS in HMA Overlays – Trial Projects and Field Performance, Public Works Department, City of Winnipeg, Interim Report#1.

3. Esfandiarpour, S., Shalaby, A., 2012, Utilization of Recycled Carpet Waste Fibres, Waste Glass and By-Product for Clay Stabilization, ANTEX WESTERN.

APPENDIX

Appendix A: Field performance evaluation of Mix-0-10_2 and Mix-3-10 (The City of Winnipeg mixes)

A.1 Pavement structures, traffic and locations of the Mix-0-10_2 and Mix-3-10

Fifteen locations in the City of Winnipeg were selected for field evaluation and performance analysis in this study. Mix-3-10 overlays were placed alongside the Mix-0-10_2 at most trial locations. The locations were selected to represent a range of residential and arterial streets and traffic volumes in the City of Winnipeg. Table A.1 presents the locations of the fifteen Mix-3-10 and Mix-0-10_2 HMA overlays selected for analysis. The construction year, pavement start and end locations, lane, and section lengths are presented.

Table A.1: Locations of Mix-3-10 and Mix-0-10_2 HMA overlays

No	Year	Street	From	To	RAS Lane	Length (KM)
1	2010	Gunn	Plessis	Redonda	Full Width	3.23
2	2011	Kilkenny	Radcliffe	Burgess	N/B	1.09
3	2011	William	Isabel	Princess	Full Width	0.53
4	2011	Arlington	Notre Dame	Alexander	Full Width	0.71
5	2012	Arlington	Flora	Pritchard	Full Width	0.16
6	2012	Ryerson	Rice	Dalhousie	E/B and N/B	0.67
7	2012	Island Lakes	De La Seigneurie	Desjardins	E/B	0.83
8	2012	W/B N Leg Bairdmore	Pembina Hwy	Barnes	Full Width	0.21
9	2012	E/B N Leg Bairdmore	Barnes	Pembina Hwy	South Lane	0.20
10	2012	Headmaster	Raleigh	Mildred	W/B	0.81
11	2013	Church	Powers	McGregor	W/B	0.39
12	2013	Redwood	McGregor	Salter	W/B	0.59
13	2013	Maple Grove	Fernbank	Glencairn	S/B	0.50
14	2013	Lucas	Burrows	Barnham	E/B	0.55
15	2013	Mountain	McGregor	Arlington	W/B	0.59

Note(s): NB=north bound; SB=southbound; WB=westbound; EB=eastbound

Table A.2 presents the pavement structures and traffic volumes for the Mix-3-10 and Mix-0-10_2 HMA overlays. The percent RAS, pavement structure and two-way annual average daily traffic (AADT) are presented. The average overlay thickness placed on top of the existing plain concrete pavements was 50mm for both mixes. The exception was the Gunn Road field trial which was a flexible pavement with 50mm Mix-0-10_2 HMA top lift, over 75 mm 5% Mix-5-10 bottom lift on granular base and sub-base.

Table A.2: Pavement structure and traffic volumes at Mix-3-10 and Mix-0-10_2 overlay locations

No	Year	Street	Lift/ %RAS	Pavement Structure	Two Way Traffic[1] (AADT)
1	2010	Gunn	Bottom 5%	50 mm HMA (Mix-0-10_2) 75 mm HMA (Mix-3-10) 75 mm Granular base 550 mm Granular Sub-base	4,006/ 5,171[2]
2	2011	Kilkenny	Top 3%	50 mm HMA (Mix-3-10 or Mix-0-10_2) 150 mm Concrete	646/ 450[2]
3	2011	William	Top 3%	50 mm HMA (Mix-3-10) 200 mm Concrete	10,140
4	2011	Arlington	Top 3%	50 mm HMA (Mix-3-10) 200 mm Concrete	18,382
5	2012	Arlington	Top 3%	50 mm HMA (Mix-3-10 200 mm Concrete	14,808
6	2012	Ryerson	Top 3%	50 mm HMA (Mix-3-10 or Mix-0-10_2) 150 mm Concrete	333
7	2012	Island Lakes	Top 3%	50 mm HMA (Mix-3-10 or Mix-0-10_2) 150 mm Concrete	579
8	2012	W/B N Leg Bairdmore	Top 3%	50 mm HMA (Mix-3-10) 200mm Concrete	3,160
9	2012	E/B N Leg Bairdmore	Top 3%	50 mm HMA (Mix-3-10 or Mix-0-10_2) 200 mm Concrete	3,051
10	2012	Headmaster	Top 3%	50 mm HMA (Mix-3-10 or Mix-0-10_2) 150 mm Concrete	733/ 577[2]
11	2013	Church	Top 3%	50 mm HMA (Mix-3-10 or Mix-0-10_2) 150 mm Concrete	339/ 299[2]
12	2013	Redwood	Top 3%	50 mm HMA (Mix-3-10 or Mix-0-10_2) 200 mm Concrete	3,664
13	2013	Maple Grove	Top 3%	50 mm HMA (Mix-3-10 or Mix-0-10_2) 150 mm Concrete	N/A
14	2013	Lucas	Top 3%	50 mm HMA (Mix-3-10 or Mix-0-10_2) 150 mm Concrete	634
15	2013	Mountain	Top 3%	50 mm HMA (Mix-3-10 or Mix-0-10_2) 200 mm Concrete	9,517

Note(s): [1]Average annual daily traffic volume (AADT), [2]AADT at different road segments

Figure A.1 shows the locations of the fifteen Mix-3-10 and Mix-0-10_2 field trials on regional and residential streets across the City of Winnipeg.

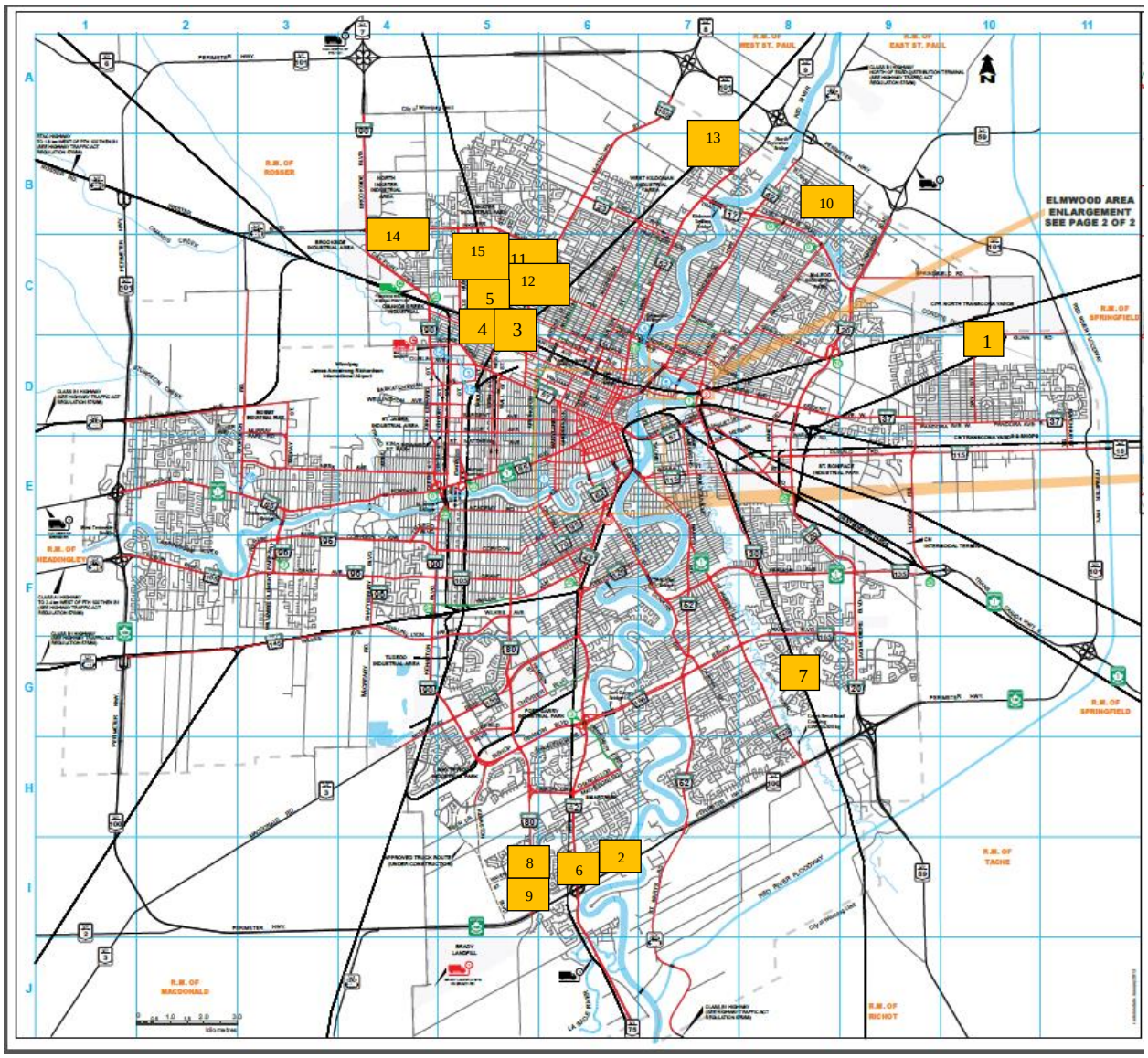

Figure A.1: Locations of Mix-3-10 and Mix-0-10_2 field trials in the City of Winnipeg

A.2 Evaluation of pre-overlay concrete joint conditions

The condition of the existing concrete pavement can have a major impact on HMA overlay performance, particularly at concrete joints. HMA overlays on underlying concrete pavements in good condition tend to outperform concrete pavements in poor conditions. Therefore, the joint conditions of the existing concrete pavement on three locations; Redwood Avenue, Maple Grove Road, and Mountain Avenue prior to the 2013 paving was documented. Only a quick visual inspection of the existing joints on Redwood Avenue was conducted prior to overlay.

Figure A.2, Figure A.3, and Figure A.4 show examples of the existing concrete joint conditions on Redwood Avenue, Maple Grove Road, and Mountain Avenue, respectively, prior to the Mix-0-10_2 and Mix-3-10 overlays in 2013.

Joint intersection damage was found severe on Mountain Avenue as it can be seen in Figure A.4 No major repair was considered for damaged joints before placing HMA overlay. The damaged joint was filled with asphalt before paving only on Maple Grove Road (Figure A.3).

Figure A.2: Pre –Overlay concrete joint condition on Redwood Avenue

Figure A.3: Pre –overlay concrete joint condition on Maple Grove Road

Figure A.4: Pre –overlay concrete joint conditions on Mountain Avenue

A.3 Reflecting cracking and distress mapping of Mix-0-10_2 and Mix-3-10 Overlay Sections

Between July and October 2013, the distress surveys on Mix-0-10_2 and Mix-3-10 overlays were conducted. The extent and severity of random longitudinal and transverse cracks, reflective cracking over concrete joints, and areas of raveling, bleeding, and polishing were measured. The severity (low, medium, or high) of the cracks and surface defects were based on the LTPP Distress Survey manual criteria.

During October 2013, the rut depth and pavement roughness measurements on the Mix-0-10_2 and Mix-3-10 overlays were conducted using a high speed laser profiler. The pavement roughness and rut depths measurements were taken in the inner wheelpath (IWP) and outer wheelpath (OWP) of lanes.

To provide direct comparisons between the Mix-0-10_2 and Mix-3-10 overlays at different locations, the total length of random cracking was normalized to a unit length per lane kilometer, and the reflective cracking and surface defects were converted to percentage.

Figure A.5 shows the graph of the normalized random longitudinal and transverse cracking for the Mix-0-10_2 and Mix-3-10 HMA overlays at each trail locations. Figure A.6 shows the graph of the percent reflection cracking (at concrete joints) for the Mix-0-10_2 and Mix-3-10 HMA overlays at each trial locations.

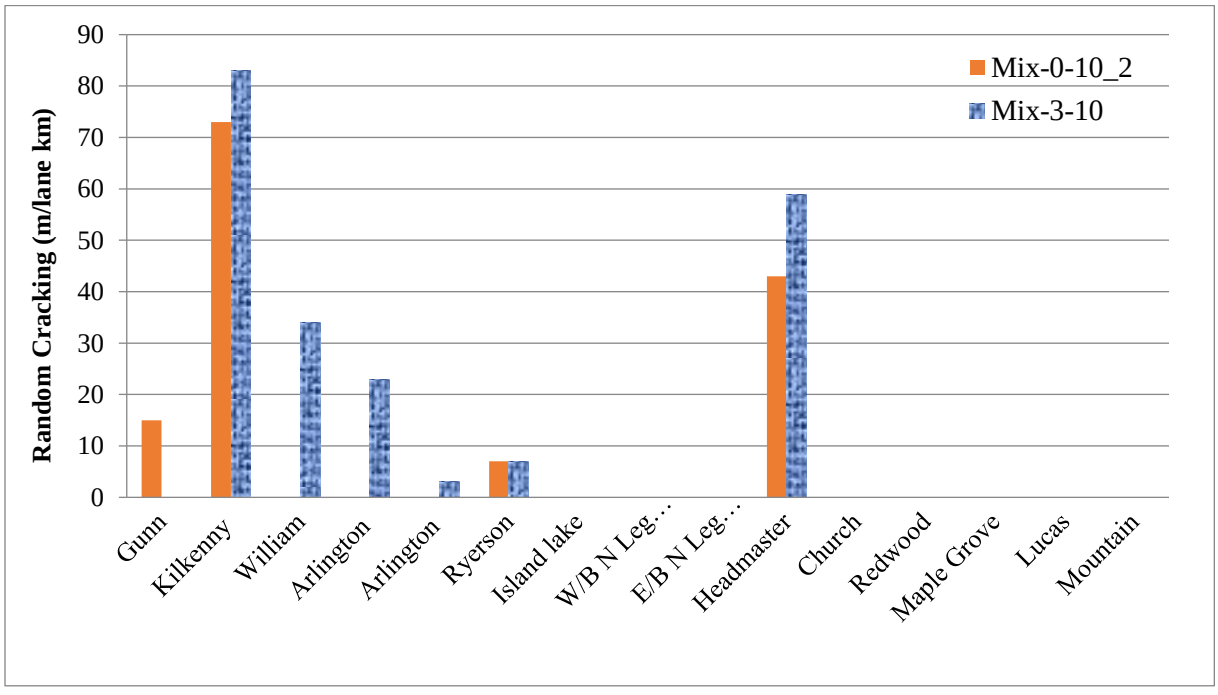

Figure A.5: Longitudinal and transverse cracking of Mix-0-10_2 and Mix-3-10 HMA overlays

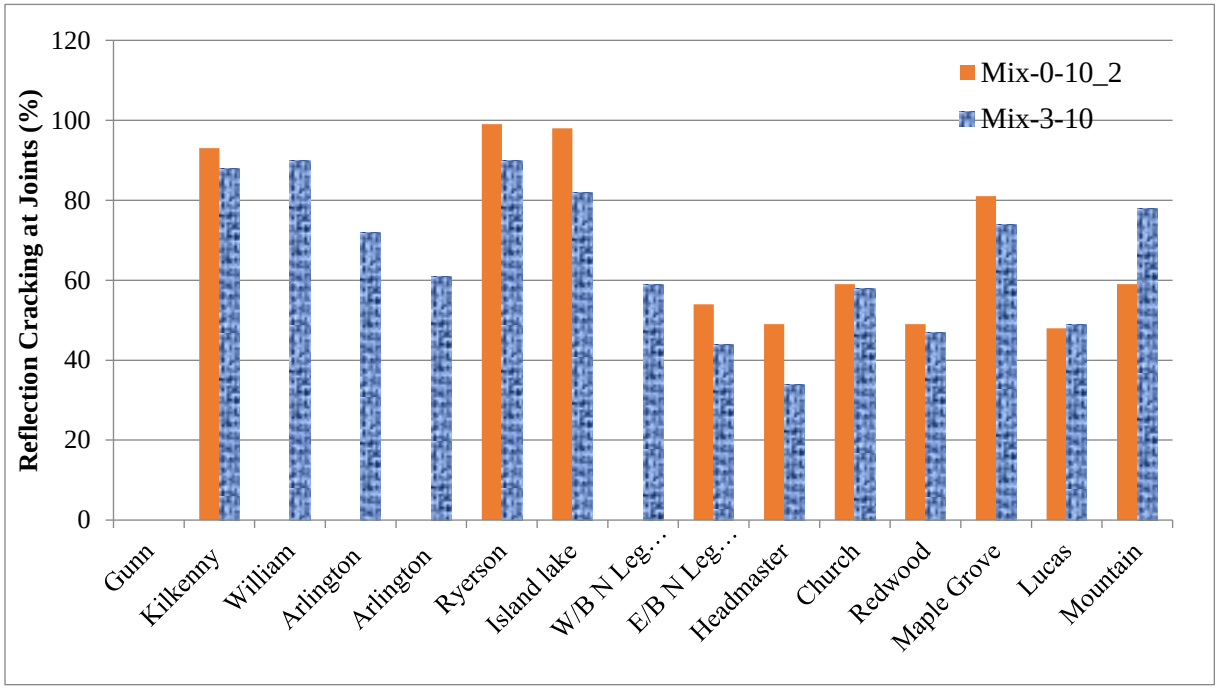

Figure A.6: Reflection cracking at joints for Mix-0-10_2 and Mix-3-10 HMA overlays

Table A.3 presents a summary of the longitudinal, transverse and reflection cracking and percent surface defects for the Mix-0-10_2 and Mix-3-10 HMA overlays, by year. The summary is based on distresses at locations with both Mix-0-10_2 and Mix-3-10 overlays.

The results show reflection cracking in the Mix-3-10 overlay was 5%, 16%, and 11% lower (on average) than reflection cracking in the Mix-0-10_2 overlay, for 2011, 2012, and 2013 respectively. However, longitudinal and transverse cracking in the Mix-3-10 overlays was 14% and 31% higher (on average) than longitudinal and transverse cracking in the Mix-0-10_2 overlay, for 2011 and 2012, respectively. The longitudinal and transverse cracking was less than 10 meters per lane-kilometer for both Mix-0-10_2 and Mix-3-10 overlay in 2013 overlays. It is unclear

whether the higher longitudinal and transverse cracking in the Mix-3-10 overlay is a function of the mix type or differences in the existing concrete on the Mix-3-10 lane prior to overly. Surface defects were minor in both Mix-0-10_2 and Mix-3-10 overlays.

Table A.3: Summary of longitudinal, transverse and reflective cracking and surface defects for Mix- 0-10_2 and Mix-3-10 HMA overlays

		Random Longitudinal and Transverse Cracking (m/lane-km)	Reflective Cracking (%)	Surface Defects (%) (bleeding, raveling, pop-outs)
2011[1]	Mix- 0-10_2	73	93	Minor (100% Pop-outs Kilkenny Street)
	Mix-3-10	83	88	
	Difference (%)	14	-5	
2012[1]	Mix- 0-10_2	13	75	Minor (Bleeding on Bairdmore Blvd)
	Mix-3-10	17	63	
	Difference (%)	31	-16	
2013[1]	Mix- 0-10_2	0.7	63	Minor polishing on Mountain street
	Mix-3-10	1.3	57	
	Difference (%)	-	-11	

Note(s): [1] Average of locations with both Mix-0-10_2 and Mix-3-10 HMA Overlays. Negative sign indicate Mix-3-10 distress is lower than Mix- 0-10 distress

A.4 Rutting and roughness performance of Mix- 0-10 and Mix-3-10 HMA overlays

The extent of rutting and pavement roughness was determined from the rut depths and IRI measurements for the 2010-2013 Mix-0-10_2 and Mix-3-10 overlays.

The rut depth and IRI were in the outer wheel path of each lane. The results show rut depths were low to moderate (2mm to 13mm) for both the Mix-0-10_2 and Mix-3-10 overlays. The pavement

roughness (IRI) was moderate (1.5mm/m to 5.0mm/m) at both Mix-0-10_2 and Mix-3-10 overlays. A direct comparison between the Mix-0-10_2 and Mix-3-10 overlays was difficult since only a few locations had rut depths and IRI measurements on both Mix-0-10_2 and Mix-3-10 lanes.

Figure A.7 shows a graphical representation of the average rut depth measured in the OWP at the Mix-0-10_2 and Mix-3-10 overlay locations. Figure 5.8 shows a graphical representation of the average IRI in the OWP at the Mix-0-10_2 and Mix-3-10 overlay locations.

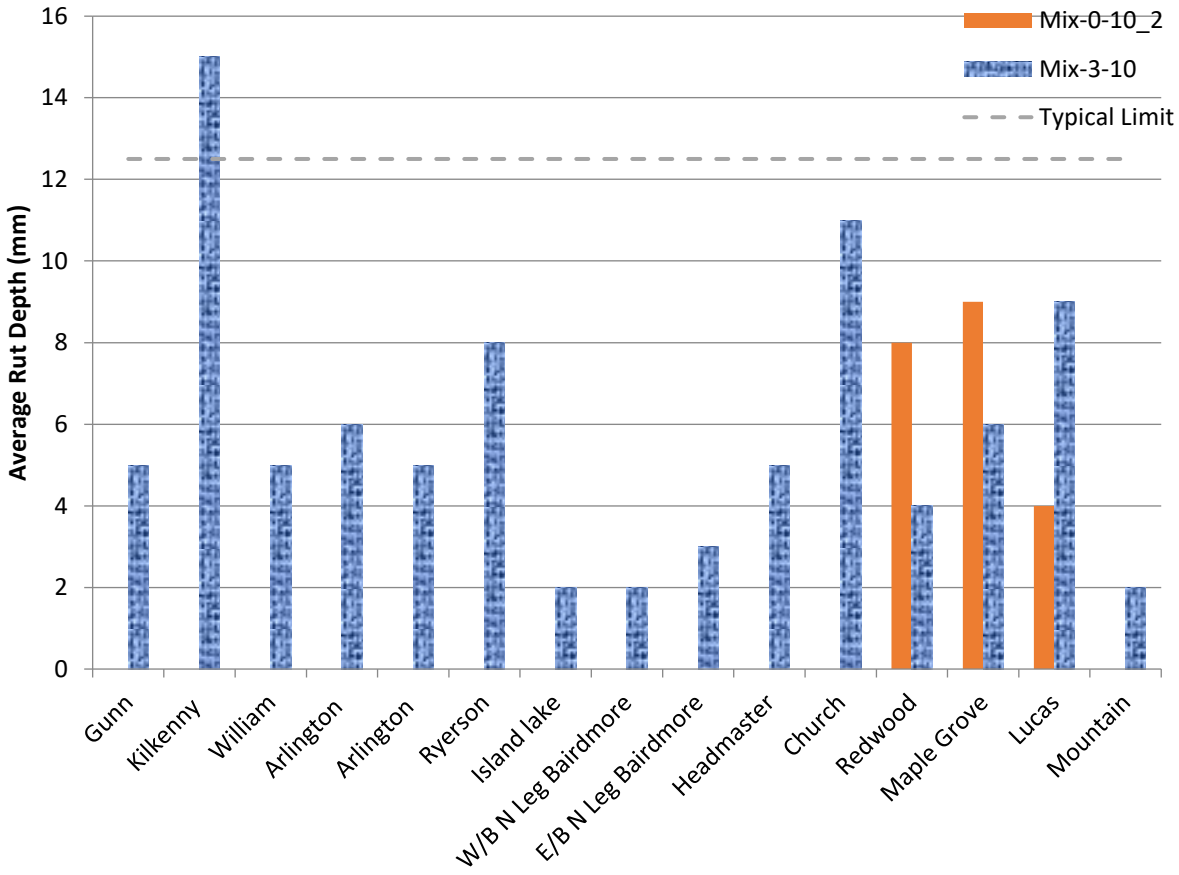

Figure A.7: Average rut depth in OWP for Mix-0-10_2 and Mix-3-10 HMA overlays

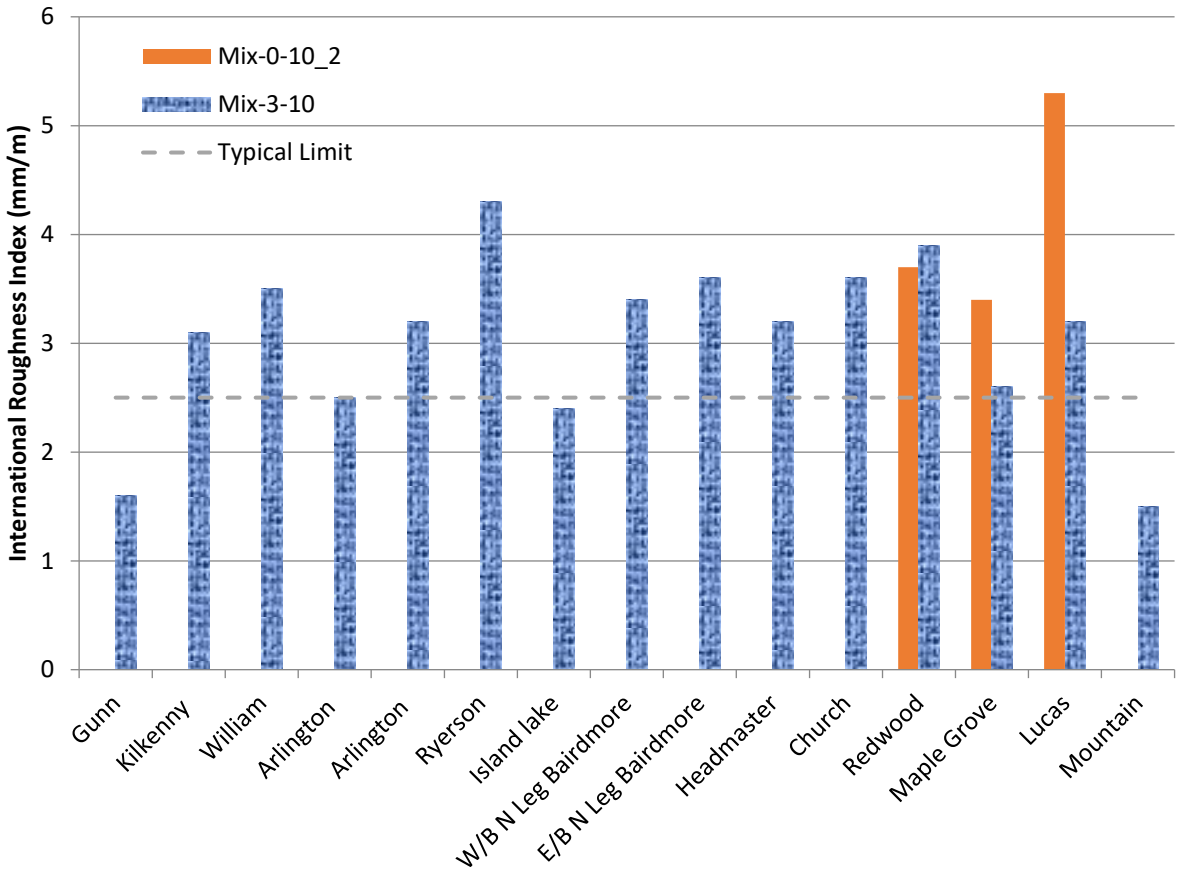

Figure A.8: Average IRI in OWP for Mix-0-10_2 and Mix-3-10 overlays

A.5 Summary

The field performance of the Mix-3-10 overlay was comparable with the Mix-0-10_2 overlays. Longitudinal and transverse cracking of Mix-3-10 overlays were 14% and 31% higher (on average by year) than longitudinal and transverse cracking of Mix-0-10_2 overlays. Reflective cracking of Mix-3-10 overlays was 5%, 16% and 11% lower (on average by year) than reflective cracking of Mix-0-10_2 overlay. Surface defects were minor in both overlays.

Rut depths were low to moderate overall (2mm to 13mm) for both Mix-3-10 and Mix-0-10_2 overlays. The IRI were moderate (1.5mm/m to 5.0mm/m) at both Mix-3-10 and Mix-0-10_2 overlays. It was difficult to compare the rut depth and roughness data between the Mix-3-10 and Mix-0-10_2 overlays since only a few locations had both Mix-3-10 and Mix-0-10_2 data.